On the Partitioning of Tropical Precipitation between Land and Ocean

Luca Schmidt

Hamburg 2024

On the Partitioning of Tropical Precipitation between Land and Ocean

Luca Schmidt

Hamburg 2024

Luca Schmidt

aus Bad Boll, Deutschland

Max-Planck-Institut für Meteorologie
The International Max Planck Research School on Earth System Modelling
(IMPRS-ESM)
Bundesstrasse 53
20146 Hamburg

Tag der Disputation: 31. Mai 2024

Folgende Gutachter empfehlen die Annahme der Dissertation:
Dr. Cathy Hohenegger
Prof. Dr. Victor Brovkin

Vorsitzender des Promotionsausschusses:
Prof. Dr. Hermann Held

Dekan der MIN-Fakultät:
Prof. Dr.-Ing. Norbert Ritter

Titelbild: Aquarellzeichnung von Luca Schmidt: Convection over a tropical landscape

For my grandparents
Wendelin, Anna, Hermann, Marta, and Walter

ABSTRACT

Tropical precipitation accounts for about two thirds of the Earth's global precipitation: What determines and constrains how this huge amount of precipitation gets partitioned between tropical land and tropical ocean? And how is it possible that tropical mean precipitation is enhanced over land, as indicated by observations?

These seemingly simple questions are difficult to answer due to the complex nature of atmospheric convection as the main source of tropical precipitation, and its manifold interactions with the land and ocean surfaces. Despite profound advances in our understanding of tropical convection, we still lack a comprehensive theory for the climatological mean state of tropical precipitation, and for the land-ocean contrast associated with this mean state. Modern satellite observations enable us to quantify related precipitation characteristics such as χ, the ratio of spatiotemporal mean precipitation over tropical land and ocean, but physical theories are needed to understand *why* these characteristics emerge. In this dissertation, I set out to investigate the physical controls and fundamental constraints on χ in a two-step approach.

In a first study, I use the fundamental law of water conservation to develop a conceptual box model of the tropical hydrology. This model treats land and ocean, as well as their overlying atmospheric volumes as moisture reservoirs that exchange moisture with one another based on empirical but physically motivated expressions for evaporation, evapotranspiration, precipitation, atmospheric advection, and soil runoff. A parameter sensitivity analysis of the system's equilibrium state reveals that χ is mostly controlled by the efficiency of moisture transport in the atmosphere, and less so by surface properties. Furthermore, χ is bounded between zero and one, meaning that the mean precipitation over ocean always exceeds mean precipitation over land. This constraint on χ is explained as a fundamental consequence of the existence of runoff together with the model assumption that the relationship $P(r)$ between precipitation P and column relative humidity r is unaffected by the underlying surface type. However, stronger mean precipitation over ocean is at odds with the observational evidence that on large scales, tropical mean precipitation is enhanced over land. This discrepancy inspires the hypothesis that the land surface modifies $P(r)$ in such a way that an atmospheric column with a given humidity r yields more precipitation over land than it does over ocean.

In a second study, I test this hypothesis using ten years of daily ERA5 reanalysis data. Even though a systematic influence of the land surface on $P(r)$ exists, this influence turns out not to be the reason for precipitation enhancement over tropical land. Instead, differences in the column relative humidity distribution, $pdf(r)$, between land and ocean, and specifically a stronger tail of the land distribution at high r values, explain the enhancement. This result is corroborated by qualitatively similar results obtained from a storm-resolving ICON simulation run with explicit convection and a grid spacing of 5 km.

Taken together, the work compiled in this thesis advances our theoretical understanding of the tropical land-ocean-atmosphere coupling through moisture fluxes, and it highlights interactions of surface properties with the atmospheric circulation as key for setting the climatological land-ocean contrast of tropical precipitation.

ZUSAMMENFASSUNG

Tropische Konvektion is verantwortlich für etwa zwei Drittel des globalen Niederschlags: Was bestimmt, wie sich diese gewaltige Wassermenge zwischen tropischem Land und tropischem Ozean aufteilt? Und wie ist es möglich, dass, wie Beobachtungsdaten zeigen, tropischer Niederschlag bevorzugt über Land fällt?

Diese vermeintlich einfachen Fragen sind schwer zu beantworten aufgrund der komplexen Natur von atmosphärischer Konvektion, der Hauptquelle tropischen Niederschlags, und ihrer zahlreichen Wechselwirkungen mit der Land- und Ozeanoberfläche. Trotz beträchlicher Fortschritte in unserem Verständnis von tropischer Konvektion, fehlt noch immer eine umfassende Theorie, die den klimatologischen Durchschnittszustand von tropischem Niederschlag und den damit verbundenen Kontrast zwischen Niederschlag über Land und Ozean erklärt. Moderne Satellitenbeobachtungen ermöglichen es, Niederschlagscharakteristiken wie χ, das Verhältnis von räumlich und zeitlich gemitteltem Niederschlag zwischen Land und Ozean, zu quantifizieren. Um jedoch zu verstehen, *wie* die beobachteten Charakteristiken zustande kommen, bedarf es physikalischer Theorien. In der vorliegenden Dissertationsschrift untersuche ich in zwei Schritten, welche physikalischen Faktoren den klimatologischen Wert von χ bestimmen und begrenzen.

In einer ersten Studie nutze ich das Prinzip der Wassererhaltung, um ein konzeptionelles Modell des tropischen Wasserkreislaufes zu entwickeln. In diesem Modell stellen Land und Ozean, sowie die jeweils darüberliegende Atmosphäre Feuchtereservoirs dar, welche basierend auf empirischen, aber physikalisch motivierten Ausdrücken für Evaporation, Evapotranspiration, Niederschlag, atmosphärische Advektion und Abflüsse im Boden Feuchte miteinander austauschen. Eine Analyse der Parametersensitivität des systemischen Gleichgewichtszustands ergibt, dass χ primär von der Effizienz des atmosphärischen Feuchtetransports bestimmt wird, und weniger stark von Oberflächeneigenschaften. Darüber hinaus ist χ auf Werte zwischen null und eins beschränkt, was bedeutet, dass es über dem Ozean grundsätzlich stärker regnet als über Land. Diese Beschränkung von χ ergibt sich als Konsequenz aus der Existenz von stetem Feuchteabfluss im Boden, sowie der Modellannahme, dass die Beziehung $P(r)$ zwischen Niederschlag P und relativer Luftfeuchtigkeit r nicht vom zugrundeliegenden Oberflächentypus abhängt. Allerdings steht der stärkere Regen über dem Ozean im Widerspruch zu der großskaligen Beobachtung von stärkerem Regen über tropischem Land. Diese Diskrepanz führt zu der Hypothese, dass die Landoberfläche die Beziehung $P(r)$ dergestalt modifiziert, dass derselbe Wert relativer Luftfeuchtigkeit über Land du mehr Niederschlag führt als über dem Ozean.

In einer zweiten Studie teste ich diese Hypothese mithilfe von zehn Jahren täglicher ERA5 Reanalysedaten. Obwohl eine systematische Modifizierung von $P(r)$ durch die Landoberfläche existiert, stellt sich heraus, dass diese Modifizierung nicht zu stärkerem Regen über tropischem Land führt. Stattdessen erklären Unterschiede in der Verteilung von relativer Luftfeuchtigkeit, $\mathrm{pdf}(r)$, zwischen Land und Ozean, und insbesondere eine erhöhte Häufigkeit sehr feuchter Orte über Land, die beobachtete Verstärkung von tropischem Landniederschlag. Qualitativ ähnliche Ergebnisse, basierend auf einer ICON-Simulation mit expliziter Konvektion und einer horizontalen Auflösung von 5 km, untermauern dieses Resultat.

Insgesamt verbessert diese Dissertation unser theoretisches Verständnis der tropischen

Land-Ozean-Atmosphären-Kopplung durch Feuchteflüssen. Sie hebt inbesondere hervor, dass Wechselwirkungen zwischen Oberflächeneigenschaften und der atmosphärischen Zirkulation den klimatologischen Kontrast zwischen tropischem Land- und Ozeanniederschlag maßgeblich bestimmen.

ACKNOWLEDGEMENTS

A dissertation seldom reflects the efforts of a solitary individual. Thus, I want to express my gratitude to all the people who contributed to the existence of this work in major ways. Firstly, I would like to thank my supervisor Cathy Hohenegger for her guidance throughout my PhD. You taught me how to approach scientific riddles, encouraged me to question the seemingly simple, challenged me, provided valuable feedback at all stages of this endeavor, and ensured that I would stay the course.

I am also grateful to Victor Brovkin for his consistent support in various capacities, and to Bjorn Stevens for critical input and the opportunity to conduct my doctoral research at the MPI for Meteorology, surrounded by inspiring people.

My time in Hamburg would not have been nearly as enjoyable without all the fantastic colleagues and friends I met at MPI and beyond. While it is impossible to acknowledge everyone, I would like to mention Moritz, Clarissa, Abisha, Arim, Hernan, Paul, Laura, Dan, Raphael, Marius, Janina, and Meike for sharing both the highs and lows, engaging in countless brain-refreshing lunch breaks, and participating in all the fun leisure activities; George for his energy and lessons on Julia; Robert for our discussions of science and life; Lukas for his technical support and uplifting cynicism; Lea and Valentina for their cheery company and creativity during the long months of lockdown; Chris for pushing my innerer Schweinehund in the climbing gym; and Ole for supporting me with much kindness and empathy on the finishing line of this PhD.

I am also indebted to Antje, Angela, Connie, and Michaela, who not only sort out bureaucratic hurdles, often without us doctoral researchers even noticing, but also provide emotional support where needed. Even more invisible but hard to overestimate is the work of people who clean and maintain our institute's infrastructure.

Some people had a great influence on who I am and how I look at the world. Foremost among them are my godmother Charis, who encouraged me to be daring; Hermann, who sparked my enthusiasm for science; Adam, whose perspectives broadened my horizon, who taught me the art of optimizing for the right thing, and who, more than once, improved my research through fruitful discussions; my "Swedish grandmother" Ingrid, whose determination and love of life is contagious; Ophelia and both Nicoles, who – each in their own special way – add richness to my world; and my homebase girls, Lisa, Ira, Kathy, Laura, Corinna, Svenja, and Rosa, who inspire me, give me confidence and solace when I need it, and add the pinch of madness and humor to my life that is needed to spice things up.

This acknowledgement would be incomplete without mentioning my parents Anton and Dorothe, as well as my brother Tim, whose support and unconditional love form the stable platform from which I ventured into every major undertaking of my life, including this PhD. And also not without my grandparents Wendelin, Anna, Hermann, Marta, and Walter, who each lived a life, so different from mine, and who sometimes tip me on my shoulder when my focus gets too narrow and I should look up to see what really matters.

CONTENTS

ACRONYMS

ERA ECMWF ReAnalysis

ET EvapoTranspiration

GCM General Circulation Model

ICON Icosahedral Nonhydrostatic (Weather and Climate Model)

ITCZ InterTropical Convergence Zone

LH Latent Heat

LHS Left Hand Side

pdf probability density function

RHS Right Hand Side

SH Sensible Heat

SST Sea Surface Temperature

Part I

UNIFYING ESSAY

MOTIVATION

The ocean is typically considered to be the starting point for water molecules on their journey through the hydrological cycle. However, not all atmospheric moisture was evaporated from the ocean surface, and likewise, not all of it will precipitate back over the ocean. How much of the total amount of evaporated water should we expect to precipitate over land instead? The answer to this question is unknown and difficult to find since the spatial distribution of precipitation hinges on a plethora of atmospheric processes and surface-atmosphere interactions. Some of these interactions depend on the underlying surface type, being land or ocean. While an overview of such interactions is provided in Chapter 2, two examples seem worth mentioning. First, the land-ocean temperature contrast generates atmospheric circulations which facilitate atmospheric moisture transport from ocean to land. Second, surface controls on local evaporation differ between land and ocean in that ocean evaporation is primarily controlled by available energy, while moisture fluxes from the land surface are additionally constrained by soil moisture availability. It is the overarching goal of this thesis to better understand the physical controls on the land-ocean precipitation contrast with a focus on the tropics, as the region receiving the bulk of the global precipitation, and whose precipitation dynamics are both poorly understood and of vital importance for the global climate as well as human and ecosystem wellbeing.

As I am writing this essay in 2024, the belt of temperate climate between $\pm 30°$N, known as the tropics, is home to about 40% of the world's human population and the majority of the planet's terrestrial and marine biodiversity (Edelman et al., 2014). Given the importance of precipitation for natural vegetation, agriculture, and freshwater resources (Phillips et al., 2009; Krishna Kumar et al., 2004; Sivakumar et al., 2005), this alone makes the tropics a highly interesting region, worthy of scientific efforts to understand the processes shaping tropical precipitation today and in the future. In addition, impacts of tropical precipitation reach well beyond the regional scale. Tropical circulations in the atmosphere such as the Hadley and Walker circulation, or various monsoon circulations are propelled by the latent heat release associated with precipitation, and they influence how the large amounts of solar energy received near the equator get distributed across the globe (Held and Hou, 1980). These circulations also play a key role in determining how effectively the planet can radiate energy back to space, which manifests in Earth's climate sensitivity (Pierrehumbert, 1995; Tomassini et al., 2015). Moreover, tropical precipitation is linked to extratropical weather and climate phenomena through a number of teleconnections, an example being the interaction of tropical waves, generated by deep convection, with extratropical storm tracks (Liu and Alexander, 2007; Stan et al., 2017).

Despite its importance in the climate system, tropical precipitation is a particularly notorious variable, associated with large and long-standing biases in state-of-the-art climate model simulations. For instance, models yield too large or too small precipitation mean amounts, and simulate a double Intertropical Convergence Zone (ITCZ) over the Pacific and Atlantic ocean, irrespective of whether convection is parametrized or explicitly re-

solved (Zhang et al., 2015; Fiedler et al., 2020; Tian and Dong, 2020; Becker et al., 2021; Hohenegger et al., 2023). These biases also manifest in a poor representation of the land-ocean precipitation contrast, quantified by χ, the ratio between spatiotemporal mean precipitation rates over tropical land and ocean. For instance, most CMIP6 models simulate a wrong value of χ, or capture it correctly but for wrong reasons (Hohenegger and Stevens, 2022, hereafter HS22).

What is needed to improve climate models, and to make sense of our increasingly accurate observations, is the development of a robust process understanding of what drives and potentially constrains the mean state of tropical precipitation and its associated land-ocean contrast. While energetic constraints have been identified as controlling factors for tropical mean precipitation (e.g. Allen and Ingram, 2002), constraints on the partitioning of this mean precipitation between land and ocean has received comparably little attention in the scientific literature. Existing studies on land-ocean precipitation contrasts either restrict themselves to monsoon precipitation (e.g. Chou et al., 2001; Fasullo, 2012), or to small scale features such as tropical islands where sea and mountain breezes, as well as interactions of the synoptic flow with orography play the dominant role (Qian, 2008; Sobel et al., 2011; Ulrich and Bellon, 2019). While these studies have advanced our mechanistic understanding of surface-atmosphere interactions and their influence on local and regional precipitation characteristics, they lack the full-tropical perspective in which conservation laws can be leveraged as constraining factors.

To my knowledge, HS22 is the first study that systematically assessed the climatology of the full tropical precipitation partitioning, represented by χ, based on satellite observations. Depending on the satellite product, the climatological χ value computed for the latitudinal band between $\pm 30\,°\mathrm{N}$ lies between 0.90 and 1.04, meaning that, on average, it rains similar amounts per unit area and time over tropical land and ocean (each about $3\,\mathrm{mm\,day^{-1}}$). This is somewhat surprising, given the soil moisture limitation of evapotranspiration from the land surface which may suggest that land should receive less mean precipitation than the ocean. However, using a conceptual rainbelt model, HS22 further demonstrated that any value of χ above 0.86 must even be interpreted as an enhancement of precipitation over tropical land with respect to the tropical ocean. This finding is essentially due to the fact that the land fraction in the subset of tropical latitudes that get visited by the rainbelt during its seasonal migration (approximately $\pm 10\,°\mathrm{N}$), is smaller than the full tropical land fraction within $\pm 30\,°\mathrm{N}$ which is used to compute χ. Consequently, the observed value of χ close to one is a mere coincidence arising from the chosen definition of tropical latitudes, and tropical precipitation in the real world is enhanced over land.

Since $\chi = 1$ turned out not to be a special number, χ may be free to range between zero and $+\infty$ if either all precipitation ends up over ocean, or all precipitation ends up over land. However, intuitively, neither of these extreme cases seems plausible. So, what are the basic controls on χ, and do large-scale constraints exist that limit the range of values χ can attain? These questions inspired the development of a conceptual box model of the tropical land-ocean-atmosphere system based on water balance equations. This model forms the basis for the first study included in this thesis, and the obtained insights in general controls and constraints on χ are the subject of Chapter 3.

Furthermore, I wanted to understand why precipitation is enhanced over tropical land, as indicated by the observed χ values above 0.86. While HS22 offer a widening and stronger movement of the rainbelt over tropical land as a first explanation, this question is far from being conclusively answered. The box model from study 1 informs a number of testable hypotheses for mechanisms that could explain precipitation enhancement over tropical land. One possibility is that the enhancement is due to a modification of the statistical relationship between precipitation and column relative humidity by the land surface. In a second study, which is summarized in Chapter 4, I test this hypothesis based on ERA5 reanalysis data.

ERA5 relies on convective parametrizations which are known to contribute to precipitation biases (Stevens and Bony, 2013). At the same time, recent model developments now enable global climate simulations with explicitly resolved convection. To test whether the conclusions of study 2 regarding the reasons for precipitation enhancement over land are sensitive to the use of convective parametrizations, I performed a similar analysis with a high-resolution ICON model simulation with explicit convection. The findings from this investigation are discussed in Chapter 5.

As a whole, this dissertation sets out to advance our fundamental understanding of the tropical land-ocean precipitation contrast using basic conservation laws and robust mean relationships, which only come to light when we reduce the complexity of real world processes. In this spirit, the remainder of this thesis is a demonstration of what we can learn when we *go simple to understand the complex*.

BACKGROUND

This chapter provides some basic information on the concepts underlying the work presented in this thesis. In particular, I give a brief overview of characteristic properties of tropical climate and precipitation, and I discuss how land and ocean, as two different surface types, interact with precipitation in their own distinct ways. To this end, I introduce water balance equations which connect the different interactions and form the basis of the conceptual box model developed in Study 1. Furthermore, this chapter covers a discussion of the statistical model of tropical precipitation known as the moisture-precipitation relationship, whose dependence on surface type and influence on the partitioning of precipitation between land and ocean is the subject of Study 2.

2.1 TROPICAL PRECIPITATION – A BRIEF INTRODUCTION

The tropical climate is spatially and temporally diverse and depends strongly on latitude. Due to the location near the equator, the deep tropics receive the highest amount of incoming solar radiation per unit area which leads to a moist and warm boundary layer. The warming and moistening of near-surface air destabilizes the atmospheric profile and triggers frequent convection, which acts to restore atmospheric stability and results in large amounts of precipitation as moist air rises, cools, and condenses. In fact, tropical precipitation amounts to about two thirds of the annual global precipitation (Chahine, 1992).

Together with the gradient of surface heating between the equator and higher latitudes, the release of latent heat associated with the formation of this precipitation drives a large-scale, meridional circulation, known as the Hadley circulation. By transporting large amounts of water vapor from the subtropics to the deep tropics, thereby converging moist air near the equator, the Hadley circulation reinforces strong deep tropical precipitation (Peixóto and Oort, 1983; Dey et al., 2024). The decending branch of the Hadley circulation is located in the subtropics where slow, large-scale subsidence of dry air balances the rapid rising motion of moist air in the deep tropics. Subsidence regions receive relatively little precipitation due to the dryness of the subsiding air and a largely stable atmospheric profile. This stability owes to a fairly strong inversion at the top of the boundary layer where the comparably cool mixed-layer air meets the warm, moist-adiabatic temperature profile of the tropical free troposphere, set by deep tropical ascent regions (e.g. Augstein et al., 1974; Charney, 1963).

2.1.1 *The role of land in shaping tropical precipitation*

This first-order picture of tropical climate with a narrow band of precipitation located near the equator, works well over tropical oceans but gets modified by the presence of land. The modification by the land surface happens in three major ways: First, land has a lower heat capacity and therefore heats up more under the influence of incoming solar radiation. The

differential heating between land and ocean establishes pressure gradients, additional to the poleward gradient driving the Hadley circulation. The resulting circulations often have a strong zonal component due to the predominantly meridional orientation of tropical continents (Halley, 1686). Examples for such circulations are the Walker circulation, which is strongest in the tropical Pacific, various monsoon circulations in the Atlantic, Pacific, and Indian ocean, and smaller scale sea breezes. In terms of precipitation, these circulations distort the first-order picture of rainy deep tropics and dry subtropics in that they enable heavy, seasonal or diurnal precipitation in subtropical regions, especially over land (Ananthakrishnan, 1977).

Second, the land's orography redirects atmospheric flow, especially near mountain ranges. By blocking and lifting of moist air, orography can further support precipitation in one place, and suppress it in another (Wohl et al., 2012). The mountain range of the Andes, for instance, blocks and redirects moist air travelling westward from the Atlantic, thereby supporting rainfall in the eastern part of the Amazon basin while turning the Pacific coast west of the mountain range into one of the driest places on Earth (Insel et al., 2010).

Third, the land surface undergoes constant drying because some of the water that precipitates over land returns to the ocean in the form of surface or sub-surface currents termed runoff. This water cannot participate in subsequent evapotranspiration (ET), meaning that the moisture input from land into the atmosphere is limited by soil moisture availability. In the subtropics, which receive little rainfall due to subsidence, this limitation leads to dessicated landscapes such as the Sahara desert with correspondingly dry atmospheric conditions due to the lack of ET. The constraint of surface moisture availbility does not exist over ocean where air, travelling from the subtropics to the deep tropics, can draw moisture from an unlimited water reservoir at the surface. Hence, through this third pathway, land reduces the amount of moisture that is carried to the deep tropics as the fuel for equatorial precipitation.

However, while the limited moisture availability of the land surface overall reduces evapotranspiration to the atmosphere, its effect is not necessarily detrimental for local precipitation. In particular, the amount of soil moisture determines how the incoming solar radiation gets partitioned into sensible and latent heat fluxes at the surface: The drier the soil, the more energy is converted to sensible heat which increases the surface temperature. On large scales, the dryness of soils relative to the ocean manifests in the land's lower heat capacity and causes the temperature gradients that drive the landward circulations discussed above. On smaller scales, inside continents, the interaction between soil moisture heterogeneities and precipitation can generate shallow circulations similar to sea breezes that carry moisture, and eventually precipitation, from moist to dry soil patches (Taylor et al., 2011; Taylor et al., 2012; Hohenegger and Stevens, 2018).

2.1.2 *A two-ingredient framework for precipitation*

After this brief overview over tropical precipitation characteristics and the roles of land and ocean in shaping them, I now want to introduce a more general, conceptual framework for precipitation, based on which I discuss how different surface types interact with precipi-

tation in their own ways. This framework starts from the assumption that two ingredients are needed for precipitation to occur at some point in space and time:

1. Atmospheric moisture as the fuel for precipitation.

2. Favorable environmental conditions together with a chain of local processes that turn available moisture into precipitation.

I will refer to this second ingredient as the conversion efficiency. In the following two sections, I describe how moisture availability and conversion efficiency each depend on the underlying surface type, being land or ocean, and how these two ingredients for precipitation interact with one another.

2.2 SURFACE CONTROLS ON MOISTURE AVAILABILITY

To understand how the surface type controls the amount of atmospheric moisture over a given location, it is instructive to first revisit the concept of water balance. In general, water balance means that water neither gets created nor destroyed but merely changes its location or phase. In the Earth system, this condition manifests in the global water cycle (e.g. Peixóto and Oort, 1983). Water molecules that get evaporated or transpired from the Earth's surface are at the mercy of atmospheric motion for an average duration of about 10 days (Trenberth, 1998). During this time, the water vapor gets transported both horizontally and vertically, and at some point encounters atmospheric conditions that lead the vapor to condense and form raindrops, ice crystals, or other forms of condensate. At this point, the water molecules have a good chance to return to the surface as precipitation, where in the tropics, this mostly means in the form of rain.

Mathematically speaking, water in the Earth system obeys the mass continuity equation which can be formulated for any given volume, and serves as the starting point for deriving the atmospheric water balance equation (see for example Trenberth and Guillemot, 1995). For our purpose here, I consider the volume of an atmospheric column containing water vapor only, i.e. neglecting other phases such as liquid or frozen moisture. The atmospheric water balance equation for this scenario describes the rate of change of column water vapor w, the vertical integral over vapor phase specific humidity, and reads

$$\frac{\delta w}{\delta t} = E - P - \vec{\nabla}_h \cdot \vec{Q}, \tag{1}$$

where E denotes evaporation or ET, P stands for precipitation, and $\vec{\nabla}_h \cdot \vec{Q}$ is the horizontal moisture flux divergence.

The horizontal moisture flux divergence in pressure coordinates can further be written in terms of the vertical integral over the product of vapor phase specific humidity $q_v(x, y, p)$ and horizontal wind speed $\vec{u}_h(x, y, p)$,

$$\vec{\nabla}_h \cdot \vec{Q} = \vec{\nabla}_h \cdot \int_{p_s}^{0} q_v \vec{u}_h \frac{dp}{g}$$

$$= \underbrace{\int_{p_s}^{0} q_v \vec{\nabla}_h \cdot \vec{u}_h \frac{dp}{g}}_{\text{convergence}} + \underbrace{\int_{p_s}^{0} \vec{u}_h \cdot \vec{\nabla}_h q_v \frac{dp}{g}}_{\text{advection}}, \tag{2}$$

The vertical integration is performed from the surface with pressure p_s, all the way to the top of the atmosphere, where pressure practically vanishes.

I separated the right hand side (RHS) of Equation (2) into two components, representing two distinct modes of horizontal moisture transport in the atmosphere: Convergence, driven by a gradient in the wind field, and advection, driven by a gradient in the moisture field. While evaporation/ET and precipitation are clear sources and sinks of atmospheric moisture, respectively, advection and convergence may either dry or moisten the atmospheric column, depending on the humidity and wind field in the column's immediate surrounding.

If we neglect the moisture exchange between the tropics and extratropics, which may not generally be a good assumption (Dessler and Minschwaner, 2007; Galewsky et al., 2005), the large-scale horizontal moisture transport in the tropics by advection and convergence is predominantly controlled by the atmospheric circulations outlined in section 2.1. For the oceanic atmosphere, the lateral moisture transport has a net drying effect, while for the terrestrial atmosphere, it has a net moistening effect. Recent global estimates (dominated by the tropics) find that about twice as much moisture gets carried from ocean to land than from land to ocean (Dey et al., 2024). To some extent, the moisture export from ocean to land happens all year around as part of the first-order Hadley cell picture, in the form of trade winds which get bent westward by the Coriolis force, and at some point meet a continent. An example is near-surface air flow moistening over the Atlantic before it reaches South America and carries moisture into the Amazon basin (Arraut et al., 2012). Even though such air leaves the continents again, net moisture transport from ocean to land happens because terrestrial mean precipitation exceeds mean ET due to runoff, so that the outflowing air is typically drier than the inflowing air. But there are additional, more important circulations facilitating moisture convergence over land, which are directly influenced by the presence of land and the temperature gradient between land and ocean.

Chief among these circulations are monsoon systems which are very complex in nature but can typically be characterized by seasonally varying wind patterns, leading to two seasons of tropical land climate, namely a rainy summer season with moisture convergence, and a less rainy winter season with reduced convergence. Monsoon systems are found over all tropical continents (e.g. Geen et al., 2020, Figure 1), and they were typically interpreted as large-scale thermally driven sea breezes (Halley, 1686). Another important circulation type is the tropical Walker circulation, generated by a mix of sea surface temperature (SST) gradients, and land-ocean temperature contrasts (Stone and Chervin, 1984). The Walker circulation's two primary ascending branches are located over tropical land, one over the warm Maritime Continent (Dayem et al., 2007), and another one over South America (Veiga et al., 2005), both with balancing sinking motion over the cool Eastern Pacific. More recently,

the ITCZ, Walker circulation, and regional monsoons have been united in the framework of "the global Monsoon" (Trenberth et al., 2000). Even though the exact role of land in this framework is not yet fully explored, I think it is fair to say that differential heating between tropical land and ocean modulates the global Monsoon in a way that leads to mean moisture convergence over land.

Apart from lateral transport, moisture availability is also affected by local processes of evaporation and ET from the ocean and land surfaces, respectively. Over ocean, evaporation is never moisture-limited and its magnitude is primarily determined by the incoming solar energy. Over tropical land, the situation is different. Moisture influx from the ocean typically creates moist atmospheric conditions and ample precipitation near the coasts but further downwind into the continent, atmospheric moisture availability increasingly hinges on "recycled" moisture that got re-evaporated from the land surface (e.g. Ent et al., 2010, Figure 3). In some sense, the land acts like a sponge or moisture buffer in the climate system. After a precipitation event, some of the water is lost to surface runoff but the remainder infiltrates into the soil where it stays available for subsequent evapotranspiration or slow runoff over time. If the soil is very wet, then ET acts much like evaporation from the ocean surface in that the vast majority of incoming solar energy is turned into latent heat (LH), as opposed to sensible heat (SH). But if the soil dries out, then soil moisture availability becomes the dominant factor that sets the partitioning between LH and SH, and ET is first reduced and eventually becomes zero when the soil suction, holding the moisture within the soil matrix, becomes too strong, and all incoming energy is turned into SH (Seneviratne et al., 2010).

This qualitative dependence of ET on soil moisture availability can be used to classify a given location at a given time into one of the following three soil moisture regimes, determined by the relative soil moisture saturation s and time-invariant properties of the given soil type, namely permanent wilting point s_{pwp} and field capacity s_{fc}:

- In the **dry regime**, s lies below s_{pwp}, and ET is zero.

- In the **soil moisture-limited regime**, s lies between s_{pwp} and s_{fc}, and ET increases roughly linearly with s.

- In the **energy-limited regime**, s lies above s_{fc}, and ET takes on the value of potential evapotranspiration E_p which is determined by available energy rather than soil moisture, meaning that ET stays constant under an increase in s.

While these regimes are a good approximation in most cases, it needs to be noted that different vegetation types modulate the dependence of ET on s. In particular, deep-rooting species found in tropical forest biomes can access moisture in deeper soil-layers, thereby continuing to evaporate substantial amounts of moisture when upper soil layers are already fairly dessicated (Nepstad et al., 1994; Rocha et al., 2004).

Due to the soil moisture dependency of evapotranspiration, the atmospheric moisture availability over land, expressed by the atmospheric water balance in Equation (1), is coupled to the soil moisture balance equation,

$$\frac{\delta s}{\delta t} = \frac{1}{n z_r} \left(P - E - R \right),$$

(3)

where R denotes runoff and nz_r is the product of soil porosity n and hydrologically active depth z_r, both properties of the local soil. In contrast to the atmospheric water balance, precipitation P and evapotranspiration E in the soil moisture balance show up as a moisture source and sink terms, respectively. As mentioned earlier, we can also see from Equation (3) that the existence of runoff, as a pure moisture sink, necessitates a typical excess of terrestrial precipitation relative to evapotranspiration, i.e. $E - P < 0$, if land is to be anything but a dry desert. Hence, the fact that we see abundant vegetation in many parts of the world is a direct consequence of the net transport of atmospheric moisture from ocean to land.

In summary, we have seen in this section that the surface type, being land or ocean, influences moisture availability in the atmosphere broadly in two ways: directly, through the surface control on evaporation/ET, and indirectly, through the influence of the surface on the atmospheric circulation which then facilitates moisture convergence and advection.

2.3 SURFACE CONTROLS ON CONVERSION EFFICIENCY

Conversion efficiency shows up in the water balance equations (1) and (3) as the precipitation rate P which can be expressed by a function of environmental conditions that determine how much precipitation is produced at some location, given the moisture availability in the overlying atmosphere. What controls the conversion efficiency in tropical regions is still a subject of active research and many variables and derived quantities have been identified as important factors, including surface temperature (e.g. Gadgil et al., 1984), humidity (e.g. Raymond and Torres, 1998), wind speed (e.g. Back and Bretherton, 2005), convective available potential energy (e.g. McBride and Frank, 1999; Tompkins, 2001), or moist static energy (e.g. Masunaga and L'Ecuyer, 2014). I will restrict the discussion here to surface temperature and atmospheric humidity as those controls relevant for the studies compiled in this thesis.

A priori, the conversion efficiency can range from producing zero precipitation for a given moisture content in the atmospheric column up to converting all available moisture into precipitation, leaving the column completely dessicated. While the latter case is never observed in reality, not least because of the constant influx of water vapor from neighboring columns and the surface, situations with zero precipitation are common, suggesting nonlinear processes and the existence of thresholds for triggering precipitating convection.

Surface temperature constitutes such a threshold quantity over both land and ocean, even though in somewhat different ways. Over ocean, observations shows that the SST needs to lie above about $26\,°\text{C}$ in order for deep convection to set in (Zhang, 1993). This dependence can be explained by the influence of SST on convective stability (Hu et al., 2023). However, several studies documented that crossing the SST threshold is only a necessary and not a sufficient condition for oceanic precipitation (Gadgil et al., 1984; Graham and Barnett, 1987). Especially for SSTs above $28\,°\text{C}$, other factors such as wind speed, moisture convergence, and vertical velocity often dominate the conversion efficiency and mask the positive influence of SST on convection (Zhang, 1993). Over land, the situation is different in that convection exhibits a strong diurnal cycle, driven by surface temperature changes.

During the night, when surface temperatures are low, convective inhibition builds up and suppresses convection. During the day, surface warming leads to a deepening of the turbulent boundary layer and thereby reduces the convective inhibition. Convection sets in as air parcels from the boundary layer are able to reach the level of free convection above which the release of latent heat from condensation makes the parcels positively buoyant (Chaboureau et al., 2004). Hence, surface temperature plays an active role in triggering convection but just like over ocean, it has a limited influence on the subsequent precipitation yield.

What turns out to be most critical for determining the strength of tropical precipitation, both over land and ocean, is atmospheric humidity, and especially humidity of the lower to mid troposphere (Raymond and Torres, 1998; Derbyshire et al., 2004; Tompkins, 2001; Holloway and Neelin, 2009). Observational studies found a strong relationship between precipitation and column water vapor w, as well as column relative humidity r. The sensitivity of precipitation to w and r shows overall similar characteristics but is less variable throughout the tropics in the case of r. These characteristics are, one the one hand, a threshold or pick-up value of column relative humidity around $r = 0.75$, below which precipitation is suppressed, and on the other hand a strongly nonlinear, monotonic increase of precipitation above this pick-up value (Bretherton et al., 2004; Rushley et al., 2018).

The literature offers various explanations for this so-called moisture-precipitation relationship $P(r)$. The most common theory is that free tropospheric entrainment of environmental air into a convecting plume decreases plume buoyancy if the environment is rather dry, while this detrimental effect on convection is weaker or absent in a moister environment (Tompkins, 2001; Derbyshire et al., 2004; Holloway and Neelin, 2009; Ahmed and Neelin, 2018). Further, convective downdrafts in a moist environment inject moist air into the boundary layer, thereby enhancing convective instability (Tompkins, 2001; Muller et al., 2009). A more theoretical explanation proposed by Peters and Neelin, 2006 is that precipitating convection represents an instance of self-organized criticality in the context of continuous phase transitions. In this framework, surface heating acts as a slow driver of moisture build-up, while buoyancy and precipitation are fast dissipation processes. Together, they keep the system close to a critical value of humidity, identical to the threshold of column relative humidity identified by observational studies. Last, Masunaga, 2012 hypothesized that the moisture-precipitation relationship arises as the statistical sampling of different types of organized convection in various stages of their respective life cycle.

Several papers examined the dependence of $P(r)$ on the underlying surface type, and obtained different findings. Ahmed and Schumacher, 2017 compared the relationship over tropical land and ocean regions, and found a lower pick-up value over land, which the authors explain by the role of enhanced surface warming in triggering convection and the potential influence of orographic forcing as mentioned in section 2.1. Another difference between land and ocean shown by Ahmed and Schumacher, 2017 is that the $P(r)$ curve for land flattens more towards high column relative humidity values than does the curve for ocean. In other words, for very moist columns, it rains less over land than over ocean. Schiro et al., 2020, comparing the relationship between peak precipitation rates from mesoscale convective systems and column water vapor over tropical land and ocean, did not find the same land-ocean differences but rather strikingly similar behavior over the two

surface types, with the exception of the Maritime Continent, where the relationship shows an earlier pick-up value and weaker precipitation at high humidities, consistent with the findings by Ahmed and Schumacher, 2017. Further support for a dependence of $P(r)$ on surface type comes from a study by Bergemann and Jakob, 2016, who compared oceanic with coastal and inland precipitation in the tropics. However, all evidence taken together, the exact nature of this dependence remains ambiguous.

For my two-ingredient conceptual picture of precipitation, the dependence of conversion efficiency on atmospheric humidity is especially interesting because it means that moisture availability is not only a passive ingredient, setting an upper limit to the precipitation amount, but also plays an active role in setting the conversion efficiency. Moisture availability and conversion efficiency are, thus, connected with each other through a negative feedback: The moister the atmospheric column, the more moisture will be removed from the column by precipitation. Mathematically, this coupling is implemented in the atmospheric water balance equation (1) by expressing the precipitation term by a function of column water vapor, $P(w)$.

In the next chapter, I present a summary of my first study, in which I developed a simple box model of the tropical water cycle based on the water balance equations (1) and (3), with the aim of better understanding the drivers and constraints of the tropical precipitation ratio χ between land and ocean.

SUMMARY OF STUDY 1 : CONSTRAINTS ON THE PARTITIONING OF TROPICAL PRECIPITATION DERIVED FROM A WATER BALANCE BOX MODEL

Modern satellite observations make it easy to quantify the climatological partitioning of tropical precipitation between land and ocean, for example in terms of the precipitation ratio χ. However, it is largely unknown what controls and potentially constrains this partitioning. The first study of this dissertation, included in Appendix A, aims to build a better understanding of the fundamental controls and constraints on χ using a highly simplified box model of the tropical land-ocean-atmosphere system governed by water balance equations. Rather than striving for realism, the idea is to use a comprehensible model to develop an intuition for basic physical interactions, to explore constraints arising from the fundamental law of water conservation, and to formulate hypotheses about the real world that can then be tested with more complex models or observational datasets.

In particular, this study addresses the following research questions:

1. **Do large-scale constraints on the tropical precipitation partitioning arise from the condition of water balance?**

2. **Which are the key parameters controlling the value of the tropical precipitation ratio χ?**

3. **Which physical processes may be responsible for precipitation enhancement over tropical land, as found in observations?**

In the following, I introduce the developed conceptual model and summarize the key findings obtained from a parameter sensitivity analysis of the model's equilibrium solution.

3.1 A CONCEPTUAL BOX MODEL BASED ON WATER BALANCE EQUATIONS

It is well-established that water is a conserved quantity in the Earth system, and that land, ocean, and atmosphere form a coupled system of moisture reservoirs (Peixóto and Oort, 1983). To first order, we may assume that water conservation also holds within the tropics. This allows us to use water balance equations to derive a highly simplified box model of the tropical water cycle. This model consists of four boxes, representing land and ocean as well as the atmospheric volumes overlying land and ocean, respectively. The modelled moisture fluxes between these boxes are evaporation/evapotranspiration E, precipitation P, atmospheric advection A, and runoff R from land to ocean. All fluxes have units mm day^{-1}. A schematic of the box model is shown in Figure 1, with black arrows representing the moisture fluxes.

The methodology to answer the research questions posed above consists of three steps: First, I developed the conceptual box model by coupling water balance equations, describing the time evolution of the boxes' moisture content, and parameterizing the water balance

components by empirical or theoretically derived expressions. Second, I randomly sampled the parameter space, spanned by a total of 11 model parameters, such as soil properties, horizontal wind speed, or the model's land fraction. For each combination of parameter values, I computed the equilibrium solution to the model equations as well as the corresponding equilibrium value of χ. Third, I analyzed the obtained equilibrium solutions with respect to emerging constraints on χ, and tested the sensitivity of χ to parameter choices.

The time evolution of the boxes' moisture content, quantified by mean integrated water vapor path w in mm in the case of atmospheric boxes, and relative soil moisture saturation s in the case of land, is described by coupled water balance equations, where a sink term for one box appears as a source term for another box. The model equations read

$$\frac{ds}{dt} = \frac{1}{nz_r} \left[P(w_\ell) - R(s, w_\ell) - E_\ell(s) \right] \tag{4}$$

$$\frac{dw_\ell}{dt} = E_\ell(s) - P(w_\ell) + A_\ell(w_\ell, w_o) \tag{5}$$

$$\frac{dw_o}{dt} = E_o - P(w_o) + A_o(w_\ell, w_o). \tag{6}$$

The subscripts ℓ and o refer to land and ocean, respectively, and soil porosity n as well as hydrologically active depth z_r in mm are model parameters. A fourth prognostic equation for the oceanic moisture content is omitted because the ocean is saturated at all times.

Because the model assumes a constant temperature throughout the domain, the ocean evaporation is prescribed by a constant parameter, $E_o = e_o$. In contrast, evapotranspiration from the land surface is parameterized as a nonlinear, monotonically increasing function of s, following the qualitative picture of the three soil moisture regimes separated by permanent wilting point and field capacity as introduced in Chapter 2. Following the approach by Rodriguez-Iturbe et al., 1991, I parameterize runoff as the soil moisture-dependent fraction $R_f(s)$ of precipitation that does not infiltrate into the soil but gets removed by surface or subsurface currents. The wetter the soil, the more precipitation is channeled into runoff. Precipitation is parameterized by the exponential moisture-precipitation relationship formulated by Bretherton et al., 2004. Note that Bretherton et al., 2004 expressed precipitation as a function of column relative humidity, $r = w/w_{sat}$. The box model uses w as a variable because column saturation vapor path w_{sat} is treated as a model parameter, independent of the underlying surface. Lateral transport of moisture in the atmosphere is reduced to advection due to the simplifying assumption of a constant background wind speed u in $\mathrm{mm\,day^{-1}}$. The result is a down-gradient net transport of water vapor. After simplifying the atmospheric moisture budget from Equation (1) by applying the box model assumptions, advection becomes a linearly increasing function of the moisture difference between the two atmospheric boxes. The slope of this function is determined by the atmospheric transport parameter τ in $\mathrm{day^{-1}}$, which in turn depends on wind speed and total domain length, as well as the box fraction, i.e. land fraction α for the land box and ocean fraction $(1 - \alpha)$ for the ocean box.

Figure 2 displays exemplary parametrization curves for evapotranspiration (Fig. 2a), runoff fraction (Fig. 2b), precipitation (Fig. 2c) and land advection (Fig. 2d) together with their mathematical expressions. The curves differ in the chosen parameter values which
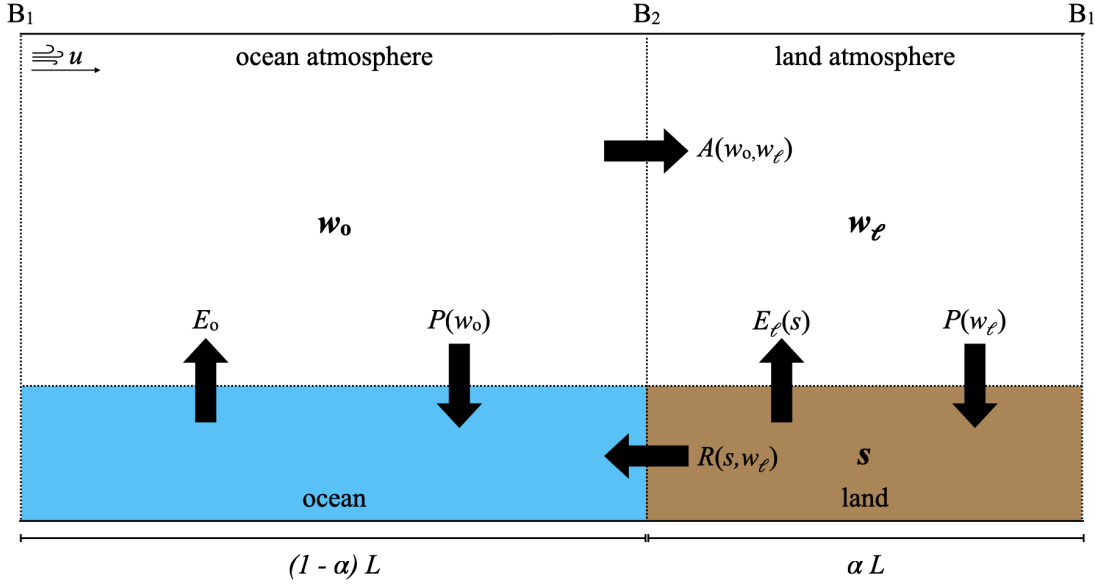
Figure 1: Box model sketch of a land-ocean-atmosphere system, coupled by mean moisture fluxes shown as black arrows. All fluxes other than ocean evaporation E_o, which is a constant model parameter, are functions of mean relative soil moisture saturation s, and/or the atmospheric mean water vapor paths over land and ocean, w_ℓ and w_o, respectively. The spatial extent of the boxes is set by the total domain length L and land fraction α. Lateral moisture transport by advection A is driven by a constant horizontal mean wind speed u.

were taken from the uniform parameter ranges provided by Table 1 in Appendix A. For the black curves, serving as a benchmark, parameter values were set to their respective mean value. Colored lines represent curves for which one parameter was set to its minimum/maximum value, while the other parameter(s) were kept at their mean value. A comparison of the colored lines with the black benchmark gives a feeling for the qualitative dependence of the parametrization curves on the individual parameters. Note, however, that the sensitivity analysis of equilibrium solutions presented in this study involved a simultaneous variation of all model parameters, rather than changing parameters one by one. Parameter interactions can, thus, lead to a wider spread of curves than displayed in Figure 2.

3.2 WATER BALANCE CONSTRAINTS ON χ_{eq}

To investigate the model behavior and potential emerging constraints on χ arising from the condition of water balance, I computed the equilibrium solution to the model equations (4) to (6) for 100 000 different combinations of parameter values, randomly chosen from the ranges listed in Table 1. The solutions each consist of a set of equilibrium values for the moisture variables, $\{w_{o,eq}, w_{\ell,eq}, s_{eq}\}$, and the equilibrium χ value is computed as

$$\chi_{eq} = \frac{P(w_{\ell,eq})}{P(w_{o,eq})}. \tag{7}$$
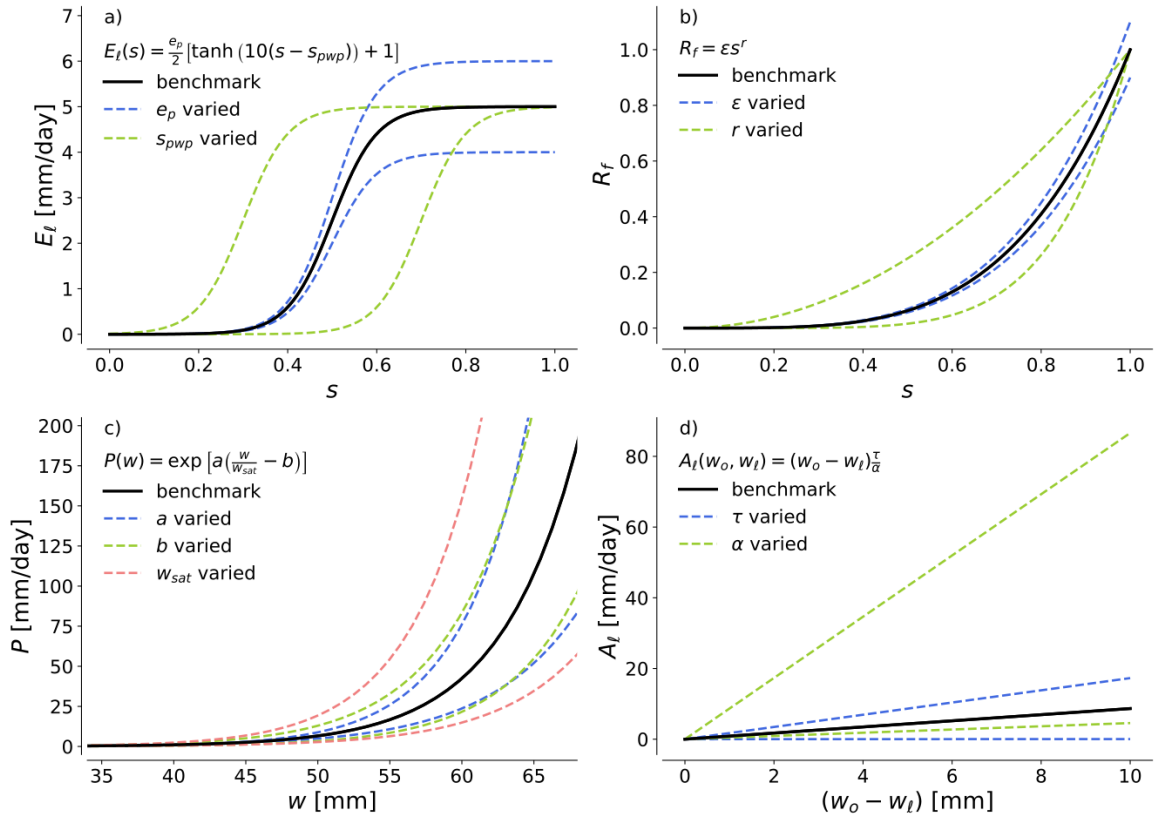
Figure 2: Exemplary curves of the moisture flux parametrizations employed by the conceptual box model. The panels show a) evapotranspiration E_ℓ, b) runoff fraction R_f, c) precipitation P, and d) land advection A_ℓ. For the black benchmark curves, all parameters were set to their mean value, while blue, green, and red dashed curves represent cases for which one parameter was changed and set once to its minimum vaue and once to its maximum value.

Probability density functions (pdf) of the obtained equilibrium moisture states are shown in Figure 3. One can see from Figure 3a that the equilibrium state of the land box spans a wide range of soil moisture saturation values. However, it is more instructive to interpret soil states with respect to their location on the evapotranspiration curve. For instance, the green curves in Figure 2a showcase that a value of $s = 0.5$ could lie in the energy-limited regime of an $E_\ell(s)$-curve for which s_{pwp} was set to its minimum value, or in the very dry regime below the permanent wilting point if s_{pwp} was set to its maximum value – two physically very distinct scenarios. Figure 3b therefore shows the position of the equilibrium soil moisture values relative to the three soil moisture regimes, visually separated by vertical dashed lines. This visualization reveals that soil moisture mostly equilibrates to values in the transition range between the permanent wilting point and the field capacity. Similarly, the atmospheric boxes tend to equilibrate to water vapor path values in the range where the moisture-precipitation relationship begins to steeply increase with increasing w (compare Figure 3c to Figure 2c). Even though a direct comparison is inapt, note that the w_{eq} values of the conceptual model span a range of values commonly found in the real tropics (e.g. Mapes et al., 2018).

Figure 3d shows the pdf of the equilibrium precipitation ratio which exhibits a narrow spike near $\chi_{eq} = 1$. What is striking, except for the spike, is the fact that no values above $\chi_{eq} = 1$ exist. Under the condition of water balance, χ_{eq}, thus, seems to be constrained to a range between 0, where land precipitation is zero, and 1, where land and ocean precipitation rates are the same. The lower bound is set by scenarios of a very large land fraction near $\alpha = 1$. In such cases, the moisture exported out of the tiny ocean atmosphere gets distributed over a large land atmosphere where it sustains a moisture value $w_{\ell,eq}$ corresponding to a near-zero precipitation rate. The upper bound of $\chi_{eq} = 1$ is independent of the parameter choices and instead a fundamental consequence of the existence of runoff combined with some of the model assumptions: Any soil with nonzero soil moisture saturation looses some amount of moisture to runoff which needs to be compensated by an equally large atmospheric flow of moisture from ocean to land in order to reach equilibrium. Advection can only facilitate this compensating moisture flow if the ocean atmosphere is moister than the land atmosphere, which poses the equilibrium condition that $w_{o,eq} > w_{\ell,eq}$. Because the model assumes that the surface type, being land or ocean, does not influence the monotonically increasing relationship between atmospheric moisture and precipitation, meaning $P_\ell(w) = P_o(w)$, the moister ocean atmosphere necessarily yields stronger rain rates than the land atmosphere. Consequently, χ_{eq} stays strictly below 1.

3.3 PARAMETER SENSITIVITY OF χ_{eq}

I evaluated the sensitivity of χ_{eq} to variations in the different model parameters by computing the mutual information index $I_{MI}(\chi_{eq}, p_i)$ for χ_{eq} with each individual parameter p_i (see Eq. (21) in Appendix A for a definition of I_{MI}). The mutual information index is essentially a measure of how much knowing the value of a certain parameter reduces the uncertainty about the value of χ_{eq}. The higher the index, the higher the sensitivity of χ_{eq}
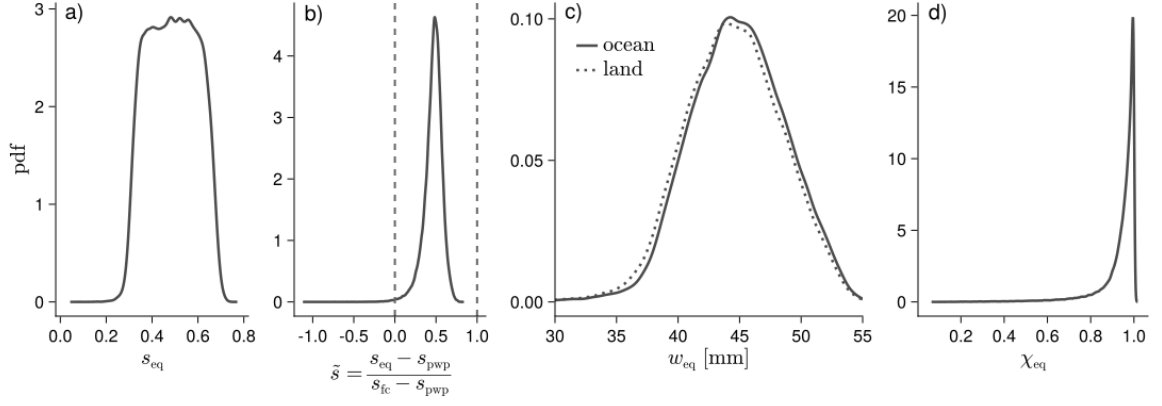
Figure 3: Pdfs of equilibrium values of the box model's state variables. The panels show a) relative soil moisture saturation, b) same as a) but rescaled such that the permanent wilting point and field capacity values, marking the beginning and end of the moisture-limited transition regime of E_ℓ, coincide with 0.0 and 1.0 (dashed lines), respectively, and c) water vapor path of the land and ocean atmospheres (tails, representing less than 0.38 % of the simulations, cut for better visibility of land-ocean differences). Panel d shows the pdf of computed equilibrium χ values.

to that parameter.

It turns out that the atmospheric transport parameter τ, quantifying the ratio between wind speed and full domain length, is by far the most sensitive parameter with a mutual information index of $I_{MI}(\chi_{eq}, \tau) = 359$, followed by the two soil parameters permanent wilting point, $I_{MI}(\chi_{eq}, s_{pwp}) = 61$, and runoff exponent, $I_{MI}(\chi_{eq}, r) = 50$, as well as land fraction, $I_{MI}(\chi_{eq}, \alpha) = 45$. All other parameters have a negligible control on χ_{eq}. Figure 4 displays scatter plots of χ_{eq} values against the values of τ and α, with white lines denoting the χ_{eq}-mean along the respective parameter.

The high sensitivity of χ_{eq} to τ can be seen from the strongly nonlinear dependence shown in the left panel of Figure 4. In particular, the spread of χ_{eq} values around the mean curve strongly decreases along increasing τ. This can be understood from the way in which τ impacts the mixing of moisture between the two atmospheric boxes: The larger τ, the stronger the mixing and the harder for the two atmospheric boxes to sustain large moisture differences $\Delta w = (w_o - w_\ell)$ which are associated with low values of χ_{eq}. In contrast, when τ is small, large moisture differences are possible and the value of χ_{eq} is mostly set by other model parameters. The influence of τ can be summarized as setting a limit to the magnitude of Δw, and thereby to the lower bound of χ_{eq}.

It can also be seen from the left panel of Figure 4 that the upper limit of χ_{eq} is one, independent of the value of τ. This upper limit can be attributed to the influence of variations in the land fraction α. The right panel of Figure 4 shows the scatter plot of χ_{eq} versus α which is characterized by a large spread of χ_{eq} throughout most of the range of α, except near the end points of its range, where $\alpha \to 0$ and $\alpha \to 1$. These end points correspond to a situation in which either the land or ocean box is tiny and the respective other box is huge. In these cases, atmospheric export or import of moisture from or to the small box is highly efficient and it becomes impossible to sustain a large Δw which is the reason why χ_{eq} goes
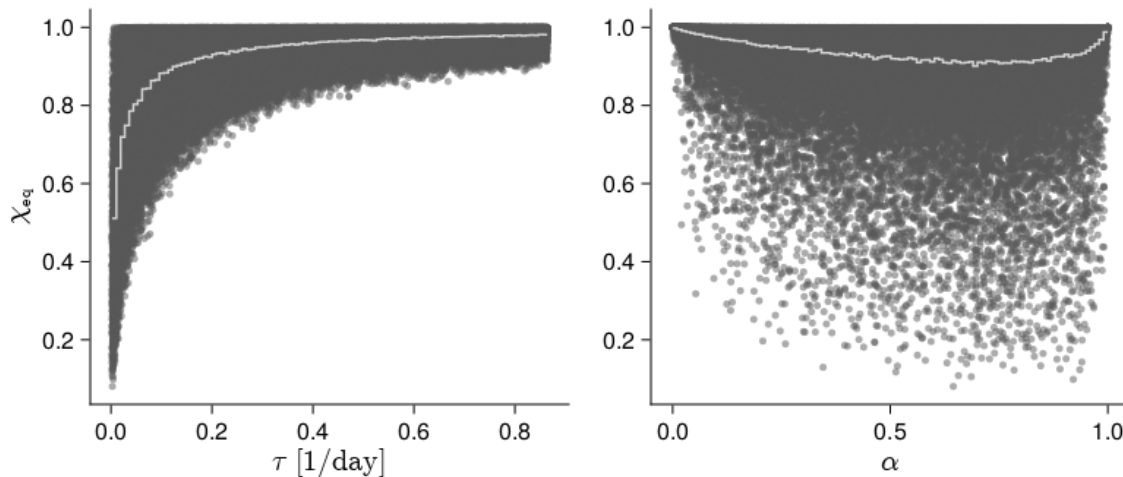
Figure 4: Equilibrium precipitation ratio χ_{eq} plotted against atmospheric transport parameter τ (left panel), and land fraction α (right panel). White lines show the χ mean values, computed for 100 bins along the parameter axis.

to 1 in these limits. In these two scenarios, the overall moisture conditions in the system get dictated by the large box. If the ocean box is large, all boxes attain a moist equilibrium state, and if the land box is large, all boxes attain a dry equilibrium state because the tiny ocean surface can only supply a small amount of moisture to the hydrological cycle.

Scatter plots for s_{pwp} and r (not shown) exhibit a similarly large spread in χ_{eq} as does the χ_{eq}-α plot, but their mean curves show an approximately linear decrease in the case of s_{pwp}, and increase in the case of r. A detailed analysis of the mechanisms through which these soil parameters influence χ_{eq} reveals that it is essentially their effect on advection or, more specifically, Δw which matters for setting χ_{eq}.

3.4 PRECIPITATION ENHANCEMENT OVER LAND

We are now left with the question of whether the box model can help formulate hypotheses for how precipitation enhancement over land, as seen in observations, may be caused. Unlike in the real world, where precipitation enhancement over land is indicated by values of χ larger than 0.86 due to the geometry of tropical land masses (HS22), precipitation enhancement over land in the box model means a χ value larger than one. As discussed before, the box model only yields χ_{eq} values smaller than one and, hence, it does not show any precipitation enhancement over land. I can therefore only indirectly reason about mechanisms leading to such precipitation enhancement by examining the physical processes not included in the box model. Based on these considerations, I formulate four hypotheses for how χ_{eq} could become larger than one in the simple box model.

First, the precipitation relationship $P(w)$ might, in reality, be influenced by surface properties and systematically differ over land, compared to over ocean, as suggested by Ahmed and Schumacher, 2017 and Bergemann and Jakob, 2016. If these differences manifest in a steeper $P(w)$ curve over land, the ocean atmosphere could still equilibrate to a moister state but yield a lower precipitation rate than the land atmosphere. As a proof of principle,

I modified the precipitation relationship by setting the b parameter values over land to a value just 0.1 % smaller than the value over ocean, and recomputed the equilibrium states. Even with only such a small modification of $P(w)$, about 20 % of the model runs yielded a χ_{eq} value larger than 1.

Second, land and ocean, especially on scales as large as the tropics, show a wide variety of climatic conditions and are therefore physically not well-described by a mean moisture state. Given the nonlinearity of $P(w)$, mean precipitation computed from distinct spatial humidity distributions over land and ocean could be very different from precipitation computed from the humidity mean values. Spatial heterogeneity of w cannot be represented in the simple box model but may be the decisive factor in producing real world precipitation enhancement over land.

Third, the assumption of constant temperature and background wind speed eliminates moisture convergence and thereby reduces lateral atmospheric transport to down-gradient moisture advection. In reality, diurnal and seasonal temperature gradients between land and ocean can drive circulations on various scales, ranging from land-sea breezes all the way to monsoon systems and the Walker circulation, which carry atmospheric moisture landward. While the real tropical ocean atmosphere is moister than the tropical land atmosphere on average, suggesting that the assumption of a down-gradient moisture transport is justified, there may exist regions and time periods with higher w values over land compared to the adjacent ocean. A representation of convergence and potentially up-gradient moisture transport in the model could, thus, lead to equilibrium solutions with $\chi_{eq} > 1$.

Last, the box model as a representation of a closed system, appropriate for large spatial scales, does not allow for precipitation enhancement over land. But what if we would open the box model and let it represent a smaller system, for instance an island surrounded by ocean? In this case, the horizontal wind speed would not represent some theoretical mean flow but rather actual physical wind, blowing over the model domain as part of a large-scale circulation. We tested this scenario with a configuration of one land box in between two ocean boxes. The "openness" of this configuration is represented by an additional model parameter w_0 for the water vapor path at the windward model boundary (see Figure 21 in Appendix A for a sketch of the open model). A sensitivity analysis of the model's equilibrium states, analogous to the one performed for the closed model, reveals that precipitation can be enhanced over land if the land fraction is sufficiently small, and the w_0 value at the windward boundary is sufficiently high. Under these conditions, the ocean atmosphere windward of the land still equilibrates to a moister state than the land atmosphere, but the second ocean may be dry enough to lead to lower ocean than land precipitation, when averaged over both ocean boxes.

SUMMARY OF STUDY 2: PRECIPITATION ENHANCEMENT OVER TROPICAL LAND THROUGH THE LENS OF THE MOISTURE-PRECIPITATION RELATIONSHIP

In the previous chapter, I hypothesized that precipitation enhancement over tropical land, as diagnosed from χ values larger than 0.86 in observations (HS22), may be explained by surface controls on the relationship between precipitation and column relative humidity $P(r)$. Land-ocean differences in $P(r)$ were indeed documented by Ahmed and Schumacher, 2017 who found that the $P(r)$ curve over land picks up at a lower r value than over ocean but that it then flattens more towards high r. However, whether these differences are responsible for lifting χ above 0.86 can only be answered by also considering land-ocean differences in the humidity distribution, $pdf(r)$. Investigating surface controls on $P(r)$ and $pdf(r)$ based on more realistic data, and determining their individual contribution to precipitation enhancement over tropical land is the overarching aim of this second study. This aim can be divided into the following research questions:

1. **How much of the spatial and temporal variability of $P(r)$ do we need to account for in order to reconstruct $\chi(t)$ from $P(r)$ and $pdf(r)$?**

2. **Do land-ocean differences in $P(r)$ explain the precipitation enhancement over tropical land?**

3. **Which values of r are responsible for the precipitation enhancement?**

4.1 CONSTRUCTING $\chi(t)$ FROM $P(r)$ AND $pdf(r)$

The first question reflects the fact that the shape of $P(r)$ might be controlled by many factors other than surface type, and that surface type, as a controlling factor, might not be the significant one for precipitation partitioning. A priori, it is therefore not clear, how much we need to know about the variability of $P(r)$ in space and time to correctly reproduce the statistical properties of tropical land and ocean precipitation, and thereby $\chi(t)$. In the theoretical limit that we know how r maps to P at each point in space and time, $\chi(t)$ can be reconstructed perfectly but we would not learn a thing. To answer the first research question, I therefore take a top-down and step-wise approach in which I compute reconstructions of $\chi(t)$ from fits of the $P(r)$ relationship that reflect an increasingly detailed spatial and temporal knowledge of $P(r)$. For instance, as the first step of this approach, I use one time-independent $P(r)$ relationship, fitted to data from the full tropics (no land/ocean distinction), and assess whether it can correctly reproduce $\chi(t)$.

The data I use throughout this study are ten years of daily P and r data (1981–1990) from the ERA5 reanalysis product (Hersbach et al., 2018b; Hersbach et al., 2018a). In this period, the ERA5 mean seasonal cycle of $\chi(t)$ is close to observations, and generally lies above 0.86, indicating precipitation enhancement over land. In each step of the approach described above, I derive a functional form of $P(r)$ by sorting the selected pairs of (P, r)

by ascending r, and then averaging the data within bins of length 0.01 along r. The fit is then computed as the piecewise linear function to the bin-mean precipitation and humidity data. With the obtained fit at hand, I reconstruct daily precipitation fields by plugging the ERA5 daily humidity fields into $P(r)$, and compute the reconstructed $\chi_{rec}(t)$ from these reconstructed precipitation fields. Whether the spatial and temporal knowledge of $P(r)$ is sufficient to reproduce $\chi(t)$ is evaluated by comparing statistical properties of $\chi_{rec}(t)$ to these same properties of the benchmark $\chi_{bm}(t)$ which is directly computed from the ERA5 precipitation fields. The statistical properties I use are the 10-year mean seasonal cycle and inter-annual variability of $\chi(t)$, quantified by the interquartile range.

Figure 5 summarizes my findings for the first research question: As a first step, I compute a fit of $P(r)$ to all tropical pairs (P, r), displayed by the green line in Figure 5a. The precipitation ratio, constructed from this fit, is shown in Figure 5b in blue, and the ERA5 benchmark is shown in black. The solid lines represent the mean seasonal cycle, and shading indicates the interquartile range of monthly mean values over the 10 years. The full tropical fit clearly misrepresents both the magnitude and seasonality of $\chi_{bm}(t)$, especially in June, July, and August (JJA). In a second step, I therefore separate land and ocean pairs, (P_ℓ, r_ℓ) and (P_o, r_o), and compute a tropical land and ocean fit function, $P_\ell(r)$ and $P_o(r)$, respectively. The obtained fit functions are shown in Figure 5c along with the corresponding reconstruction of $\chi(t)$ in Fig. 5d. Accounting for differences in $P(r)$ based on surface type, greatly improves the magnitude of the seasonal cycle such that the overall 10-year mean value of benchmark and reconstruction are identical. However, the seasonality of χ_{rec} and χ_{bm} is still distinct, pointing towards a time-dependence of either or both $P_\ell(r)$ and $P_o(r)$. This is tested in a third step, where I compute fit functions for both land and ocean, and each month of the year, $P_{\ell,m}(r)$ and $P_{o,m}(r)$. The fit functions and the corresponding reconstruction, are shown in Figure 5e and f, respectively. By construction, the monthly $\chi_{rec}(t)$ and $\chi_{bm}(t)$ mean values now lie on top of each other. Some differences remain in the interquartile range, but I consider the agreement to be good enough for the purpose of this investigation. Looking at the fit functions in Fig. 5e, it becomes clear that the seasonal variability of $P_{\ell,m}(r)$ is stronger than the one of $P_{o,m}(r)$ in the range of intermediate and high r values where precipitation rates are significantly nonzero. Nevertheless, a more detailed investigation (discussed in Appendix B) reveals that also the oceanic variability needs to be accounted for in order to completely remove the mismatch between benchmark and reconstruction mean curves in Fig. 5d.

In summary, the surface type, being land or ocean, proofed to be a significant control on $P(r)$, relevant for correctly reconstructing the precipitation partitioning between tropical land and ocean. However, one further needs to account for the seasonal variability of $P_{\ell,m}(r)$ and $P_{o,m}(r)$ to capture the basic properties of $\chi(t)$ such as its mean seasonal cycle.

4.2 DO LAND-OCEAN DIFFERENCES IN $P(r)$ EXPLAIN PRECIPITATION ENHANCEMENT OVER TROPICAL LAND?

To answer the second research question of whether land-ocean differences in $P(r)$ can explain precipitation enhancement over tropical land, it is important to note that there are two influences on $\chi(t)$ in any given month: land-ocean differences in the moisture-precipitation relationship $P(r)$, and land-ocean differences in the humidity distribution $pdf(r)$. These two
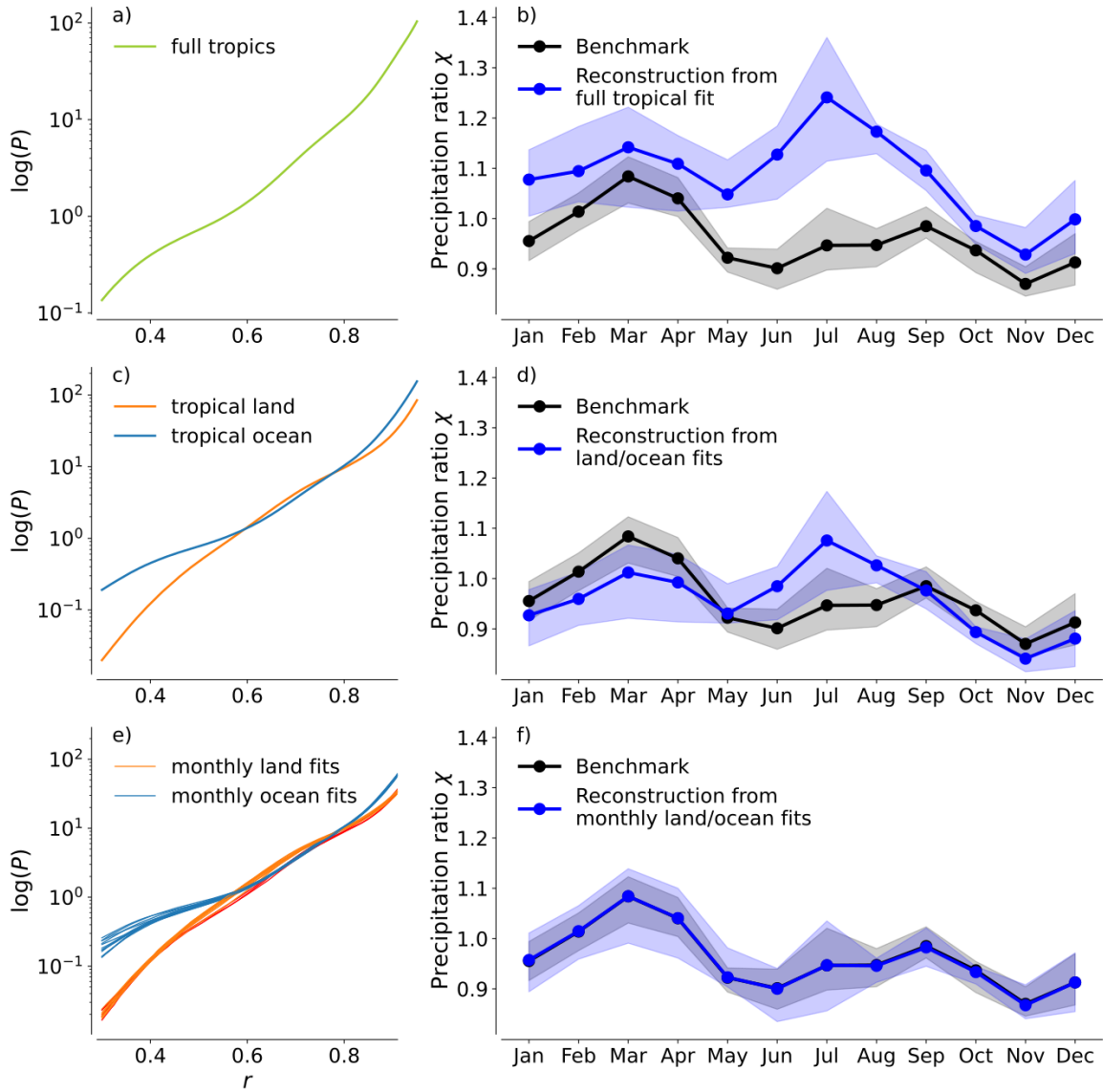
Figure 5: Empirical fits of precipitation P as a function of column relative humidity r, computed from different spatial and temporal subsets of tropical daily (P, r) data (panels a, c, and e), together with the respective reconstruction of precipitation ratio χ (blue curves in panels b, d, and f), based on the fitted relationships. The black benchmark curves were computed from ERA5 precipitation directly. Shading denotes the interquartile range of monthly mean values of different years. Red lines in panel e) highlight the land relationships $P_{m,\ell}(r)$ for June, July, and August as the only months that do not exhibit the 'bump'.

factors may act alone or in tandem to produce precipitation enhancement over land.

To disentangle those influences, let us first return to the curves of $P_{\ell,m}(r)$ and $P_{o,m}(r)$ displayed in Figure 5e. For land-ocean differences in $P(r)$ to be responsible for precipitation enhancement over land, $P_{\ell,m}(r)$ needs to be larger than $P_{o,m}(r)$ in at least some range of r. The three red lines, representing $P_{\ell,m}(r)$ in JJA, are singled out because they do not have any such range. Over the full range of r, these curves are either smaller or equal to $P_{o,m}(r)$. Thus, we can already conclude that precipitation enhancement in boreal summer is not caused by land-ocean differences in $P(r)$. Other months exhibit a range at intermediate values of r, where $P_{\ell,m}(r) > P_{o,m}(r)$. I refer to this range as the 'bump'.

In order to investigate whether land-ocean differences in $P(r)$ are responsible for χ values above 0.86, I conduct two sensitivity experiments: First, I test the effect of all land-ocean differences in $P(r)$ together by using the ocean fit functions, $P_{o,m}(r)$, to reconstruct precipitation over both land and ocean. The idea behind this experiment is that the resulting reconstructed $\chi_{rec}(t)$ should lie below 0.86 if the modification of $P(r)$ by the land surface, which is here removed, causes terrestrial precipitation enhancement. Figure 6a shows the reconstruction from this first sensitivity experiment together with the ERA5 benchmark and a red solid line indicating the threshold of precipitation enhancement over land. Much like the reconstruction from the full tropical fit in Figure 5b, the reconstruction here strongly overestimates $\chi_{bm}(t)$ which is not surprising given that the ocean is expected to leave a strong imprint on the full tropical fit due to its large spatial extent. That the reconstructed precipitation ratio lies not only above 0.86 but even above the benchmark proofs that all land-ocean differences in $P(r)$ together are not responsible for precipitation enhancement over tropical land, and that they even act to *disfavor* precipitation over land. In other words, even if there were no differences between land and ocean in $P(r)$, the land-ocean differences in $pdf(r)$, which we will examine in the next section, would still cause precipitation enhancement over land.

What is not yet clear from the first sensitivity experiment is the role of the 'bump', as the only range of r in which land-ocean differences in $P(r)$ support precipitation enhancement over land. Is the 'bump' required for keeping $\chi(t)$ above 0.86? To test this, I conduct a second experiment where I reconstruct ocean precipitation with the ocean relationships $P_{o,m}(r)$, and land precipitation with modified land relationships, $\tilde{P}_{\ell,m}(r)$. The modification consists of a removal of the 'bump' by setting $\tilde{P}_{\ell,m}(r) = P_{o,m}(r)$ in the range, where formerly $P_{\ell,m}(r) > P_{o,m}(r)$. The obtained reconstruction of $\chi(t)$ is shown in Figure 6b. Even without the 'bump', precipitation remains enhanced over land in all months except November, in which case precipitation enhancement was weakest to begin with.

Overall, my investigation demonstrated that land-ocean differences in $P(r)$ are not responsible for precipitation enhancement over tropical land. The initial hypothesis, inspired by the box model study described in Chapter 3, can therefore be refuted.
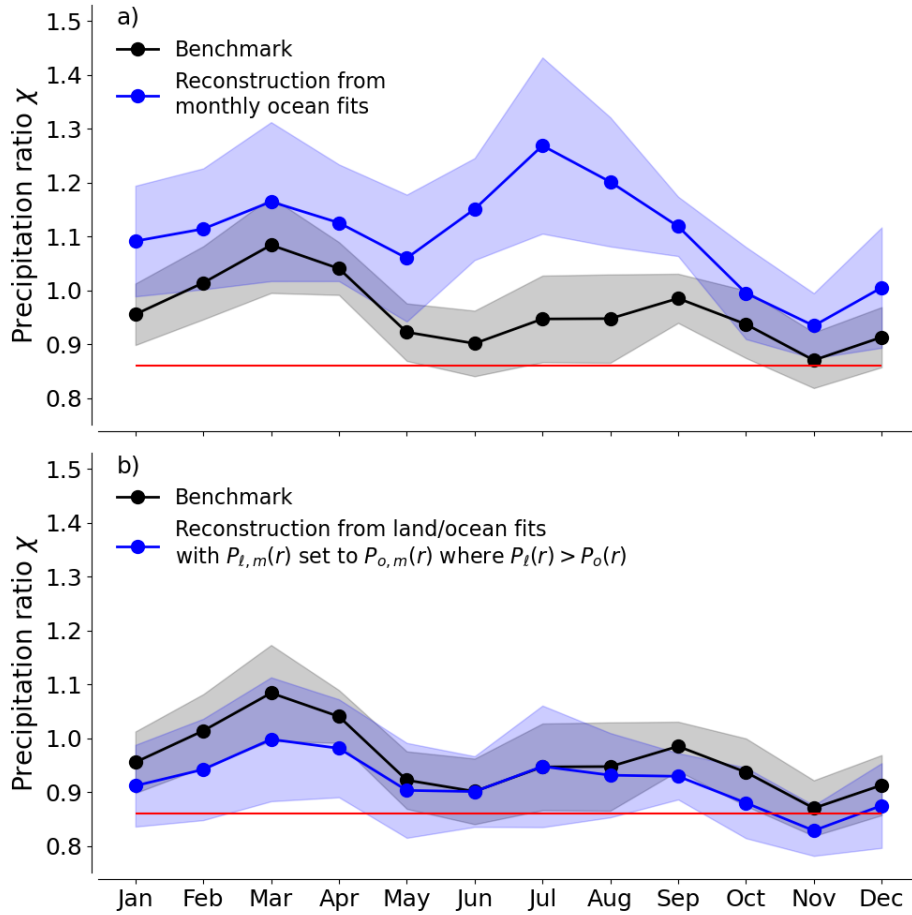
Figure 6: Reconstructions of χ from sensitivity experiments compared with the benchmark (lines and shading analogous to Fig. 5). Panel a: Reconstruction from oceanic relationship $P_{o,m}(r)$, applied to both land and ocean grid cells. Panel b: Reconstruction for which ocean precipitation was computed from $P_{o,m}(r)$, and land precipitation was computed from a modified land relationship which was set to $P_{o,m}(r)$ in the range where $P_{\ell,m}(r) > P_{o,m}(r)$, effectively removing the 'bump'. Red lines show the threshold for precipitation enhancement over land.

4.3 IDENTIFYING THE HUMIDITY VALUES ASSOCIATED WITH PRECIPITATION ENHANCEMENT OVER LAND

Since the precipitation enhancement is not explained by land-ocean differences in $P(r)$, it must be caused by land-ocean differences in $pdf(r)$. To understand the influence of the humidity distributions in more detail, it is the goal of this section to assess the differences in $pdf(r)$ between land and ocean, and to identify the parts of the humidity distributions, i.e. the ranges of r, which are key for precipitation enhancement over land.

The second row of Figure 7 displays land and ocean humidity distributions for three exemplary months, computed from all 10 years of data. In all months, the humidity distribution over land shows a stronger bimodality than the distribution over ocean. While bimodality is also seen in the ocean distribution, the probability of both very dry and very wet columns is higher over land. I chose March, July, and November because they represent three different combinations of distinctive features in the land-ocean differences of $P(r)$ and $pdf(r)$: March and November exhibit the 'bump' in $P(r)$, while July does not, and March and July exhibit a pronounced tail of the land humidity distribution towards the highest values of r, while November does not.

Considering the very low precipitation rates for small values of r, we can already guess that it will be the enhanced tail of $pdf(r)$ over land towards high r values which facilitates the precipitation enhancement over tropical land, despite the fact that land-ocean differences in $P(r)$, shown in the top row of Figure 7, penalize land precipitation in this range. To formally test this expectation, it is convenient to recast the 10-year mean precipitation ratio $\chi_{mean,m}$ for month m in terms of the land and ocean moisture-precipitation relationships, $P_{\ell,m}(r)$ and $P_{o,m}(r)$, and humidity distributions, $pdf_{\ell,m}(r)$ and $pdf_{o,m}(r)$,

$$\chi_{mean,m} = \frac{\int_0^{r_e} P_{\ell,m}(r)\,pdf_{\ell,m}(r)dr}{\int_0^1 P_{o,m}(r)\,pdf_{o,m}(r)dr} > 0.86, \tag{8}$$

with $r_e = 1$. The inequality in Equation (8) holds for precipitation enhancement over tropical land.

The contribution of different values of r to precipitation enhancement over land can be evaluated by modifying Equation (8) in two steps: First, I express $pdf_{\ell,m}(r)$ and $pdf_{o,m}(r)$ in terms of the fraction of the land and ocean domain that is occupied by a given value of r. Second, I rewrite the integrals in Equation (8) as the total accumulated rainfall, $P_{\ell,cum}(r_e)$ and $P_{o,cum}(r_e)$, where the accumulation is performed from $r = 0$ to the variable end point r_e. With these modifications (see section B.4.2 in Appendix B for more details), Equation (8) can be reformulated to

$$\frac{P_{\ell,cum}(r_e)}{\alpha} - 0.86\frac{P_{o,cum}(r_e)}{1 - \alpha} > 0, \tag{9}$$

and one can identify humidity values that contribute to precipitation enhancement over land as those values of r_e at which the left hand side (LHS) of Equation (9) increases.
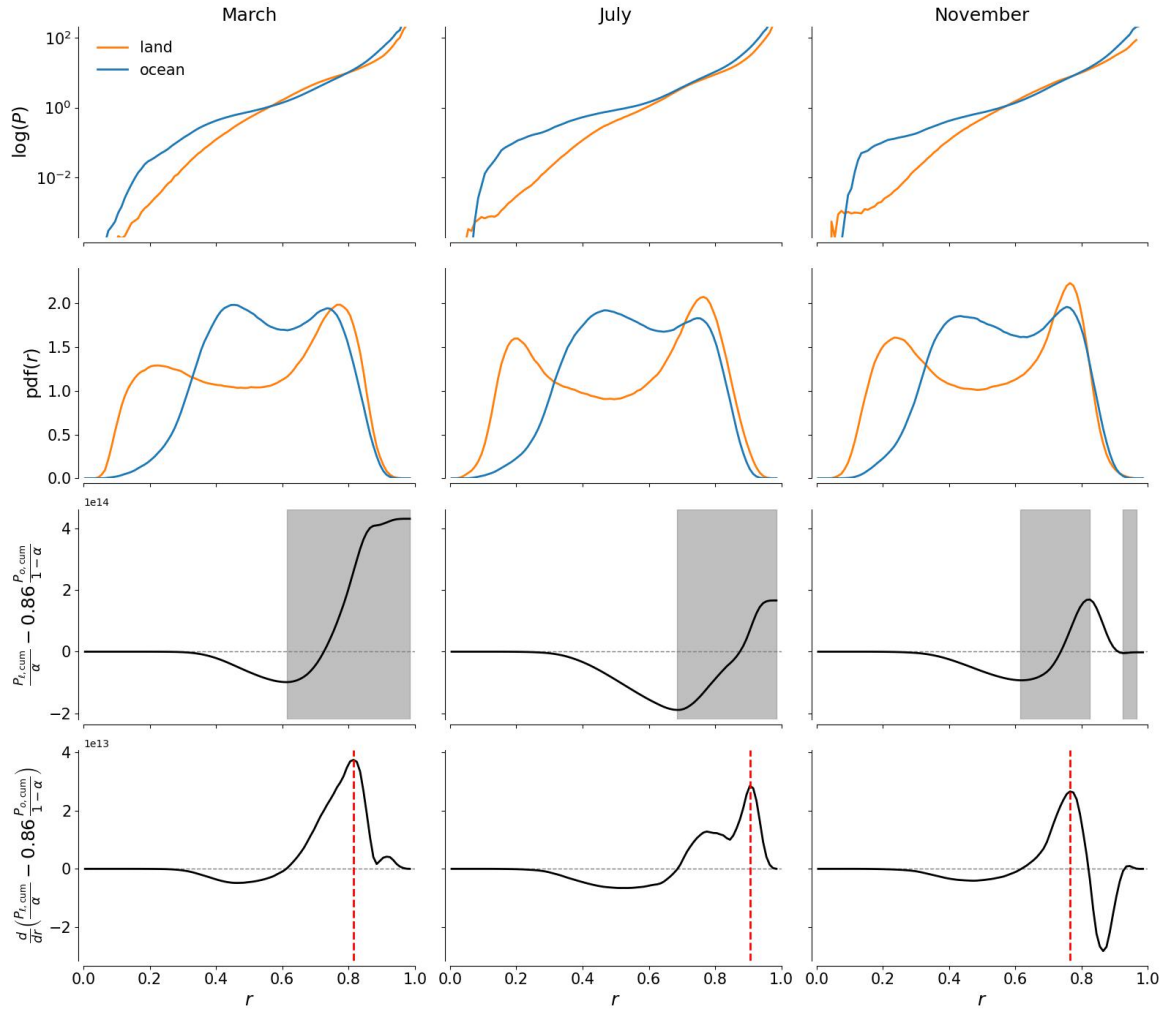
Figure 7: Land and ocean moisture-precipitation relationships (top row) and pdfs of column relative humidity (second row) for three exemplary months (columns). The third row shows the curves of the LHS of Equation (9) in black, with gray shading highlighting ranges of r that contribute to precipitation enhancement over land. The derivative of the LHS of Equation (9) is shown in the fourth row. Positive values contribute to the precipitation enhancement, and red dashed lines indicate the locations of maximum contribution.

The LHS of Equation (9) is plotted in the third row of Figure 7, with gray shading indicating the ranges of r which contribute to precipitation enhancement over land. Similarly, the bottom row of Figure 7 shows the derivative of the LHS of Equation (9) with respect to r_e, and the humidity value which most strongly contributes to the precipitation enhancement is indicated by a red dashed line. The expectation that high humidity values cause precipitation enhancement over land is confirmed with $r = 0.6$ constituting an approximate lower bound (also in other months that are not shown). The r value most relevant for precipitation enhancement over land lies at around $r = 0.8$ in March and November, where the 'bump' in $P(r)$ exists, and slightly higher, at around $r = 0.9$, in July, where no 'bump' is present but the land humidity distribution has the most pronounced tail towards highest r values.

DO LAND-OCEAN HUMIDITY DIFFERENCES CAUSE PRECIPITATION ENHANCEMENT OVER TROPICAL LAND IN CONVECTION-RESOLVING SIMULATIONS?

The results presented in Chapter 4 were solely based on ERA5 reanalysis data and it is not clear to which extent the qualitative findings generalize. Even though ERA5 is currently considered to be our best "simulated reality", owing to the assimilation of observational data, the product is based on a General Circulation Model (GCM) with horizontal grid resolution of about 30 km, insufficient to resolve convection. Precipitation in the tropics is largely dependent on moist convection which is governed by the intricate interplay of water and the atmospheric circulation, that is not adequately represented by conventional convective parametrizations (Stevens and Bony, 2013). In addition, the feedback between soil moisture and precipitation, including its sign, depends on whether convection is parameterized or represented explicitly in models (Taylor et al., 2013). In response to these problems, the scientific community directed great efforts at the development of km-scale, convection-resolving global climate models which are now becoming operational. One example is the ICOsahedral Nonhydrostatic (ICON) model in its high-resolution ICON-Sapphire configuration, developed for horizontal resolutions below 10 km (Hohenegger et al., 2023).

To get an indication for whether the differences in the moisture-precipitation relationship and humidity distributions found in the 10-year ERA5 data (1981–1990) are sensitive to the use of convective parametrizations, I repeat the analysis from Chapter 4 with simulation output from a 5-year coupled ICON-Sapphire run with 5 km horizontal resolution and explicit convection. The simulation was performed as part of the nextGEMS project (Koldunov et al., 2023) and is hereafter referred to as ICON ngc3028. The simulated period runs from January 2020 to July 2025. Even though the ICON simulation comes with its own biases, such as too much rainfall over the tropical ocean, I conjecture that similarities between the ERA5 and ICON results increase the likelihood that the diagnosed phenomenon is true to nature while differences suggest an influence of convective parametrizations. However, robust conclusions about the role of model biases as opposed to actual physics cannot be drawn without a careful comparison of the obtained results with observations.

Figure 8 shows a comparison of the mean seasonal cycle of $\chi(t)$ in ERA5 and ICON ngc3028. The threshold for precipitation enhancement over land, $\chi = 0.86$, is indicated by a red line, and only about half of the months in Figure 8b lie above this threshold. Nevertheless, the overall shape of the seasonal cycle bears some resemblance to the ERA5 cycle. Some of the differences could be due to the fact that the two datasets contain different years. More recent decades in the ERA5 product, e.g. the period 2011–2020, show a similarly weak precipitation enhancement over land, with the mean value of χ lying above 0.86 in only about half of the months. While satellite products consistently show precipitation enhancement over land in the long-term mean (HS22), I cannot preclude that processes controlling $\chi(t)$ are sensitive to time-dependent phenomena such as the phases of ENSO or global warming. In the case of ICON ngc3028, however, the low $\chi(t)$ stems from a strong
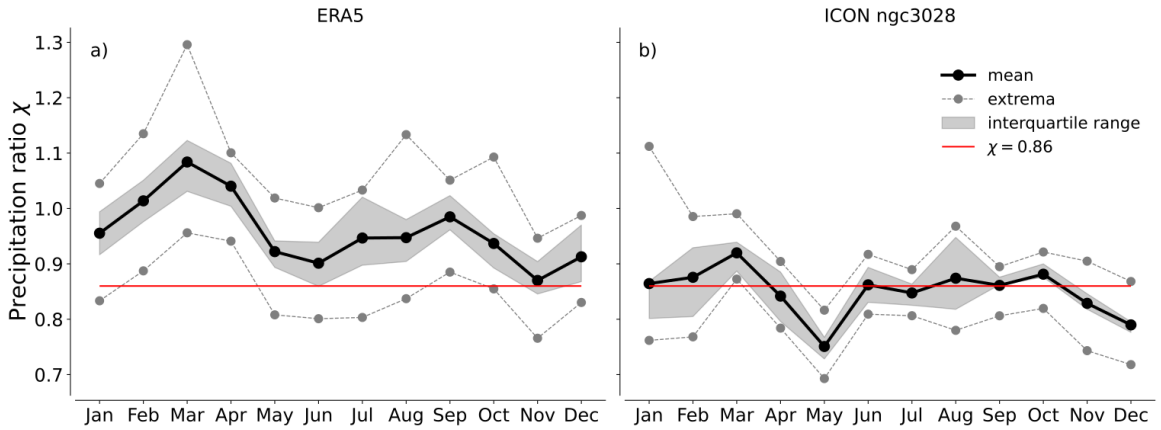
Figure 8: Comparison of mean seasonal cycles of χ (black solid lines), interquartile ranges of annual mean values (gray shading), and extreme years (gray dashed lines) between a) ERA5 (1981–1990) and b) ICON ngc3028 (01-2020 – 07-2025). The red lines show the threshold for precipitation enhancement over tropical land.

overestimation of oceanic precipitation with a mean value of about $4\,\mathrm{mm\,day^{-1}}$, which lies significantly above the observed mean of about $3\,\mathrm{mm\,day^{-1}}$ (HS22). I will return to this point when discussing how $P(r)$ and $\mathrm{pdf}(r)$ contribute to the simulated χ values in ICON ng3028.

A first agreement between the ERA5 and ICON analysis is that monthly, surface type-specific fit functions of the moisture-precipitation relationship, $P_{\ell,m}(r)$ and $P_{o,m}(r)$, can adequately reconstruct the mean seasonality of $\chi(t)$ (see Fig. 5f for ERA5, similar plot for ICON not shown). However, the obtained fit functions exhibit significant differences as illustrated in Figure 9. In particular, two differences are noteworthy: First, the ICON curves no longer exhibit the 'bump', which divided the ERA5 humidity space into three regimes, visually separated by the dashed vertical lines in Figure 9a. Instead, only two regimes exist in Figure 9b, one for low r values in which $P_{\ell,m}(r) > P_{o,m}(r)$, and another one for high r values in which $P_{\ell,m}(r) < P_{o,m}(r)$. (Strictly speaking, there exists another regime below $r \approx 0.25$ in which $P_{\ell,m}(r) < P_{o,m}(r)$, but this regime contributes insignificant amounts of precipitation and was omitted in Figure 9 for better visibility of the relevant differences.) Second, both land and ocean curves exhibit a larger month-to-month variability in the ICON simulation compared to ERA5.

Regarding the differences in month-to-month variability, the higher variability of the ICON curves may reflect the fact that precipitation fields from resolved convection are less smooth and allow for stronger extremes. An interesting similarity between ICON and ERA5 in their variability are the land curves from June, July, and August which are shown in red and, in the ERA5 case, did not exhibit the 'bump'. Likewise in the ICON case, these curves yield the lowest precipitation rates for most values along r. Given that these months are associated with northern hemisphere monsoon activity and large amounts of continental rainfall, it is puzzling that their land-ocean differences in $P(r)$ are particularly detrimental for land precipitation.
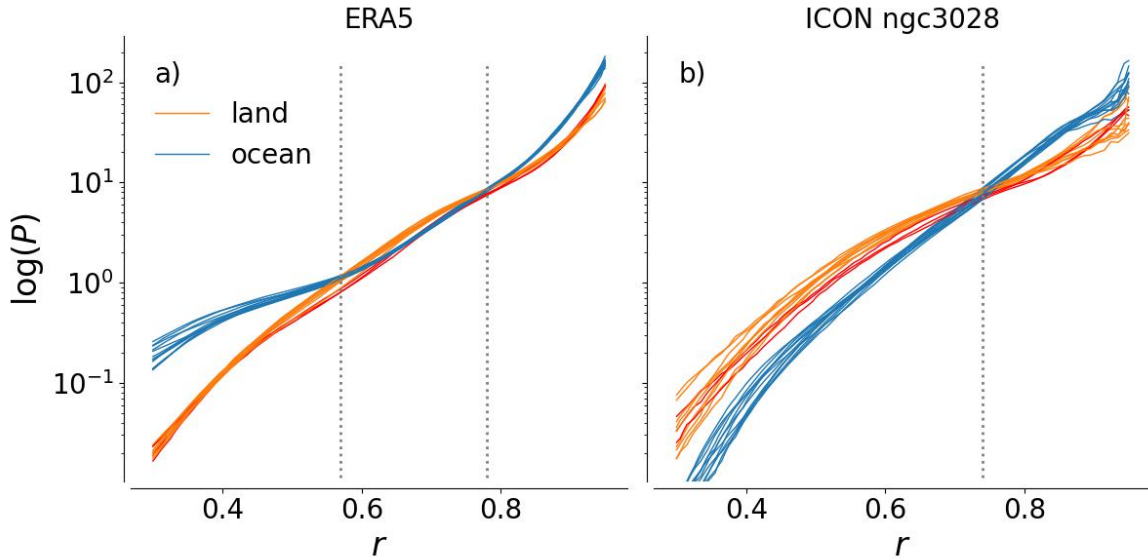
Figure 9: Comparison of monthly moisture-precipitation relationships $P_{m,\ell}(r)$ and $P_{m,o}(r)$ between ERA5 and ICON. Red lines denote the land relationships for June, July, and August. Dashed vertical lines visualize the location of the approximate intersection points of land and ocean relationships.

Regarding the differences in the low-r regime, I speculate that the ICON feature is more trustworthy, not only because the feature in ERA5 is inconsistent with observational studies that investigated land-ocean differences in $P(r)$ (Ahmed and Schumacher, 2017), but also because convective parametrizations are known to struggle in dry environments (Derbyshire et al., 2004). In Figure 10a, I further investigate the ERA5 feature, by comparing $P(r)$ curves obtained from all tropical grid cells (solid lines) to ones that I conditioned on being rainy, using a threshold value of $0.1\,\mathrm{mm\,day^{-1}}$ (dashed lines). The dashed lines can be interpreted as actual precipitation intensities, while the solid lines include the influence of grid cells without any precipitation. At high r values, the dashed and solid lines are in good agreement, indicating that all moist cells are rainy. At low r values, the curves from rainy cells show that land-ocean differences nearly disappear, implying that land-ocean differences in the abundance of non-rainy grid cells are the primary reason for differences between the solid orange and blue lines. Figure 10b depicts oceanic and terrestrial distributions of rainy and non-rainy cells along r: Over land, the distributions are relatively well separated. For values below $r = 0.4$, it practically never rains, and above $r = 0.6$ it practically always rains. Over ocean, the overlap of the two distributions is much larger, with relatively numerous rainy grid cells between $r = 0.3$ and 0.6, which lift the solid blue curve in Figure 10. Thus, while I cannot provide an answer here, the relevant question for explaining the low-r regime in ERA5 seems to be what controls the triggering or inhibition of convection in dry environments, rather than what controls precipitation intensity once convection sets in.

The fact that the ICON $P(r)$ relationship over land exceeds the oceanic one over a wide range of low and intermediate r values up to about $r = 0.75$ prompts the question of whether land-ocean differences in $P(r)$ still act to disfavor precipitation over land, as they did in ERA5, or whether they actually enhance it. Analogous to the experiment conducted
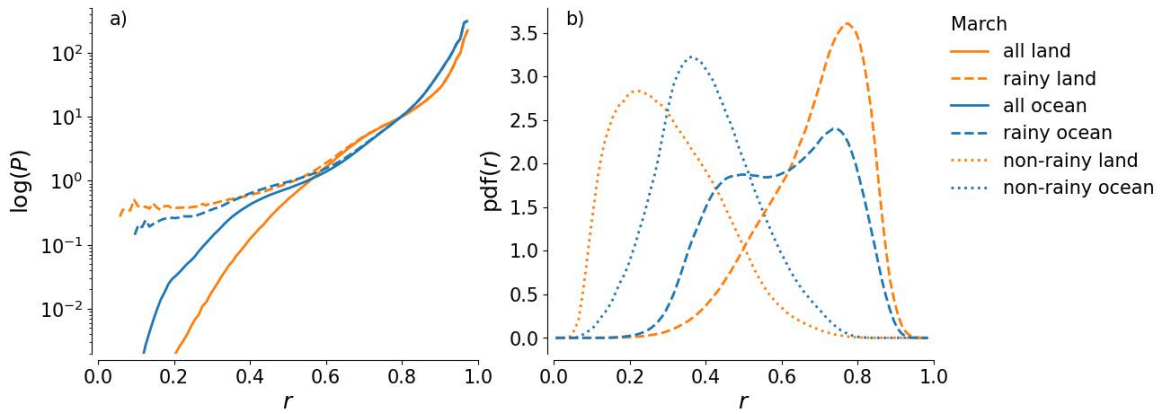
Figure 10: Comparison of ERA5 land and ocean moisture-precipitation relationships (panel a) and humidity distributions (panel b) between rainy (dashed lines) and non-rainy (dotted lines) grid cells, shown for the exemplary month of March. The solid lines in panel a represent the relationships without distinction between rainy and non-rainy.

in Chapter 4 and shown in Figure 6a, I test this by computing a reconstruction of $\chi(t)$ for which I compute precipitation over both land and ocean from the monthly oceanic $P_{o,m}(r)$ relationship. The result is shown in Figure 11. Similar to the ERA5 case, the reconstructed $\chi_{rec}(t)$ lies above the benchmark in most months, and especially during JJA. However, September and November represent exceptions in that land-ocean differences in $P(r)$ have no effect on the $\chi(t)$ mean value, and October stands out as an example for precipitation enhancement over land (even though small in magnitude), that can be attributed to the $P(r)$ differences between land and ocean.

The ICON differences in $P(r)$ can also be expected to impact the identified ranges of r that contribute to precipitation enhancement over tropical land. To examine these impacts, Figure 12 shows exemplary ICON land-ocean differences in $P(r)$ and $pdf(r)$ as well as the ranges contributing to land precipitation enhancement, analogous to Figure 7 for ERA5. This time, I selected May, July, and October because of their distinct behavior: May represents the month furthest away from precipitation enhancement over land, as shown in Figure 8, July is the month in which land-ocean differences in $P(r)$ have the most detrimental influence on land precipitation, as seen in Figure 11, but in which $\chi(t)$ still ends up close to the enhancement threshold, and October is the only month in which the $P(r)$ differences actually cause the precipitation enhancement over land. On first sight, the humidity pdfs obtained from ICON look similar to the ones obtained from ERA5. May and July exhibit an extended tail of the land pdf towards high r, relative to the ocean, and this feature disappears in October. However, there also exist notable differences between ICON and ERA5 which explain the weak or missing precipitation enhancement over land in ICON.

Chief among these differences is the reduced bimodality and increased skewness of the ocean distribution, with a tendency to lean towards high r values. In May, this circumstance is accompanied by an only weakly enhanced high-r tail and a much reduced moist peak in the land pdf. Even though some enhancement of precipitation over land is seen in the intermediate humidity range around $r = 0.5$, the associated precipitation rates are too weak to compensate for the precipitation enhancement over ocean in the mid to high
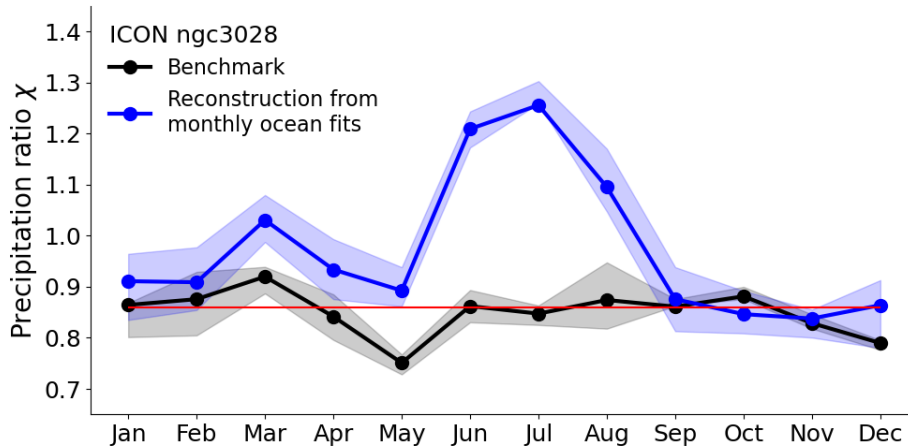
Figure 11: Reconstruction of χ from oceanic monthly relationships $P_{m,o}(r)$, applied to both oceanic and land grid cells, compared with benchmark (analogous to Figure 6a). The red line denotes the threshold for precipitation enhancement over tropical land.

r regime. In July, the situation is similar to ERA5 in that the pronounced tail of the land distribution at high r values creates considerable enhancement of precipitation over land. But also here, the skewness of the ocean distribution counteracts the precipitation enhancement over land, and even dominates over it, so that $\chi(t)$ ends up slightly below 0.86. Last, in October, the land pdf does not exhibit a stronger tail than the ocean pdf but instead, it exhibits a relatively broad second peak which coincides with the upper end of the range in which $P_{\ell,m}(r) > P_{o,m}(r)$, and in which precipitation rates are already fairly high. This allows the land-ocean differences in $P(r)$ that favor precipitation over land to leverage their potential.

Taken together, and including the characteristics of land-ocean differences in $P(r)$ and $pdf(r)$ of other months not discussed here, I would argue that several results from the ICON analysis are consistent with the findings from Chapter 4, especially the role of the enhanced tail of $pdf_\ell(r)$ at high r values in JJA, and that maximum enhancement of precipitation over land comes from r values between approximately 0.7 and 0.9 in all but two months. Identified discrepancies are mostly rooted in a too moist ocean atmosphere in ICON, yielding spuriously large precipitation amounts, and keeping $\chi(t)$ close to or below the threshold for precipitation enhancement over land. How relevant land-ocean differences in $P(r)$ at intermediate r values really are for the precipitation enhancement over land, especially when being combined with a more realistic oceanic humidity distribution, cannot be answered conclusively without further investigations using observations. However, the ICON analysis suggests that their importance might be underestimated by ERA5.

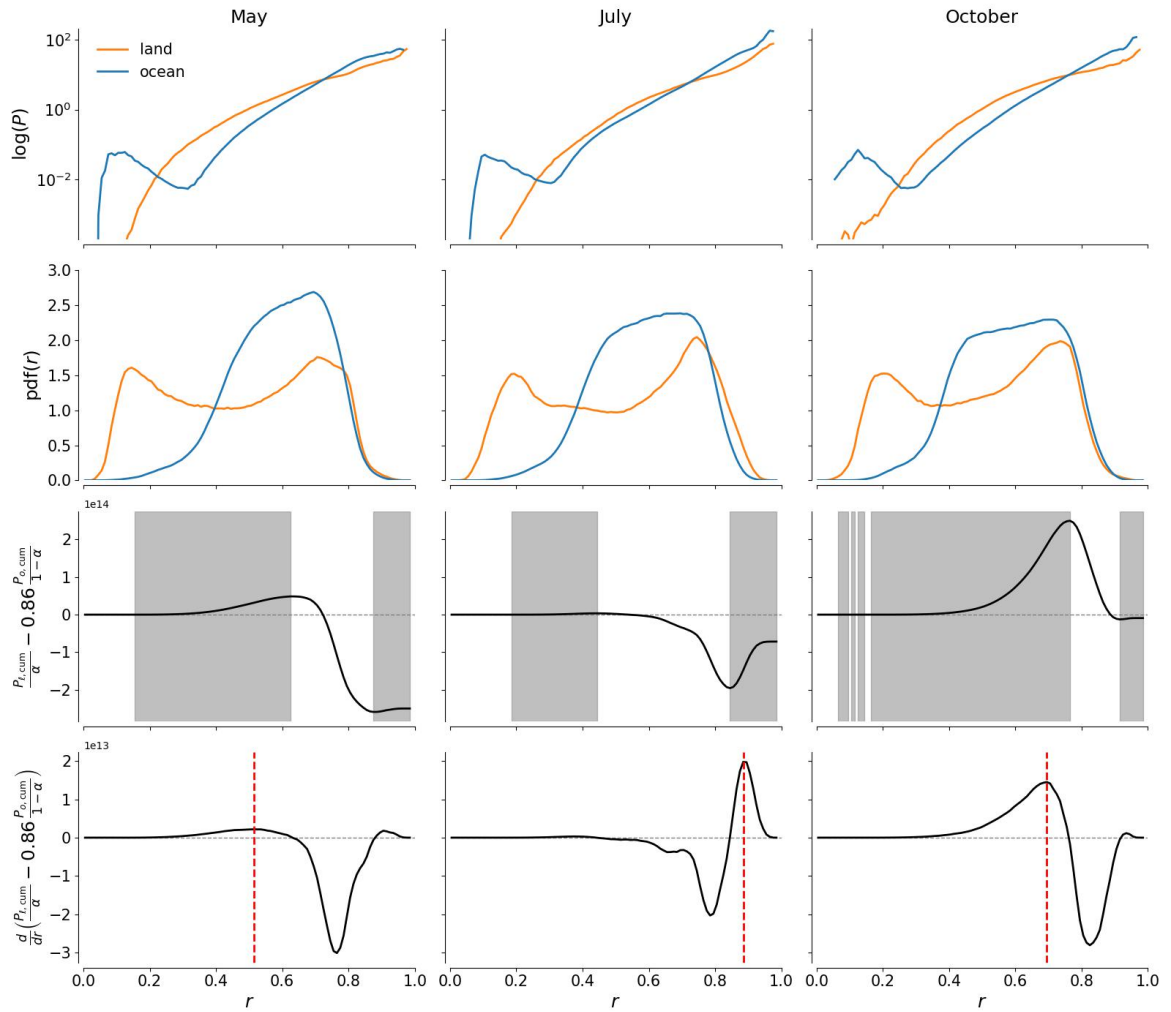Figure 12: Analogous to Figure 7 but based on the ICON ngc3028 data.

SUMMARY AND CONCLUDING THOUGHTS

The overall goal of this dissertation was to better understand what fundamentally controls the way in which tropical precipitation gets partitioned between land and ocean, and how it is possible that precipitation gets enhanced over tropical land with respect to the tropical ocean.

6.1 SUMMARY OF MY RESEARCH FINDINGS

To this end, I first developed a simple box model governed by water balance equations, describing the tropical land, ocean, and atmosphere as a coupled system of moisture reservoirs (boxes) that exchange moisture with one another, following empirical functions of the reservoirs' moisture content.

A parameter sensitivity analysis of the model's equilibrium solution revealed that the efficiency of horizontal atmospheric moisture transport is the dominant factor controlling the precipitation ratio χ. Soil properties, influencing evapotranspiration and runoff, turned out to be of lesser importance. Furthermore, regardless of the chosen parameter values, the ocean atmosphere always equilibrated to a moister state than the land atmosphere, thereby facilitating the net atmospheric moisture advection from ocean to land that is needed to balance soil runoff. Because the model assumes a monotonic increase of precipitation with atmospheric humidity, whose mathematical expression is independent of the underlying surface type, the moister ocean atmosphere consistently yielded a higher rain rate than the land atmosphere, thus, restricting χ to values between zero and one.

While real world observations confirm that the tropical land atmosphere is drier than the ocean atmosphere on average, the model's inability to produce stronger mean precipitation over land than over ocean is counterfactual, given that real world observations show a climatological enhancement of tropical precipitation over land. This disagreement between the box model mechanics and observations inspired a number of hypotheses that could explain precipitation enhancement over land in reality.

One of these hypotheses conjectured that the land surface may modify the relationship between precipitation P and column relative humidity r. If the same r value would lead to sufficiently more precipitation over land than over ocean, then the ocean atmosphere could still equilibrate to a higher humidity value and enable landward advection, while at the same time yielding less precipitation than the land atmosphere. In my second study, I tested and refuted this hypothesis using 10 years of ERA5 reanalysis data: The surface type, being land or ocean, indeed affects $P(r)$ in a systematic manner, but these land-ocean differences overall disfavor precipitation over land, rather than enhancing it. Instead, precipitation enhancement over tropical land is explained by land-ocean differences in the probability distribution of column relative humidity $pdf(r)$, in particular at high values of

r where the terrestrial distribution exhibits a stronger tail than the oceanic distribution.

A convection-resolving ICON simulation overall confirms that distinct humidity distributions over land and ocean are important for explaining precipitation enhancement over land. However, the results of this analysis also suggest that ERA5 misrepresents the land-ocean differences in $P(r)$ at low and intermediate r values, with the effect of diminishing their role in enhancing precipitation over land.

6.2 OPEN QUESTIONS AND IDEAS FOR FURTHER RESEARCH

The studies presented in this thesis provided answers to the research questions I set out to answer, but they also sparked new questions and ideas for further investigations.

For instance, the box model largely ignored energetic constraints, in particular by assuming a constant horizontal wind speed and a fixed temperature, shared among all boxes. These choices strongly reduced the complexity of the modelled interactions but also disabled potentially relevant processes that could allow the equilibrium χ value to lie above one. One example is the generation of atmospheric circulations by land-ocean temperature differences, which could facilitate up-gradient moisture transport by convergence. Such up-gradient moisture transport is known to occur in the tropical mean picture, for instance, when the near-surface branch of the Hadley cell carries moisture from the comparably dry subtropics to the moist deep tropics. To which extent up-gradient moisture transport happens between ocean and land is less clear and may vary between individual continents and their adjacent oceans. However, regardless of the sign of the land-ocean moisture gradient, convergence can be expected to increase landward moisture transport and should be accounted for.

While I argued in the previous paragraph that energetics impact the horizontal moisture transport, likely with a positive net effect on moisture availability over land, also local impacts on atmospheric humidity and conversion efficiency are to be expected. First, temperature strongly controls the rate of evaporation from the ocean surface, and evapotranspiration from the land surface, wherever energy-limited soil moisture conditions prevail. Second, surface warming destabilizes the atmospheric profile by deepening the turbulent boundary layer, and decreasing the inversion strength at its top. These effects on stability have been argued to cause the lower pick-up value of $P(r)$ over land (Ahmed and Schumacher, 2017). Third, surface warming, especially over moisture-limited land, may have a negative effect on column relative humidity due to the associated increase in saturation specific humidity, dictated by the Clausius-Clapeyron equation. If moistening factors cannot compensate for the increased moisture holding capacity of the atmosphere, r will drop and precipitation will be reduced. Given the partly counteracting nature of energy-related mechanisms, it is not clear what their combined effect on the equilibrium χ value and its theoretical bounds would be. Thus, investigating energetic constraints is an interesting direction for further conceptual work.

However, given the insight from study 2 that land-ocean differences in the spatial distribution of r values, rather than their mean value, are key for understanding controls on χ, a simple box model as presented in study 1 seems inapt for investigating energetic controls.

While I see potential for idealized model simulations to shed light on the role of energetics in setting and constraining χ, the employed model should be sophisticated enough to develop thermally driven circulations, for example in a two-dimensional setup, and resolve spatially heterogeneous atmospheric temperature and moisture profiles, as well as soil moisture conditions.

I expect that energetics also play a key role in explaining the land-ocean differences in $P(r)$ and $pdf(r)$, discovered in study 2, both through their dynamic influence in the form of circulations, and their local thermodynamic control. I would like to know how the different humidity distributions over land and ocean come about and, more specifically, how the land is able to maintain its numerous moist locations which are responsible for the enhancement of land precipitation with respect to the ocean. What is the relative importance of moistening through convergence of remotely sourced moisture, as opposed to moistening through local evapotranspiration, and the temperature control on r? Disentangling the roles of these processes in shaping the current land-ocean precipitation contrast would enable us to formulate expectations for how $\chi(t)$ may evolve in the future.

In the decades to come, surface temperatures are expected to change due to anthropogenic climate change. How does global warming impact the tropical precipitation partitioning? The maintenance of very moist land locations might be threatened by constraints arising from projected increases of the temperature contrast between tropical land and ocean. Under global warming, both models and observations show that tropical land warms disproportionately more than the tropical ocean (Manabe et al., 1991; Sutton et al., 2007), which implies that the water holding capacity of the terrestrial atmosphere is increased relative to the one over ocean. The moisture content of air over ocean is therefore constrained to a lower value than that over land, and as air, imported from the ocean, warms over land, its relative saturation is lowered (Sherwood and Fu, 2014). As a consequence, one may conjecture that land atmosphere moistening through advection and convergence will be less efficient in a warmer world. In addition, the increased warming contrast between land and ocean may affect the strength of thermally driven circulations, which facilitate the horizontal moisture transport. Two competing mechanisms seem plausible: On the one hand, a reduction in relative humidity over land would reduce precipitation and the associated latent heat release that propels both the landward Walker and monsoon circulations. As a consequence, circulations would weaken and transport less moisture towards the land – a negative feedback loop develops. On the other hand, larger temperature differences increase the pressure gradient force near the surface which could strengthen the circulation, thereby balancing or at least limiting the reduction of relative humidity over land. Which one of these mechanisms will dominate is currently unknown and opens exciting avenues for future research.

Last, even though land-ocean differences in $P(r)$ turned out to diminish land precipitation rather than enhancing it, I would like to understand where these differences come from. Previous works such as Ahmed and Schumacher, 2017 only provide qualitative arguments such as orographic lifting and the destabilization of the land atmosphere by daytime surface warming to explain why the land relationship features a lower pick-up value and therefore a stronger mean precipitation rate at intermediate r values. While these are plausible hypotheses, a rigorous evaluation is yet to confirm or refute them, and they do not

explain the high-r regime where $P_o(r)$ exceeds $P_\ell(r)$.

In contrast to low and intermediate r values, where $P(r)$ is not identical with the mean intensity of precipitation events due to the contribution of numerous grid cells without any precipitation, precipitation from high r values exclusively stems from rainy grid cells, and can therefore be interpreted as mean intensity. Given a very moist atmospheric column, what prevents the land atmosphere from leveraging this potential and reaching similarly strong precipitation rates as those over ocean? One may speculate that the pronounced diurnal cycle over land limits the time frame within a day in which deep convection can develop and precipitate, before the night time stabilization of the atmospheric profile shuts it down. This could reduce the mean precipitation rate over land relative to over ocean when comparing daily averages. Another, more uncertain hypothesis concerns shallow circulations, forming between moist and dry soil patches over land, that have been shown to bring precipitation from the moist to the dry patches in idealized convection-permitting simulations (Hohenegger and Stevens, 2018). One could imagine that, through this mechanism, real world soil moisture heterogeneities could lead to a dissipation and re-establishment of land convection elsewhere before its full precipitation potential is reached. However, whether the real world time scale of these circulation reversals supports this hypothesis, whether the effects would be seen in the tropical mean signal, and whether ERA5 with its relatively coarse horizontal resolution would capture the effect is unclear.

In conclusion, this thesis has advanced our conceptual understanding of how moisture coupling in the tropical land-ocean-atmosphere system controls and constrains the land-ocean precipitation contrast. The way in which atmospheric humidity gets structured in space, either through lateral transport by atmospheric circulations, or through local moistening processes, was found to be key for explaining the tropical precipitation ratio χ, including the diagnosed precipitation enhancement over land. It is the hope that the findings compiled in this dissertation inform and inspire further research activities in the fascinating field of tropical hydrology.

Part II

APPENDIX

CONSTRAINTS ON THE RATIO BETWEEN TROPICAL LAND AND OCEAN PRECIPITATION DERIVED FROM A CONCEPTUAL WATER BALANCE MODEL

A

The work in this appendix has been published as:

Constraints on the Ratio between Tropical Land and Ocean Precipitation Derived from a Conceptual Water Balance Model

Luca Schmidt[1,2] and Cathy Hohenegger [1]

[1]Max Planck Institute for Meteorology, Hamburg, Germany
[2]International Max Planck Research School on Earth System Modelling, Hamburg, Germany

ABSTRACT

Which processes control the mean amounts of precipitation received by tropical land and ocean? Do large-scale constraints exist on the ratio between the two? We address these questions using a conceptual box model based on water balance equations. With empirical but physically motivated parametrizations of the water balance components, we construct a set of coupled differential equations which describe the dynamical behavior of the water vapor content over land and ocean as well as the land's soil moisture content. For a closed model configuration with one ocean and one land box, we compute equilibrium solutions across the parameter space and analyze their sensitivity to parameter choices. The precipitation ratio χ, defined as the ratio between mean land and ocean precipitation rates, quantifies the land-sea precipitation contrast. We find that χ is bounded between zero and one as long as the presence of land does not affect the relationship between water vapor path and precipitation. However, for the tested parameter values, 95% of the obtained χ values are even larger than 0.75. The sensitivity analysis reveals that χ is primarily controlled by the efficiency of atmospheric moisture transport rather than by land surface parameters. We further investigate under which conditions precipitation enhancement over land ($\chi > 1$) would be possible. An open model configuration with an island between two ocean boxes and nonzero external advection into the domain can yield χ values larger than one, but only for a small subset of parameter choices, characterized by small land fractions and a sufficiently large moisture influx through the windward boundary.

A.1 INTRODUCTION

All water that evaporates from Earth's land and ocean surfaces must eventually return to the surface as precipitation. This water mass balance also holds approximately in the tropics. But which physical processes or parameters of the system determine how much it rains over land versus over ocean? A useful quantity in the context of the large-scale tropical land-sea contrast of precipitation is the precipitation ratio χ, defined as the ratio of spatio-temporally averaged precipitation rates over tropical land and ocean. Modern observations make it easy to quantify χ but do not explain its value. Similarly, the complexity of sophisticated climate models limits clear process understanding and, apart from that, these models frequently fail to reproduce observed precipitation patterns (Fiedler et al., 2020) as well as the right land-sea contrast of precipitation (Hohenegger and Stevens, 2022). It is therefore the aim of this study to provide theoretical understanding of the large-scale constraints on χ that arise from the water mass balance, as well as the sensitivity of χ to different physical processes and properties of the system. To this end, we consider a simple box model with

44

a small number of free parameters such as land fraction or land surface characteristics. As such, this model is not meant to realistically describe the real tropics. Rather, it helps us understand fundamental relationships and identify relevant mechanisms for which more sophisticated investigations are needed.

Hohenegger and Stevens, 2022 is the first study to compute χ from different observation products and to use a conceptual rainbelt model to interpret the obtained values with respect to the role of land for precipitating convection. Accounting for the tropical land-ocean geometry as well as width, intensity, and latitudinal position of the rainbelt, the χ values from observations, ranging between 0.9 and 1.04, could only be explained if the nature of the surface, being land or ocean, affects the rainbelt characteristics. In other words, the presence of land affects the way it rains. The authors concluded that land receives more precipitation than what is expected from the mere geometry of the tropical land masses. Similar to Hohenegger and Stevens, 2022, we study the physical controls on χ and draw indirect conclusions about the relationship between precipitation and the underlying surface. However, we take a different, independent approach which is agnostic about the land geometry and spatial structure of precipitation. With our box model consisting of one ocean and one land domain, we examine the theoretical upper and lower bounds of χ that arise solely from the condition of water balance.

While the large-scale land-sea contrast of precipitation remains poorly investigated, much work using box models and water balance equations has been directed at the question of how the presence of land impacts local rainfall. Unlike the ocean, land can dry out and thereby significantly reduce its evaporative moisture flux. The degree to which precipitation hinges on local evapotranspiration, determines how susceptible precipitation is to changes in soil moisture conditions and therefore to the underlying surface. With their one-dimensional land-atmosphere model based on water balance equations, Budyko and Drozdov, 1953 lay the foundation for quantifying land-atmosphere coupling by computing moisture recycling ratios for different continental regions. The recycling ratio measures the share of precipitation inside a region that is derived from locally evaporated moisture, as opposed to advected moisture from outside the region. Important subsequent studies that computed recycling ratios include Brubaker et al., 1993, Eltahir and Bras, 1994, and Ent et al., 2010. While the obtained contributions from local evapotranspiration to rainfall varied between 10 and 90 %, depending on the selected region and employed method, all studies agreed on that soil moisture availability leaves an imprint on the terrestrial precipitation signal.

Such moisture recycling studies as well as the hydrological studies by Rodriguez-Iturbe et al., 1991 and Entekhabi et al., 1992, who used a land box model based on water balance equations to understand the controls on soil moisture variability, inspired our approach and helped us design our conceptual model. However, because these studies only consider terrestrial precipitation with prescribed contributions from advected moisture. Advected moisture itself, which likely plays a role in setting χ, is not part of their solution. We therefore couple our land and ocean domains through advection and runoff, and allow for an interactive exchange of moisture between them. As a consequence, land and ocean precipitation rates and, hence, χ arise as part of the solution to our model equations.
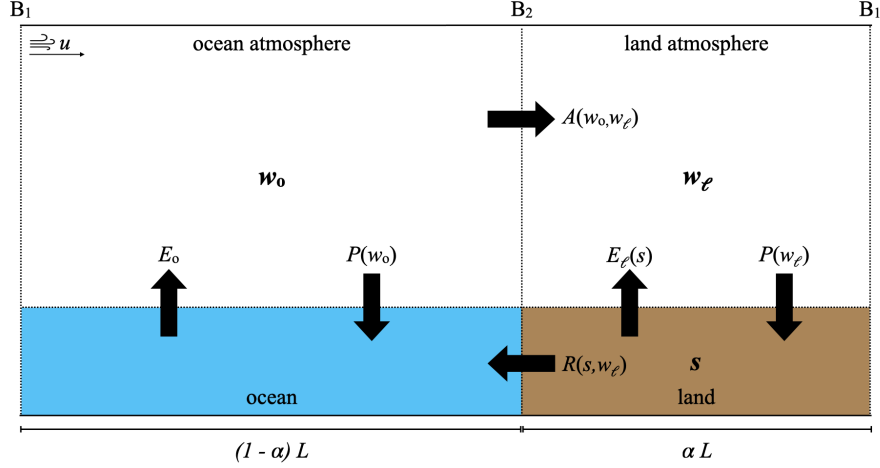
Figure 13: Model sketch of the land-ocean-atmosphere system with periodic boundary conditions. The length of the boxes is determined by the total domain length L in km and land fraction α. Black arrows represent the box-averaged moisture fluxes in $\mathrm{mm\,day^{-1}}$ between the four model boxes. An exception is the advective net exchange A between the atmospheres which represents the total net amount of transferred moisture in $\mathrm{mm^2\,day^{-1}}$ and translates to different mean fluxes, A_o and A_ℓ, in $\mathrm{mm\,day^{-1}}$ out of or into these boxes due to the different box lengths. The atmospheric moisture transport is driven by a constant horizontal background wind speed u. All fluxes other than ocean evaporation E_o, which is treated as a constant model parameter, are functions of the relative soil moisture saturation s, or water vapor paths of land and ocean atmospheres, w_ℓ and w_o, respectively.

A.2 MODEL DESCRIPTION

To understand the controlling factors and constraints for the land-sea precipitation contrast, we propose a box model as sketched in Figure 13. The model consists of an ocean subdomain denoted by subscript 'o', and a land subdomain denoted by 'ℓ' whose sizes are determined by the full domain length L and land fraction α. Each subdomain contains a ground box at the bottom (ocean or land) and an atmospheric box above. The vertical extent of the atmospheric boxes is chosen as the height over which water vapor is transported and stored. Similarly, the vertical depth of the land box is given by the hydrologically active soil depth z_r. In the horizontal direction, the model has periodic boundary conditions, which makes it a closed system that conserves water. Such a *closed* model (CM) is suitable to describe the entire Earth or, if net moisture exchange with the extratropics is negligible, the tropics. In section A.6, we discuss an *open* model (OM) version which allows for nonzero net advection from outside the model domain.

A.2.1 *Water balance equations*

To formulate the underlying water balance equations, we express all moisture fluxes between the boxes as functions of the system's moisture state. For atmospheric boxes, the moisture state is given by the mean water vapor path w in mm, and for the land box by the unitless mean relative soil moisture saturation s. Since the ocean does not dry out, it

does not require a moisture variable. Hence, the full information on the moisture state of the land-ocean-atmosphere system at any moment in time t is given by the set of state variables $\{w_o(t), w_\ell(t), s(t)\}$.

The time-evolution of the state variables is expressed by coupled water balance equations in which the water fluxes represent moisture sinks and sources (see e.g. Brubaker et al., 1991):

$$\frac{ds}{dt} = \frac{1}{nz_r}\left[P(w_\ell) - R(s, w_\ell) - E_\ell(s)\right] \tag{10}$$

$$\frac{dw_\ell}{dt} = E_\ell(s) - P(w_\ell) + A_\ell(w_\ell, w_o) \tag{11}$$

$$\frac{dw_o}{dt} = E_o - P(w_o) + A_o(w_\ell, w_o). \tag{12}$$

Note that the time-dependence of s, w_ℓ and w_o is implicit in Equations (10) to (12). The relevant fluxes, indicated by the black arrows in Figure 13, are precipitation P, land evapotranspiration E_ℓ, ocean evaporation E_o, soil runoff R, and atmospheric advection A. The advection terms A_ℓ and A_o in Eqs. (11) and (12) represent the *net* advection rates into the land and ocean atmosphere, respectively, and are positive for net moisture import and negative for net moisture export. In a closed system, the domain-mean advection vanishes, i.e. $\alpha A_\ell + (1-\alpha)A_o = 0$. All fluxes are given as spatial mean flux rates in mm day^{-1}. The product of dimensionless soil porosity n and hydrologically active soil depth z_r in mm is a model parameter.

A.2.2 *Empirical relationships for water fluxes*

To solve the water balance equations (10) - (12), we need expressions for the water fluxes. While the conservation of water is a fundamental condition, there are no simple fundamental laws governing the moisture exchange between the model boxes. Instead, we use empirical relationships, as has been done, for instance, by Rodriguez-Iturbe et al., 1991. As in their study, we express runoff as the fraction R_f of precipitation that does not infiltrate into the soil,

$$R(s, w_\ell) = R_f(s)P(w_\ell), \tag{13}$$

with

$$R_f(s) = \epsilon s^r, \tag{14}$$

and the two dimensionless parameters ϵ and r. Equation (14) tells us that runoff intensifies as the soil moistens. Runoff water is returned to the ocean but has no effect on the ocean's moisture properties.

For precipitation, Rodriguez-Iturbe et al., 1991 followed the approach of Budyko and Drozdov, 1953 which assumes that the advected part of land precipitation is known. This is not a desirable assumption in our case where the focus is on the factors controlling the land-to-ocean precipitation ratio. We want a free interaction between the two subdomains and therefore choose to parametrize precipitation as a function of w, as established by Bretherton et al., 2004 based on observations,

$$P(w) = \exp\left[a\left(\frac{w}{w_{\text{sat}}} - b\right)\right]. \tag{15}$$

Equation (15) introduces two dimensionless parameters a and b and the saturated water vapor path w_{sat} in mm. Whether the exact shape of the $P(w)$ relationship, here set by the choice of a, b, and w_{sat}, is identical over land and ocean is still under debate. While Schiro et al., 2016 and Schiro et al., 2020 reported only slight differences in the $P(w)$ relationship between tropical land and ocean regions, a similar study by Ahmed and Schumacher, 2017 found that land precipitation increases more strongly at lower water vapor path values than ocean precipitation, and that it exhibits a diurnal cycle, presumably due to stronger surface heating and orographic effects. Our hypothesis here is that the processes which turn water vapor into precipitation depend only on the atmospheric vapor concentration and not on the underlying surface. Hence, we use Eq. (15) with the same parameter values over land and ocean. Indirectly, by comparing our model results to observed values of χ, we can return to this debate and assess whether the nature of the underlying surface affects the $P(w)$ relationship (see Section A.6a).

The qualitative dependence of evapotranspiration on soil moisture saturation is long-known, see e.g. Budyko, 1958. Seneviratne et al., 2010 present a schematic, where E_ℓ is close to zero for soil moisture values below the permanent wilting point, $s < s_{\text{pwp}}$, increases approximately linearly in a transition range between the permanent wilting point and a critical value close to the field capacity, $s_{\text{pwp}} < s < s_{\text{fc}}$, and reaches a plateau for higher s values, $s > s_{\text{fc}}$, where evapotranspiration is nearly constant at its potential rate e_p. For computational convenience, we parametrize evapotranspiration by the following smooth function which has the qualitative properties described above,

$$E_\ell(s) = \frac{e_p}{2}\left[\tanh\left(10\left(s - \frac{s_{\text{pwp}} + s_{\text{fc}}}{2}\right)\right) + 1\right]. \tag{16}$$

Unlike land, the ocean is always fully saturated and we assume the resulting ocean evaporation rate to be a constant model parameter $E_o = e_o$.

It remains to find expressions for the mean net advection rates for the land and ocean atmospheres, hereafter just land/ocean advection. The total net advection into a given box is the difference between the moisture entering and leaving the box per unit time, which is computed from the windward and leeward boundary water vapor paths (in mm) times mean horizontal wind speed u (in mm day^{-1}), respectively. Because we assume one uniform w across each atmospheric box, the wind transports the moisture amount $w_o u$ from ocean to land and $w_\ell u$ from land to ocean, resulting in a net exchange of $A(w_o, w_\ell) = \pm(w_o - w_\ell)u$. For the advection rates per unit length in mm day^{-1}, this gives

$$A_\ell(w_o, w_\ell) = \frac{(w_o - w_\ell)u}{\alpha L} = \frac{(w_o - w_\ell)}{\alpha}\tau \tag{17}$$

for land advection and

$$A_o(w_o, w_\ell) = -\frac{(w_o - w_\ell)u}{(1-\alpha)L} = -\frac{(w_o - w_\ell)}{(1-\alpha)}\tau, \tag{18}$$

for ocean advection, with α being the land fraction and L the total domain length (see Figure 13). On the right hand sides of Eqs. (17) and (18), we introduced the atmospheric transport parameter $\tau = u/L$ in day^{-1}. Its inverse value τ^{-1} represents a characteristic timescale

for atmospheric transport. Similar concepts were used by Brubaker et al., 1991, Sobel and Bellon, 2009, and Lintner et al., 2013 to model advection. In a closed system, this formulation of advection with a constant, unidirectional wind field results in a down-gradient net transport of atmospheric moisture. In our case this net transport carries moisture from a moister ocean atmosphere to a drier land atmosphere which is not always the case in reality (Brubaker et al., 1991).

A.2.3 *Parameter ranges*

We want to constrain χ for our system in equilibrium and test its sensitivity to parameter choices. To do that, we need to define plausible ranges for all free model parameters, thereby constructing our search space. The chosen ranges are summarized in Table 1.

The ranges for s_{pwp} and s_{fc} are taken from data for different soil types presented in Hagemann and Stacke, 2015, where we discard the extreme cases of pure sand and peat. After converting the provided volumetric data to relative soil moisture saturation values, s_{pwp} ranges between 0.15 and 0.55. We notice the fairly consistent relationship, $s_{fc} = s_{pwp} + 0.3$, and use it to reduce the number of free model parameters by one. Entekhabi et al., 1992 provide values for e_p, nz_r, r, and ϵ for both a semihumid and a semiarid climate. We take the values from these two climates as limits for the respective parameter ranges and vary e_p between 4 and 6 mm day^{-1} and nz_r between 50 and 120 mm. Entekhabi et al., 1992 set $r = 6$ for both cases but we let the runoff exponent range between 2 and 6, motivated by Rodriguez-Iturbe et al., 1991 who used $r = 2$ in an illustrative example. Since both studies agree on $\epsilon = 1$, we vary this parameter only slightly between 0.9 and 1.1. Note that ϵ values larger than one could lead to unphysical solutions where runoff exceeds precipitation. Such unphysical cases must be excluded from the analysis but it turns out they never occur. The precipitation parameters are taken from Bretherton et al., 2004 (where our b is called r). We use their fitting parameter values for monthly and daily data as bounds for a and b. Bretherton et al., 2004 also give a typical value, $w_{sat} = 72$ mm, for regions of tropical convection and we deem it appropriate to vary w_{sat} between 65 and 80 mm. Ocean evaporation can be constrained from observations. For instance, Kumar et al., 2017 found the mean evaporation from tropical ocean surfaces to range between 2.5 - 2.8 mm day^{-1}, while an earlier study by Zhang and McPhaden, 1995 indicates higher values of about 3.5 mm day^{-1}. Based on these findings, we let e_o range between 2.5 and 3.5 mm day^{-1}. This range also encompasses 3 mm day^{-1} – the mean value of precipitation over both tropical land and ocean. Lastly, τ is constrained by computing the smallest and largest value of u/L, respectively, where we assume plausible wind speeds in the lower troposphere between 1 and 10 m s^{-1}, and let the domain length vary between 1000 and 40000 km, the upper limit corresponding to Earth's equatorial circumference. Thus, we obtain a range for τ between about 0.002 and 0.864 day^{-1}.

A.2.4 *Model assumptions*

The simplicity of the proposed model owes to a number of assumptions, some of which are important to be made explicit. Foremost, we assume that each model box has well-mixed physical properties so that all interactions are adequately described in terms of spatial mean quantities. Second, we determine the system's moisture state by water balance equations only, ignoring the potential effects of energy balance considerations such as the

Table 1: Free parameters for the closed model simulations with uniform random sampling of parameter values.

Parameter	Minimum	Maximum	Range choice motivated by
s_{pwp}	0.15	0.55	Hagemann and Stacke, 2015
e_p [mm day^{-1}]	4.0	6.0	Entekhabi et al., 1992
nZr [mm]	50.0	120.0	Entekhabi et al., 1992
e_o [mm day^{-1}]	2.5	3.5	Kumar et al., 2017, Zhang and McPhaden, 1995
ϵ	0.9	1.1	Rodriguez-Iturbe et al., 1991, Entekhabi et al., 1992
r	2	6	Rodriguez-Iturbe et al., 1991, Entekhabi et al., 1992
a	11.4	15.6	Bretherton et al., 2004
b	0.5	0.6	Bretherton et al., 2004
w_{sat} [mm]	65.0	80.0	Bretherton et al., 2004
α	0.0	1.0	full possible range
$\tau = u/L$ [day^{-1}]	0.00216	0.864	plausible ranges for L and u

influence of a diurnal cycle. Energetic conditions are kept constant and only enter indirectly through the values of energy-dependent parameters such as e_o or w_{sat}. Third, we prescribe a background wind speed with only a horizontal and constant component. Last, and more importantly, we assume that the functional relationship between precipitation and water vapor path from Eq. (15) holds over both land and ocean with the same choice of parameter values. By comparing the range of obtained χ values from our simple model to known values from the real world, we will discuss in Section A.6a what we can conclude about the potential processes that control the land-sea precipitation contrast in the real world.

A.3 METHODOLOGY

Here, we present the different analysis methods that are employed to evaluate the model behavior and to assess the sensitivity of the land-to-ocean precipitation ratio to variations of the parameter values. The land-to-ocean precipitation ratio is defined as

$$\chi = \frac{P_\ell}{P_o} = \frac{P(w_\ell)}{P(w_o)}. \tag{19}$$

The equilibrium solution to the model equations (10) to (12) has to be found numerically. We use the DynamicalSystems.jl library from Datseris, 2018 to find all roots of the model equations which represent stable fixed points of the system. Adopting an agnostic view on the plausibility of different combinations of parameter values from the ranges in Table 1, we perform 100 000 model simulations for randomly chosen points in the 11-dimensional parameter space, each yielding a corresponding equilibrium state and resulting fluxes. Scatter plots are used to analyze the sensitivity of χ to the different model parameters.

A suitable measure for the dependence of some quantity Q on a parameter p_i which accounts for the possibility of a non-linear and non-monotonic relationship between Q and p_i is their mutual information $MI(Q, p_i)$. Mutual information quantifies how much the knowledge of p_i reduces the uncertainty about Q. The mutual information of p_i and Q is computed as

$$MI(Q, p_i) = H(Q) + H(p_i) - H(Q, p_i), \tag{20}$$

where $H(Q)$, $H(p_i)$, and $H(Q, p_i)$ are the Shannon entropies of Q and p_i values, and of their joint distribution, respectively (Shannon, 1948). To ascribe the probability distributions required for the computation of the Shannon entropies, we use amplitude binning with 10 equally-sized bins for both Q and p_i.

To put the mutual information value into perspective, we follow the approach from Datseris and Parlitz, 2022, p.106, and assess whether the obtained $MI(Q, p_i)$ is significantly different from the null-hypothesis of independent Q and p_i. From the mutual information values of 1000 shuffled surrogates of Q and p_i, we compute a probability distribution of MI values for the uncorrelated case and define $MI_{\text{uncorr},3\sigma}(Q, p_i)$ as the value that deviates by three standard deviations σ from the mean of this distribution. The mutual information index,

$$I_{MI}(Q, p_i) = \frac{MI(Q, p_i)}{MI_{\text{uncorr},3\sigma}(Q, p_i)}, \tag{21}$$

can then be used to assess how the actual mutual information $MI(Q, p_i)$ compares to the value one would expect if Q and p_i were unrelated. We choose $I_{MI} = 1$ to be the threshold for a significant sensitivity of Q to p_i, with higher $I_{MI}(Q, p_i)$ values reflecting a higher sensitivity. In this work, we compute the mutual information index $I_{MI}(\chi, p_i)$ for all free model parameters p_i in order to rank and compare the sensitivity of χ to these different parameters.

A.4 BASIC MODEL BEHAVIOR AND IMPLICATIONS FOR χ

We performed 100 000 closed model simulations with different parameter choices, each yielding exactly one stable equilibrium solution to the model Equations (10) to (12). The output of these simulations is henceforth referred to as "CM data". In this section, we analyze these data with the aim of determining the range of possible equilibrium values of χ. Note that the presented results proofed to be qualitatively robust to variations in the number of performed simulations.

We begin by characterizing the obtained equilibrium states and associated moisture fluxes. Figure 14 illustrates the characteristics of possible equilibria through probability density functions (PDF) of equilibrium soil moisture values in panel a) and b), and water vapor path values for land and ocean atmospheres in panel c). In panel b), s is rescaled to $\tilde{s} = (s - s_{pwp})/(s_{fc} - s_{pwp})$ such that the equilibrium values are located relative to the different regimes of evapotranspiration discussed in Section A.2A.2.2. The regimes are separated by the permanent wilting point and field capacity which are each indicated by a dashed vertical line. The bulk of all simulations equilibrates to intermediate soil moisture values between $s = 0.25$ and 0.75 with a sharp peak in the center part of the E_ℓ-transition
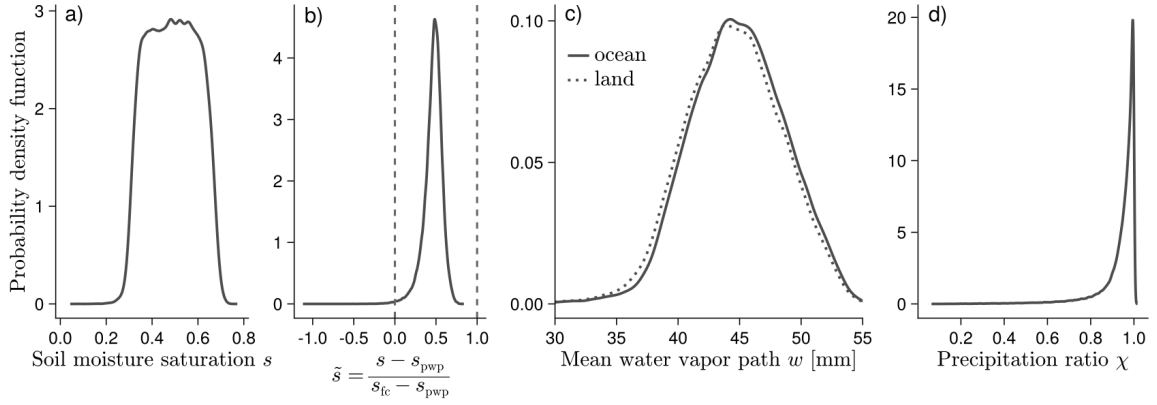
Figure 14: Smoothed probability density functions of equilibrium soil moisture values in panel a), rescaled soil moisture values with vertical lines denoting the permanent wilting point and field capacity which mark the beginning and end of the transition regime of E_ℓ, respectively, in panel b), water vapor path of the land and ocean atmospheres in panel c) and values of χ in panel d). For improved visibility of water vapor path differences between land and ocean in panel c), the distribution's tails towards very dry and very moist states, representing less than 0.38 % of the simulations, are not shown.

regime around $\tilde{s} = 0.5$. Only few simulations (0.38 %) equilibrate to a very dry state with soil moisture values below the permanent wilting point. We discuss such dry states in Section A.5b. Similarly, the atmospheres mostly equilibrate to intermediate w_o and w_ℓ values between 40 and 50 mm (see panel c)), well below w_{sat}. As a matter of comparison, a value of $w = 48$ mm is often employed to distinguish the moist deep tropics with deep convection from the dry subtropics (Masunaga and Mapes, 2020). For better visibility of the differences between w_o and w_ℓ in Fig. 14, we cut the tails of very dry and very moist atmospheric states, representing less than 0.23 % of all simulations. Figure 14c) shows that land and ocean generally equilibrate to similar atmospheric moisture values but that the land is slightly drier than the ocean.

Figure 15 shows moving averages of the equilibrium fluxes from all simulations as functions of the equilibrium soil moisture saturation. Note that the ocean advection rate A_o has negative values in all solutions and is therefore multiplied by -1 to simplify the comparison of its magnitude with other fluxes. Figure 15 contains the entire CM data so that the emerging behavior of the fluxes is a result of a plethora of different parameter choices with soil moisture values being the result, not the driver. Therefore, one should not confuse the plotted curves with the well-defined parametrizations of the water fluxes as functions of s for a fixed set of parameter values.

The purple line in Figure 15 represents both land advection and runoff. That a net moisture transport from ocean to land balances the land's loss of moisture through runoff is a long-known characteristic of the equilibrated hydrological cycle, see e.g. Horton, 1943 or Peixóto and Oort, 1983. We can use this fact to derive an upper bound of χ: According to the advection equations (17) and (18), net moisture transport from ocean to land requires the ocean atmosphere to be moister than the land atmosphere, $w_o > w_\ell$. Since the same, monotonically increasing function $P(w)$ from Eq. (15) is used over land and ocean, $P(w_o)$ is necessarily larger than $P(w_\ell)$. In other words, it rains more strongly over ocean than over land. This is confirmed by Fig. 15 where the dark blue curve for P_o always lies above the light blue curve for P_ℓ. Hence, in our water balance model, an upper bound on χ exists,
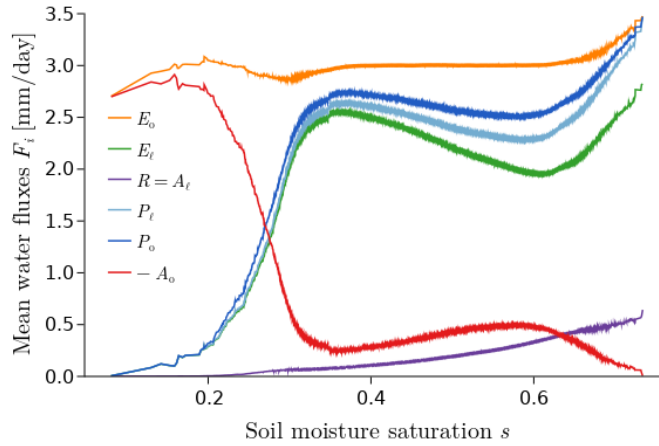
Figure 15: Moving average over different fluxes versus soil moisture saturation computed from the CM data. For the moving average, we sort the data by s and compute the average flux rates within a window of 20000 simulations symmetrically centered around each value of s. Towards the limits of s, the window's size is reduced in order to retain its symmetric positioning.

this upper bound being $\chi = 1$. That χ is bounded by one is also apparent from Fig. 14d which shows the PDF of χ values. While the lower bound is essentially zero, corresponding to cases where land precipitation vanishes, low values of χ are rare and 82.9 % of all parameter combinations yield values larger than 0.9, thereby falling into the range obtained by Hohenegger and Stevens, 2022 from observations.

The shapes of the lines in Fig. 15 indicate that three soil moisture-precipitation regimes can be distinguished: For low equilibrium soil moisture values up to $s \approx 0.36$, runoff and land advection are negligible and P_ℓ nearly equals E_ℓ which rises sharply with s. In an intermediate soil moisture regime, $0.36 \lesssim s \lesssim 0.61$, P_ℓ decreases due to a decline of E_ℓ. However, the precipitation decrease is slightly damped by a steadily growing contribution of moisture from land advection (purple line). Lastly, above $s \approx 0.61$, precipitation increases again as the evapotranspiration trend reverses and advection keeps intensifying.

The equilibrium fluxes in Figure 15 exhibit a number of surprising behaviors: Why is there hardly any rain over ocean when the soil is dry? Why does advection out of the ocean atmosphere (red line) tend to decline with increasing s while advection into the land atmosphere (purple line) increases monotonically? And why does evapotranspiration decline in the intermediate regime while soil moisture increases? To answer these questions, we need a better understanding of how the different model parameter choices and combinations thereof influence the attained equilibrium states and fluxes. The sensitivity of χ to variations in the model parameters and explanations for the seemingly unphysical behaviors in Figure 15 are the topic of the next section.

A.5   PARAMETER SENSITIVITY OF χ

Having established that χ is bounded between zero and one in our water balance model, we want to better understand the controls of different parameters on the attained equilibrium value. To this end, we quantify the sensitivity of χ to each individual model parameter by the mutual information index $I_{MI}(p_i)$ defined in Eq. (21). A comparison of the results
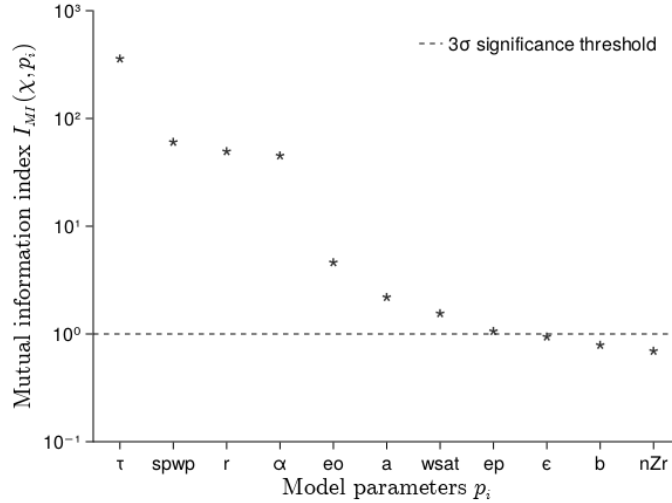
Figure 16: Relative sensitivity of χ to the different model parameters p_i measured by the mutual information index I_{MI}. Values larger than $I_{MI} = 1$ (dashed line) lie above the significance threshold.

for all model parameters p_i is provided in Figure 16. The atmospheric transport parameter τ is by far the most influential parameter, followed by the soil parameters permanent wilting point s_{pwp} and runoff exponent r, and the land fraction α. Some of the remaining parameters also have I_{MI} values above or close to the significance threshold (dashed line) but we do not discuss them in detail due to their rather small contributions to the overall sensitivity. Note that the relative importance of different parameters for χ is not caused or reflected by the relative magnitude of the moisture fluxes associated with these parameters. For instance, the fact that two important parameters, τ and α, both appear in the advection term does not imply that advection is the strongest flux, in fact it never is as illustrated in Figure 15. The importance of τ and α is also not related to the fact that advection is the only linear flux parametrization. A similar sensitivity analysis for a model version with linear expressions for all moisture fluxes (not shown) still identified τ and α as the parameters with the strongest control on χ.

Figure 17 shows scatter plots of χ versus the four most influential model parameters. The respective mean of χ values along each parameter is shown by a white line and the spread around this mean is generated by variations in all other model parameters. In this section, we discuss the physical mechanisms by which these most important parameters influence χ.

A.5.1 *Atmospheric transport parameter τ*

The relationship between χ and τ in Fig. 17a is strongly nonlinear and leads to variations of the χ mean between 0.5 and 0.98, confirming the high sensitivity determined in the mutual information analysis. Physically, τ corresponds to the fraction of the domain length that moisture can travel horizontally in the atmosphere in one day. As such, it can be interpreted as the efficiency of atmospheric moisture transport or efficiency of horizontal mixing: The higher the value of τ, the more efficient the mixing, and the lower the moisture differences, $\Delta w = w_o - w_\ell$, between the two atmospheres. Since we link precipitation and atmospheric
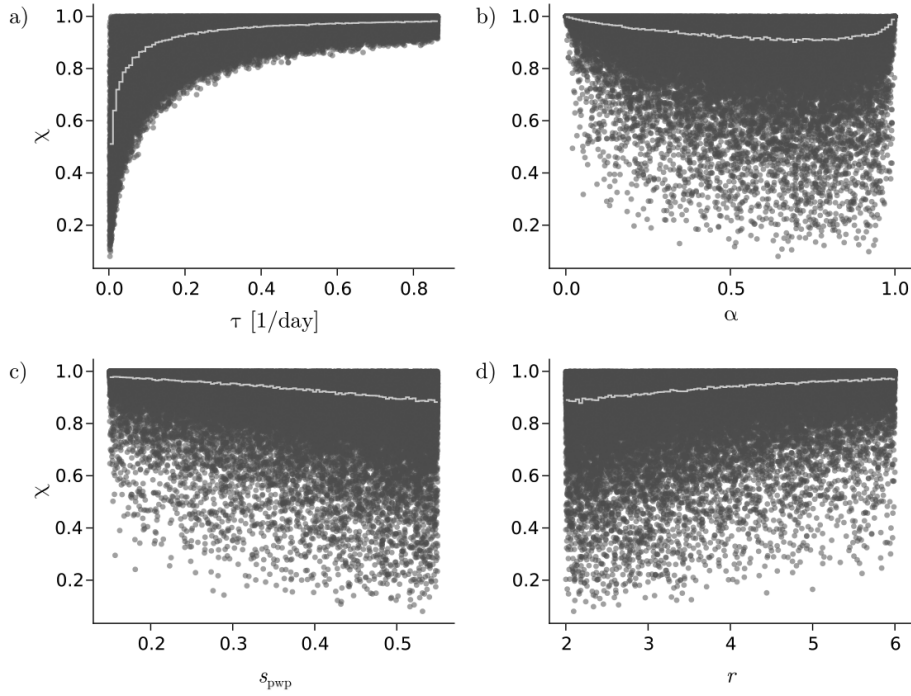
Figure 17: Precipitation ratio χ versus atmospheric transport parameter τ, land fraction α, permanent wilting point s_{pwp} and runoff exponent r. The white lines show χ mean values computed for 100 bins along the parameter axis.

moisture through the same parametrization $P(w)$ over land and ocean, a small Δw implies similar precipitation rates over land and ocean and a χ value close to one. In contrast, inefficient mixing due to small values of τ can sustain larger moisture differences between land and ocean and leads to smaller values of χ. This theoretical control of τ on χ is confirmed in Fig. 17a where χ tends to be small for low values of τ and converges towards one as τ increases. The spread around the τ mean is reduced as τ increases, making τ a better predictor for χ, the larger its value. Fig. 17a also suggests that τ has a strong control on the lower bound of the spread around the χ mean which increases with τ. In contrast, the upper bound of the spread, $\chi = 1$, seems independent of τ.

We can understand how τ influences the lower bound of the spread of χ values by returning to the advection equations (17) and (18), each of which can be rephrased as the product of Δw and an advection efficiency, namely τ/α for land advection and $\tau/(1-\alpha)$ for ocean advection. Only if both advection efficiencies are low, a large moisture difference and, hence, small χ can be sustained. The land fraction affects ocean and land advection efficiencies in opposite ways, suggesting a minimum of overall advection efficiency for intermediate α. If advection was the only process at play, this minimum would be located at $\alpha = 0.5$, and it would be left to τ to set the final value of the lowest possible advection efficiency, and thereby the smallest possible χ for that value of τ. In the following, we will see that the complexity of land-atmosphere interactions adds further parameter controls on the lower bound of χ and leads to an asymmetry in the relationship between χ and α such that the lowest χ value is found at a larger land fraction than $\alpha = 0.5$.

A.5.2 *Land fraction α*

Fig. 17b illustrates how α impacts the value of χ. The χ mean varies between 0.91 and 1.0 on a u-shaped line between the extreme cases of an ocean-only, $\alpha = 0$, and land-only, $\alpha = 1$, scenario where in both cases χ is close to one. As for τ, the impact of land fraction changes on the value of χ is rooted in their control on the advection efficiencies, τ/α and $\tau/(1-\alpha)$. The particular role of α is to differentiate between the efficiency of moisture export out of the ocean subdomain and the efficiency of moisture import into the land subdomain by setting the different areas over which the advected moisture gets distributed. If α is small, the imported moisture gets distributed over a small land size, making land advection efficient and the rate per unit area high. The reverse applies for a large land fraction. In either case, mixing between the two atmospheres is efficient and the smaller atmosphere adopts the moisture conditions of the larger one, resulting in a χ value close to one.

While the model cannot handle the exact endpoints of the α-range, we can examine them in a thought experiment: Imagine a domain fully covered by ocean. Water balance would require the ocean precipitation to balance ocean evaporation, $P_o = E_o$. If we now introduced an infinitesimal patch of land, some of the evaporated moisture would be advected into the tiny land atmosphere without significantly altering the moisture conditions over the vast ocean. Since τ/α is high, the atmospheric conditions over land would rapidly converge to those over the ocean. Hence, for such small α, the system is expected to behave as if the land did not exist. Atmospheric conditions would be overall moist with nearly the same land and ocean precipitation rates close to E_o, leading to a χ of one. At the other extreme, imagine a pure land domain but with the assumption that runoff to some external reservoir remains possible. The runoff would continuously reduce the soil moisture saturation and with it evapotranspiration and precipitation until the trivial equilibrium solution $\{s = 0, w_\ell = 0\}$ is reached. Allowing for advection from an infinitesimal ocean would not change the picture much. With high efficiency $\tau/(1-\alpha)$, almost the entire but nevertheless small amount of evaporated oceanic moisture would be exported to the land, leaving behind a fairly dry ocean atmosphere and hardly affecting the dry state of the large land atmosphere and soil. Hence, the system would behave as if the ocean did not exist with similarly low precipitation rates close to zero in both subdomains.

The transition between the ocean-only and land-only scenario is best understood by examining the individual rain rates P_o and P_ℓ over the range of α as shown in Figure 18. The two extremes are connected by a regime of monotonic drying as the ocean surface – the only true source of moisture for the system's hydrological cycle – shrinks. Although not shown, the overall reduction of available moisture as the land fraction increases also manifests itself in a soil moisture decrease. We can investigate the shapes of P_ℓ and P_o theoretically, assuming all parameters except α to be fixed. Expressions for the rain rates are found by imposing equilibrium conditions on Eqs. (11) and (12), yielding

$$P_\ell = E_\ell(s(\alpha)) + \Delta w(\alpha)\frac{\tau}{\alpha} \tag{22}$$

$$P_o = e_o - \Delta w(\alpha)\frac{\tau}{1-\alpha}. \tag{23}$$

Note that $s(\alpha)$ and $\Delta w(\alpha)$ are implicit functions of the land fraction but that we lack analytical expressions for them. As α increases in Fig. 18, P_ℓ decreases more strongly than
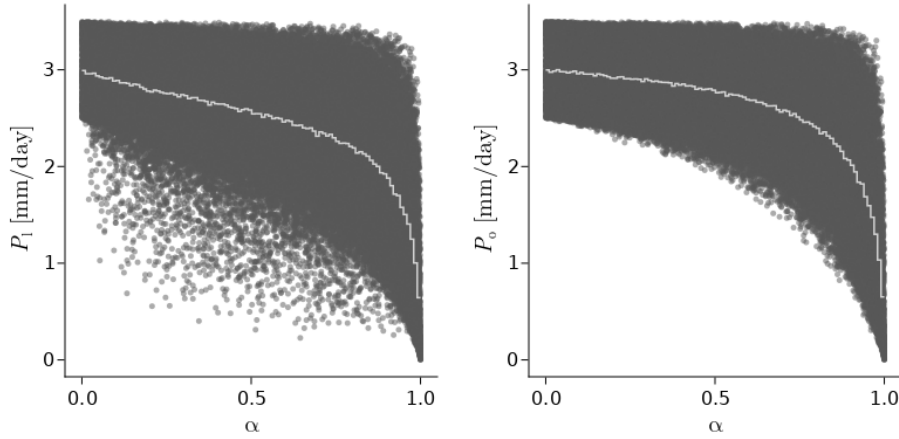
Figure 18: Ocean precipitation rate P_o and land precipitation rate P_ℓ versus land fraction α. The white lines show χ mean values computed for 100 bins along the α axis. The transition from an ocean-only to a land-only model scenario is marked by a decrease of both precipitation fluxes, indicating overall moist conditions for small land fractions and dry conditions for large land fractions.

P_o because land precipitation is not only affected by (initially sharply) decreasing $1/\alpha$ but in addition by a reduction in evapotranspiration as s declines. In contrast, ocean precipitation is only reduced by (initially weakly) increasing advection. The additional influence of α on P_ℓ through E_ℓ causes the asymmetry of the $\chi(\alpha)$-mean in Figure 17b with a minimum around $\alpha = 0.75$ instead of 0.5. Although $\chi(\alpha)$ is expected to be u-shaped for every combination of the other parameter values, the exact location of the minimum will differ. Generally, the width of the spread of χ values indicates that the land fraction is the dominant predictor for χ near its extreme values but that its influence weakens towards intermediate values.

With the understanding of the influence of α developed in this section, we can now explain the first two seemingly unphysical behaviors in Figure 3, as described at the end of Section A.4. They concern the fact that there is hardly any rain over the ocean when the soil is dry and that ocean advection tends to decrease with increasing s while land advection increases. The model runs which populate the regime of low soil moisture in Figure 15 share the property of large land fractions and therefore equilibrate to overall dry conditions, both over land and over ocean. Both atmospheres can consequently only yield very little rain. The amount of moisture exchanged between land and ocean translates to an advection rate per unit area that is high for the small ocean and low for the large land. The opposite situation is found at the largest s values in Figure 15 which originate from model runs with very small α. There, A_ℓ is at its maximum while A_o nearly vanishes. In the intermediate s-regime, values of α are intermediate and have little influence on the shape of the fluxes.

A.5.3 *Permanent wilting point s_{pwp} and field capacity s_{fc}*

Variations in the soil parameters lead to mean variations of χ similar to the effects of land fraction changes, with the mean varying between $\chi = 0.88$ and 0.98 for both the permanent wilting point (Fig. 17c) and the runoff exponent (Fig. 17d). In Figure 17c, χ shows an almost

linear decrease for an increase in s_{pwp}. To understand this behavior, another thought experiment is helpful: Let us consider a system in equilibrium for some value of the permanent wilting point, e.g. $s_{pwp} = 0.3$, and examine how the system would respond if this value was suddenly changed to $s_{pwp} = 0.4$, as illustrated in Figure 19. The presented arguments assume that the other parameter values stay fixed when varying s_{pwp} but we can see from the right panel of Fig. 19 that the influence of the permanent wilting point also leaves its imprint on the mean soil moisture state (white line) in the form of a clear increase with s_{pwp}. We therefore make use of the mean value for illustration purposes. The left panel of Figure 19 depicts the evapotranspiration curves for $s_{pwp} = 0.3$ and 0.4, respectively, with fixed $e_p = 5.0\,\text{mm day}^{-1}$. Because s_{pwp} and s_{fc} are equidistant for different soil types, a change of s_{pwp} merely shifts the evapotranspiration curve along s.

The mean soil moisture value in the CM data for $s_{pwp} = 0.3$ is $s = 0.45$. This initial state for our thought experiment and its corresponding evapotranspiration value are displayed as blue dots in Figure 19. An abrupt increase of the permanent wilting point to $s_{pwp} = 0.4$ would lead to the following sequence of events: First, evapotranspiration experiences an instantaneous drop ΔE_{inst} (first red arrow connecting the blue and green dots). The green dot represents a temporary state where the model is not in equilibrium because the soil receives more moisture from precipitation than it loses through evapotranspiration and runoff. Consequently, the soil moistens. As time progresses, the system attains a new equilibrium state (orange dot) at a higher s value. However, as the soil moistens, not only evapotranspiration but also runoff increases so that the soil does not moisten enough to reach the initial E_ℓ flux. As a consequence, the land atmosphere becomes drier and land advection increases. Since the ocean atmosphere needs to supply more moisture to the land, w_o decreases. Therefore, the increase in advection from increased Δw, needed to balance the increased runoff, is only possible if w_ℓ decreases more strongly than w_o. Accordingly, P_ℓ decreases more strongly than P_o which explains why χ declines with increasing s_{pwp}.

In effect, the new equilibrium for a larger s_{pwp} value would be characterised by a moister soil with larger runoff but reduced precipitation, thus leaving less moisture to evapotranspiration. The new E_ℓ would be ΔE_{eq} smaller than its initial value. This response to an increase in s_{pwp} is also responsible for the third seemingly unphysical behavior, namely the decline of evapotranspiration for intermediate s values previously seen in Figure 15. Precipitation and evapotranspiration are reduced because states with moister soils correspond to simulations with larger s_{pwp}.

A.5.4 *Runoff exponent* r

The relationship between χ and r in Figure 17d resembles $\chi(s_{pwp})$ but with opposite trend: χ increases with r while it decreases with s_{pwp}. Indeed, the similarity originates from a similar physical mechanism. In the formulation of the runoff fraction, $R_f = \epsilon s^r$, r enters as the exponent. As for the s_{pwp}-dependence, we can conduct a thought experiment, starting from a system in equilibrium which then responds to a sudden increase of r. Since s has values between zero and one, an increase of the runoff exponent reduces the value of R_f and soil moisture increases. As a consequence, also both atmospheres start to moisten: First, w_ℓ increases through increased evapotranspiration from the wetter soil, thereby reducing the moisture difference between land and ocean. Second, the reduction of Δw implies reduced advection with the effect that the ocean atmosphere retains more of its moisture and w_o increases. Eventually, the decreasing advection matches the runoff which started
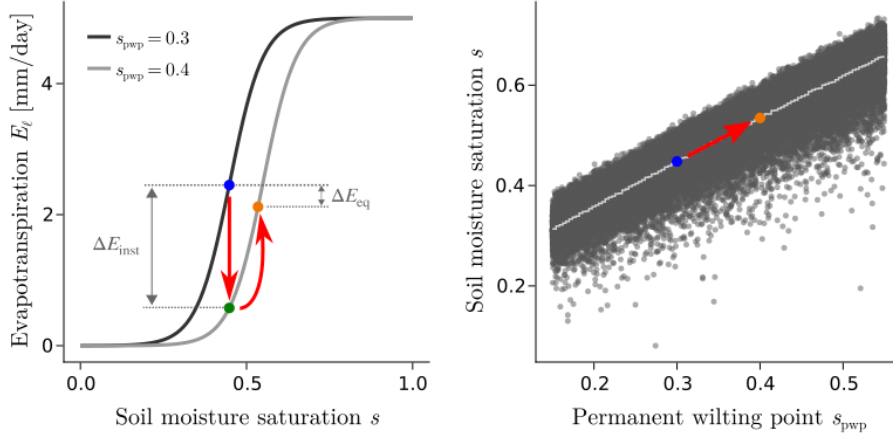
Figure 19: Influence of an increase in s_{pwp} on the equilibrium state. Left: Higher values of s_{pwp} shift the graph of the E_ℓ parametrization towards larger s. Right: Equilibrium values of the soil moisture saturation from CM data plotted against s_{pwp} values. The blue dots mark the initial equilibrium state, the green dot represents a temporary state of soil moisture imbalance due to a sudden increase of s_{pwp} and the orange dot marks the eventually attained equilibrium state for the new s_{pwp} value.

to intensify again after the initial drop. A new equilibrium is attained in which runoff is reduced compared to the initial state with lower r value. Equally reduced land advection with lower Δw reflects more similar atmospheric moisture conditions and, hence, increased χ.

Equilibrium states with higher r value also have stronger precipitation rates from higher w_ℓ and w_o. In Figure 15, we see the influence of r in both the low and high soil moisture regime, where it works in tandem with the land fraction to shape the moisture fluxes. Both precipitation increases for low and high s, respectively, correspond to a combination of increasing r and decreasing α. In these regimes, the combined influence of r and α dominates over the influence of s_{pwp} discussed earlier.

A.6   UNDER WHICH CIRCUMSTANCES CAN χ BECOME LARGER THAN 1?

So far, we concluded that χ is bounded by an upper limit of one due to the necessity of a net moisture transport from ocean to land and the assumption that the efficiency with which atmospheric moisture is turned into precipitation is the same over land and ocean. However, we know of local systems in the real world for which higher rain rates are observed over land compared to the adjacent ocean. For instance, Qian, 2008, Sobel et al., 2011, Cronin et al., 2015, Wang and Sobel, 2017 and Ulrich and Bellon, 2019 found precipitation enhancement over tropical islands and attributed this observation mainly to the development of sea breezes triggering precipitating convection over the islands. Even for the full tropics, some observations suggest a χ value slightly larger than one (Hohenegger and Stevens, 2022). By construction, our simple model cannot yield χ values larger than one which can be interpreted as a tendency to underestimate real precipitation ratios. In the following, we explore different ways in which our model framework could be modified to enable precipitation enhancement over land, i.e. $\chi > 1$.

A.6.1   *Relaxing assumptions of the closed model*

To begin with, we started out with the hypothesis that precipitation is neither favored by land, nor ocean, meaning that different surface characteristics do not affect the way it rains: for the same water vapor path, the model computes the same amount of rain over land and ocean. In reality, while we can generally expect a moister atmosphere to yield more rainfall, the shape of $P(w)$, determined by the values for the a and b parameters, could differ over different surfaces. With its tendency for too low χ values, our model suggests that our initial hypothesis about $P(w)$ was wrong and that in reality, precipitation is actually favored over land. In the model, we can favor precipitation over land most easily by choosing a smaller b parameter over land than over ocean, leading to higher precipitation rates over land than over ocean for the same water vapor path. As a proof of concept, we ran model simulations with different choices for b over land and ocean. When choosing b just 0.1 % smaller over land than over ocean, already about 20 % of the simulations yielded a χ value larger than one. That it rains differently over land and ocean would be in line with the conclusions of Hohenegger and Stevens, 2022 who found more precipitation over tropical land than what is expected based on the tropical land-sea distribution and rainbelt position, and also with the results of Ahmed and Schumacher, 2017 who found distinct differences in the $P(w)$ relationships over land and ocean based on observations. Further studies examining differences in $P(w)$ over different surface types, and constraining the realistic ranges of the a and b parameters are needed to conclude whether precipitation processes are responsible for the higher χ values found in nature.

Second, we treat all model boxes as being homogeneous and well-mixed which allows us to work with mean fluxes rather than resolving the horizontal direction explicitly. It is well-known, however, that an airstream traversing an oceanic region will moisten along its trajectory since mean ocean evaporation typically exceeds mean ocean precipitation and the reverse applies to land regions. Furthermore, Ogino et al., 2016 and Ogino et al., 2017 found that the conventional view in which Earth's surface gets divided into ocean and land misses out on particular interactions driven by the land-sea contrast which are confined to a coastal region, a few hundred kilometers seaward and landward from the coast. These coastal regions receive more rain than both the open ocean and inland continental regions. Also Bergemann and Jakob, 2016 found that tropical rainfall over land associated with coastal effects such as sea breezes can occur under drier atmospheric conditions than rainfall over the open ocean. Hence, adding coastal zones with a specific coastal precipitation parametrization to the model is another flavor of the argument that – for precipitation enhancement over land – it has to rain differently in different subdomains. Coastal zones might also capture the fact that precipitation enhancement is particularly strong over relatively small land masses where coastal effects are expected to be more influential.

Third, the model has neither an energy budget, nor a diurnal cycle. As a consequence, phenomena associated with pressure gradient forcing like diurnal sea breezes which tend to enhance precipitation over land are not captured. Energy-dependence and a diurnal cycle can be implemented in different ways – either fundamentally by coupling water balance and energy balance equations, or indirectly by introducing a diurnal cycle in energy-dependent parameters such as τ, e_p or w_{sat}. Even with the same $P(w)$ relationship across the domain, a diurnal cycle may lead to $\chi > 1$ through two pathways: Evapotranspiration might be enhanced more strongly than ocean evaporation during the day. At the same time, the wind field would become variable and might exhibit convergence over land, potentially

leading to up-gradient moisture transport which was formerly disabled due to the assumption of a constant background wind speed. The combined effect of these two pathways may lead to a high enough concentration of moisture over land during the day to yield higher temporary rain rates over land than over ocean. If the reverse transport during the night does not fully compensate for the daytime precipitation signal, then χ might be larger than one on average. In other words, the diurnal cycle of available energy may explain why χ is close to one and can even be larger than one in reality.

Last, our model configuration with one land and one ocean box is not representative of the real tropics. It is likely that a different land distribution with more boxes would lead to higher χ values because smaller box sizes generally increase the advection efficiencies. If, in addition, the boxes were differently sized, we might see instances where χ > 1. In equilibrium, each ocean atmosphere would still be moister than the leeward land atmosphere but it cannot be precluded that weighting the precipitation rates by the different box sizes would yield a stronger mean land than ocean precipitation.

A.6.2 *Opening the closed model*

The previous arguments still treat the land-ocean-atmosphere system as a closed model. This assumption may be valid over the full tropics, assuming a negligible net moisture exchange with the extratropics, but it is certainly invalid over islands, where land precipitation enhancement is typically observed. Hence, allowing for atmospheric inflow and outflow out of the domain might create χ values larger than one. We test this hypothesis in two ways.

First, moisture import or export from an external environment outside the model boundaries can be incorporated by an additional advection term, A_{ext} in mm day^{-1} in Equation (12) for oceanic water vapor. A positive A_{ext} denotes inflow of external moisture, while a negative A_{ext} means that the ocean atmosphere loses moisture through the model boundaries. This construction mimics the case of an island surrounded by an ocean under the influence of lange-scale convergence or divergence. But is this change in the model framework sufficient to create scenarios for which χ > 1?

We argue that the answer is no: Regardless of whether the system is gaining or losing moisture through its boundaries, an equilibrium state still requires a net transport of moisture from ocean to land, and therefore $w_o > w_\ell$ with χ < 1. The term A_{ext} acts in a similar fashion as ocean evaporation. Under the influence of moisture convergence, the positive A_{ext} is equivalent to an increase in E_o and merely increases the moisture content in all boxes. In the case of moisture divergence, negative A_{ext} acts like a reduction of E_o and an overall drier equilibrium state is attained as long as $|A_{ext}| < E_o$. If the loss through the model boundary is stronger than the moisture input from the ocean surface, the system will undergo drying until the trivial solution $\{w_o = 0, w_\ell = 0, s = 0\}$ is reached.

Second, we can also open the model by allowing moisture to enter the domain from one side and leave it on the other side. As an illustrative example for this type of *open model*, we consider the simplest configuration with a land box of length L_ℓ, placed between two equally big ocean boxes of lengths $L_{o1} = L_{o2}$. The subscript 'o1' refers to the ocean in front of the island as seen by the airflow horizontally traversing the domain at constant wind speed, while 'o2' refers to the ocean behind the island. The equations governing the evolution of w_{o1}, w_ℓ and w_{o2} and s are formulated in analogy to the closed model equations and can be found in the Appendix along with a model sketch. This open model

requires one additional parameter, the boundary water vapor path w_0 with values between 0 mm and w_{sat}, which denotes the water vapor path at the windward model boundary. It enters the model equations in the advection term for the first ocean. As for the closed model, we perform 100 000 simulations with randomly chosen combinations of parameter values from Table 1 with the modification that the full domain length is varied between 200 and 2000 km. The obtained set of equilibrium solutions is refer to as "OM data".

In the closed model, χ is computed from mean precipitation rates $\bar{P}_\ell$ and $\bar{P}_o$ as

$$\chi = \frac{\bar{P}_\ell}{\bar{P}_o} = \frac{2P_\ell}{P_{o1} + P_{o2}}. \tag{24}$$

As in the case of the closed model, equilibrium can only be attained if the land atmosphere receives advected moisture from the ocean. In the open model, this means that the first ocean atmosphere has to be moister than the land atmosphere which – sticking to the assumption of the same parametrization for precipitation across the domain – implies $P_{o1} > P_\ell$. It follows from Equation (24) that a χ value larger than one is possible if the inequality, $P_{o2} < 2P_\ell - P_{o1}$, is fulfilled. This means, the second ocean atmosphere must be dry enough to compensate for the relatively moist first ocean atmosphere, such that the mean ocean precipitation is smaller than P_ℓ. From the OM data, we find that only about 6.7 % of all simulations meet this condition and yield $\chi > 1$. As expected, these simulations have in common that atmospheric moisture reduces along the wind trajectory, i.e. $w_0 > w_{o1} > w_\ell > w_{o2}$.

We perform the same sensitivity analysis as for the closed model to understand which parameter combinations lead to χ values larger than one, and to which parameters χ is most sensitive. Opening the model does not fundamentally change the principal sensitivities but modifies their order of importance: The most sensitive parameter is now w_0 with $I_{MI}(w_0, \chi) = 254$, followed by α with $I_{MI}(\alpha, \chi) = 202$ and τ with $I_{MI}(\tau, \chi) = 147$. All other parameters, including the formerly relevant soil parameters, have I_{MI} values lower than 8 and can be neglected as predictors for χ. To understand which parameter combinations lead to $\chi > 1$, Figure 20 shows PDFs of the values of w_0, α and τ for simulations with χ values smaller and larger than one in blue and orange, respectively. Even though the distributions have a significant overlap, $\chi > 1$ requires a large enough boundary water vapor path $w_0 \gtrsim 38$ mm and becomes more likely with smaller land fractions. States with $\chi > 1$ do not exist for $\alpha > 0.93$ and are most likely around $\alpha = 0.05$. In contrast, a value of $\chi > 1$ seems to be possible with any value for τ. Further inspection of the state variable values (not shown) reveals that equilibrium states with $\chi > 1$ are overall moist. Soil moisture saturation values cluster close to and beyond the field capacity. Water vapor path values peak around 48 mm over both land and ocean and never get smaller than 38 mm. Simulations with $\chi < 1$, in contrast, exhibit equilibrium states across the entire moisture spectrum, including very dry states with soil moisture values below the permanent wilting point.

As in the case of the closed model, the open model results are subject to the choice of the land distribution and may change for different numbers of land boxes. In addition, the open model is sensitive to the location of the land box which affects the relative size of the two ocean boxes. However, a test of different asymmetric configurations indicates that the presented statements are only affected quantitatively, not qualitatively.
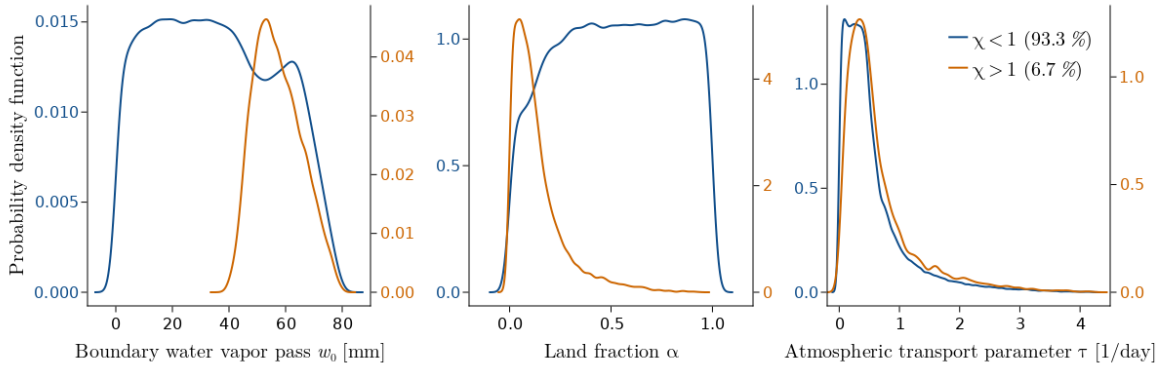
Figure 20: Probability density functions of parameter values for w_0, α and τ. Blue and orange graphs contain data from simulations with χ values smaller and larger than one, respectively. Ratios larger than one are only found for 6.7 % of all simulations.

A.7 CONCLUSIONS

This study was motivated by our lack of theoretical understanding of how tropical precipitation gets partitioned between land and ocean. To provide such understanding, we studied constraints and sensitivities of the precipitation ratio χ, quantifying the ratio between spatio-temporally averaged land and ocean precipitation rates, $\chi = P_\ell/P_o$. Estimates of χ from different observation products range between 0.9 and 1.04 (Hohenegger and Stevens, 2022). We wanted to know how various atmospheric and land processes determine the value of χ and whether constraints on χ arise from the condition of water mass balance.

We introduced a conceptual box model that describes the rate of change of soil moisture and atmospheric moisture over ocean and land, respectively. The water balance components are expressed by empirical parametric functions of the mean water content of the land and atmospheric boxes. In particular, as a hypothesis, we assumed that precipitation increases exponentially with water vapor path and that the presence of land does not affect this relationship. In order to investigate the bounds of χ and its parameter sensitivity, we analyzed a large number of equilibrium solutions for different combinations of model parameter values. The obtained results for the case of a closed model with one land and one ocean box can be summarized as follows:

- As long as the land does not affect the relationship between precipitation and water vapor path, χ is bounded by an upper limit of one. This is a direct consequence of the equilibrium condition that the land's loss of water through runoff needs to be compensated for by an equally large net moisture transport from a moister ocean atmosphere to a drier land atmosphere. As precipitation increases exponentially with water vapor path, this necessarily implies stronger precipitation over ocean.

- The lower limit of χ is zero in cases where the land precipitation is zero. Although χ can theoretically vary between zero and one, values between 0.75 and 1.0 appear most likely, with 95 % of the simulations falling into this range.

- The free model parameters are listed in Table 1. We find that χ is most sensitive to a variation of the atmospheric transport parameter τ, followed by the two soil

parameters permanent wilting point s_{pwp} and runoff exponent r, and land fraction α. Efficient atmospheric transport for high τ values assimilates the land and ocean atmospheres which results in high χ values. Land fraction is most influential near its extreme values, $\alpha \to 0$ and $\alpha \to 1$, where in both cases χ is close to one. Near these extremes, the highly efficient advection rate into or out of the respective tiny land or ocean atmosphere creates similar atmospheric conditions in both boxes. A χ minimum is located at intermediate α values. Finally, χ decreases with increasing permanent wilting point and increases with increasing r. This can be understood from the way in which these parameters control the amount of evapotranspiration (for s_{pwp}) and runoff (for r), and thereby the amount of advective moisture inflow into the land atmosphere required for equilibrium. A larger moisture inflow corresponds to a larger moisture difference between land and ocean atmospheres and, hence, to a lower value of χ.

- The closed water balance model cannot explain observed island precipitation enhancement as reported by other studies because χ is bounded by one. Our interpretation of this finding is that precipitation enhancement over land requires the land to affect the relationship between precipitation and water vapor path, that precipitation enhancement is linked to the presence of a diurnal cycle, that a different land distribution is required, or that it is only possible in an open model which allows for net advection into or out of the domain. We tested this last option with an open model configuration in which moisture can enter the model through the windward boundary and leave on the other side. For this setup, χ values larger than one exist for a small subset (6.7 %) of the performed simulations. These cases require a sufficiently large moisture inflow with a boundary water vapor path of at least $w_0 = 38\,mm$, and small land sizes, typically around $\alpha \approx 0.05$ and no larger than $\alpha = 0.93$. The most influential parameters for the open model are w_0, α and τ, while the soil parameters are no longer important.

Even though the simple conceptual model does not capture the full range of physical processes that influence the land-sea precipitation contrast in reality, it is able to constrain χ and identifies the efficiency of atmospheric transport as the dominant factor controlling the value of χ. In fact, understanding how advection changes following a change in the model parameter values turned out to be key for understanding how the value of χ changes.

Data availability statement. The code base used for generating the data and figures for this work is freely available at https://github.com/Lucalino/OcelandModel.

OPEN MODEL FORMULATION

The equations governing an open model configuration with an island (subscript 'ℓ') between two ocean boxes (subscripts 'o1' and 'o2' in the order of their appearance along the wind trajectory) are similar to the ones for the closed model introduced in Section A.2. However, four instead of three equations are needed,

$$\frac{ds}{dt} = \frac{1}{nz_r} \left[P(w_\ell) - R(s, w_\ell) - E(s) \right] \tag{25}$$

$$\frac{dw_{o1}}{dt} = E_o - P(w_{o1}) + \frac{(w_0 - w_{o1})u}{L_{o1}}. \tag{26}$$

$$\frac{dw_\ell}{dt} = E(s) - P(w_\ell) + \frac{(w_{o1} - w_\ell)u}{L_\ell} \tag{27}$$

$$\frac{dw_{o2}}{dt} = E_o - P(w_{o2}) + \frac{(w_\ell - w_{o2})u}{L_{o2}}, . \tag{28}$$

The lengths of the model subdomains can be written as $L_{o1} = L_{o2} = (1 - \alpha)L/2$ and $L_\ell = \alpha L$, where L denotes the full model domain length.

For a small number of parameter combinations, the algorithm could not determine an equilibrium solution to the open model equations.

Figure 21: Sketch of a land-ocean-atmosphere system consisting of an island between two ocean boxes with atmospheric boxes above. The lateral model boundaries are open, allowing moisture to enter and leave the modelled domain. The water vapor path value at the windward model boundary is given by the parameter w_0 and may reflect synoptic-scale atmospheric conditions. Moisture fluxes between boxes are analogous to the closed model described in Section A.2.

B

PRECIPITATION ENHANCEMENT OVER TROPICAL LAND THROUGH THE LENS OF THE MOISTURE-PRECIPITATION RELATIONSHIP

The work in this appendix has been submitted as:

Precipitation Enhancement over Tropical Land through the Lens of the Moisture-Precipitation Relationship

Luca Schmidt[1,2] & Cathy Hohenegger[1]

[1]Max Planck Institute for Meteorology, Hamburg, Germany
[2]International Max Planck Research School on Earth System Modelling (IMPRS-ESM), Hamburg, Germany

ABSTRACT

Tropical precipitation P has been found to be related to column relative humidity r by a simple relationship known as the moisture-precipitation relationship $P(r)$. Based on one decade of daily ERA5 reanalysis data, we test whether $P(r)$ is able to reproduce the tropical land-ocean precipitation contrast measured by χ, the ratio between mean precipitation over land and ocean. We find that $P(r)$ captures the mean seasonal cycle of χ as long as we account for the fact that $P(r)$ is distinct over land and ocean, and that it varies seasonally. Typical values of χ above 0.86 imply that precipitation is enhanced over land, relative to the ocean. We therefore investigate next whether this enhancement is due to the differences in $P(r)$ and/or in the humidity distribution between land and ocean. We show that, rather than enhancing precipitation, the presence of land modifies $P(r)$ in such a way that precipitation is disfavored compared to over ocean. Precipitation enhancement over land is instead explained by the modified terrestrial humidity distribution that features a more pronounced tail towards high r values compared to the one over ocean. All results rest on an accurate construction of $P(r)$ from the underlying data. Simple fit models such as an exponential function that were proposed by previous studies are unable to capture the seasonal cycle of χ and fail to explain land-ocean differences in precipitation.

B.1 INTRODUCTION

Tropical precipitation is related to atmospheric humidity through a statistical, roughly exponential relationship, known as the moisture-precipitation relationship. Using satellite observations, Bretherton et al., 2004 showed that this moisture-precipitation relationship holds over all tropical oceans. A similar, albeit not identical moisture-precipitation relationship was found over tropical land (Ahmed and Schumacher, 2017; Schiro et al., 2016). In this work, we investigate what the moisture-precipitation relationship can teach us about the controls on the land-ocean contrast of tropical precipitation.

The land-ocean contrast of tropical mean precipitation can be quantified by the precipitation ratio χ, which denotes the ratio of spatiotemporal mean precipitation over tropical land and ocean. Defining the tropics as the region between $\pm30°$N, Hohenegger and Stevens (2022, hereafter HS22) found climatological values of χ between 0.90 and 1.04 in observations. They further derived a conceptual model for the distribution of tropical precipitation in the form of a rainbelt. Given the geometry of the tropical land masses as well as the latitudinal range of the rainbelt's seasonal migration, HS22 showed that values of χ can only be explained if precipitation characteristics, such as the rainbelt's width, location, or intensity, are modified by the land surface in a way that precipitation is enhanced over

land. HS22 calculated a theoretical threshold value of $\chi = 0.86$ above which precipitation is enhanced over tropical land.

The moisture-precipitation relationship $P(r)$ which links mean precipitation rate P to column relative humidity r was formally introduced by Bretherton et al., 2004 but several previous works such as the early study by Austin, 1948 or later works by Raymond and Torres, 1998 and Tompkins, 2001 already described a strong correlation between precipitation and ambient humidity, in particular humidity of the lower free troposphere. Various explanations for this strong correlation were proposed in the literature including the impact of lateral entrainment of moist air on plume buoyancy (e.g. Tompkins, 2001; Derbyshire et al., 2004; Holloway and Neelin, 2009; Muller et al., 2009), convective downdrafts that inject moist air into the boundary layer, thereby changing the boundary layer stability (e.g. Tompkins, 2001; Muller et al., 2009), or tropical convection as an instance of self-organized criticality in the context of continuous phase transitions (Peters and Neelin, 2006).

Owing to its simplicity and apparent generality, analytical formulations of $P(r)$ have been used to parameterize precipitation in conceptual models. We employed $P(r)$ as a parametrization in a previous study aiming at understanding the controls on χ using a simple box model based on water balance equations (Schmidt and Hohenegger, 2023, hereafter SH23). Consistent with HS22, even though methodologically independent, we found that precipitation enhancement over tropical land, as observed in the real world, requires the land surface to influence the way it rains. In the framework of the box model, in which humidity over land and ocean are each represented by a single mean value, this implies that the moisture-precipitation relationship must be distinct over land and ocean such that it rains more over land for a given value of r. Ahmed and Schumacher, 2017 analyzed differences in $P(r)$ between various tropical land and ocean regions and indeed found systematic differences between the two surface types. Over land, $P(r)$ typically picks up at an earlier threshold value of r but then flattens more towards high r. Thus, the $P(r)$ curve over land does not generally lie above the one over ocean, but only in some range of r. Apart from the moisture-precipitation relationship, also the humidity distributions over land and ocean can be expected to be distinct but such differences were not investigated by Ahmed and Schumacher, 2017. It is therefore not clear whether differences in $P(r)$ or in the humidity distributions explain precipitation enhancement over land, and which range of r is key to the enhancement.

The aim of this study is to investigate which features of $P(r)$ or differences in the terrestrial and oceanic humidity distributions explain the enhancement of precipitation over tropical land. To this end, we first describe the employed data and methodology in Section B.2. In Section B.3, we evaluate on which spatial and temporal scale we need to sample the variability of $P(r)$ in order to correctly capture the mean behavior of χ over time. In Section B.4, we use the obtained moisture-precipitation relationships and perform sensitivity experiments that disentangle the role of distinct $P(r)$ relationships and distinct humidity distributions over land and ocean in creating precipitation enhancement over tropical land. Finally, we reflect on the dependence of our results on the employed fit model in Section B.5 and conclude with a general summary of our findings in Section B.6.

B.2 DATA AND METHODS

In this work, we assess whether the moisture-precipitation relationship $P(r)$, defined as the relationship between the daily mean precipitation rate P in mm day^{-1} and daily mean

column relative humidity r, can explain the precipitation enhancement over tropical land which is indicated by values of the tropical precipitation ratio higher than 0.86 (HS22). The tropical precipitation ratio is computed as

$$\chi(t) = \frac{\overline{P_\ell}(t)}{\overline{P_o}(t)},$$ (29)

where $\overline{P_\ell}(t)$ represents the daily mean precipitation averaged over tropical land, and $\overline{P_o}(t)$ the daily mean precipitation averaged over tropical ocean. The units of $\overline{P_\ell}$ and $\overline{P_o}$ are mm day^{-1} and t denotes time in days.

B.2.1 *Data selection and variables*

The study is based on 10 years of ERA5 reanalysis data provided by the European Center for Medium Range Weather Forecasts (ECMWF) with a grid spacing of 30 km (Hersbach et al., 2018b; Hersbach et al., 2018a). We consider the tropics between $\pm 30°$N, and select the time period from 1981 to 1990 because in this decade, the ERA5 precipitation ratio χ shows no significant trend related to, for instance, global warming, and the mean seasonal cycle of χ is similar to the one derived from TRMM satellite observations (compare Figure 22 to Figure 6b in HS22).

To evaluate Equation (29) and to derive the P(r) relationship, we use fields of daily mean precipitation P, as well as daily mean column relative humidity r. Column relative humidity is defined as the ratio of column-integrated specific humidity and column-integrated saturation specific humidity. To obtain daily r values, we first compute column relative humidity from hourly fields of temperature T in K, specific humidity q_v in kg kg^{-1}, and pressure p in Pa, and then perform the daily averaging. The saturation vapor pressure, which is needed for the computation of saturation specific humidity, is calculated according to Murphy and Koop, 2005, Equation (10). Note that the ERA5 data contains non-zero entries for atmospheric variables of sub-surface grid cells which need to be masked before computing vertical integrals over the atmospheric column.

B.2.2 *Reconstruction of $\chi(t)$ from P(r)*

To understand the controls on the tropical precipitation ratio through the lens of the moisture-precipitation relationship, we first have to find out what we need to know about P(r) to reconstruct the ERA5 $\chi(t)$ from it. This reconstruction happens in two steps: First, we derive the functional relationship P(r) as an empirical fit to the P and r data. To this end, we take pairs of (P, r) and sort them by ascending r. Next, we divide the r-space, ranging from 0 to 1, into bins of length 0.01, assign the pairs of (P, r) to their respective bin and average the precipitation within each bin. The empirical fit is then the piecewise linear function connecting the bin-mean precipitation values along r. In the second step, we reconstruct daily precipitation fields by applying the obtained P(r) fit to the daily r values from ERA5. The reconstructed precipitation ratio $\chi_{rec}(t)$ can then be computed from the reconstructed precipitation fields using Equation (29).

To complete the first step, we need to make two choices. First, we need to decide on the spatial and temporal resolutions of the P and r data. Second, we need to decide over which temporal and spatial scale we sample P and r when deriving the empirical fit. In
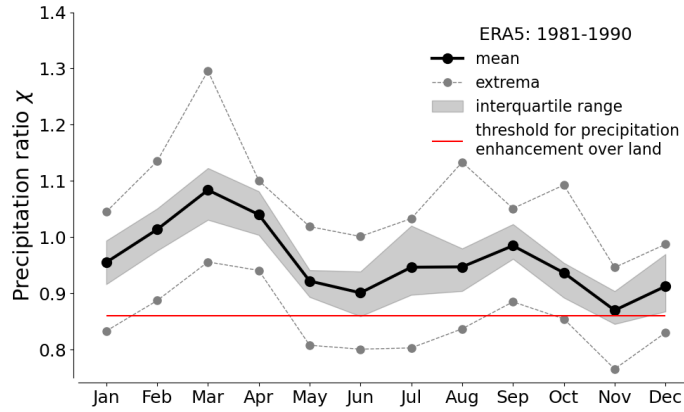
Figure 22: Mean seasonal cycle (solid line) of the precipitation ratio from ERA5 reanalysis data from 1981 to 1990. The interannual variability is shown by the interquartile range of values from individual years (shaded area) and by the extreme values for each month (dashed lines). The red line shows the threshold for precipitation enhancement over land as identified by Hohenegger and Stevens, 2022.

other words, how many empirical fits do we need to adequately account for the variability of the moisture-precipitation relationship in space and time? Regarding the first choice, we decided to use daily, rather than e.g. monthly, P and r data as well as the native grid resolution. This choice was based on two considerations: First, the physical mechanisms proposed as explanations for the tight relationship between P and r, such as entrainment of convective plumes, act locally and on short temporal scales. Second, nonlinear relationships such as $P(r)$ are not scale-invariant, meaning that averaging over r and P values in space or time not only reduces the sampled range of r and P values, it also results in a loss of information about the shape of the relationship. The second choice, namely the spatial and temporal scale for sampling P and r, is investigated in the next section, since it will give us a first answer as to how important land-ocean differences are for reconstructing $\chi(t)$ and, hence, explaining precipitation enhancement over tropical land.

B.3 WHAT DO WE NEED TO KNOW ABOUT $P(r)$ TO CORRECTLY RECONSTRUCT $\chi(t)$?

Apart from the dependence of the retrieved $P(r)$ relationship on the resolution of the underlying data discussed in Section B.2.2, the physical relationship itself may be subject to variability in space and time. To assess this, we compute reconstructions $\chi_{rec}(t)$ from $P(r)$ fit functions that reflect increasingly detailed spatial and temporal knowledge about $P(r)$. The metric for deciding whether the knowledge of $P(r)$ is detailed enough is the comparison of the mean seasonal cycle and year-to-year variability of the reconstructed $\chi_{rec}(t)$ with the benchmark $\chi_{bm}(t)$, where $\chi_{bm}(t)$ is computed directly from the 10-year ERA5 daily precipitation fields using Equation (29). Figure 22 shows the mean seasonal cycle of $\chi_{bm}(t)$ with a solid black line. The year-to-year variability is represented in terms of the interquartile range (gray shading) and 10-year extrema of monthly mean values (dashed lines). Throughout this work, we use the mean and interquartile range as the benchmark against which we test different reconstructions $\chi_{rec}(t)$. The expectation is that these statistical characteristics of $\chi_{bm}(t)$ will only be captured correctly by $\chi_{rec}(t)$ if the knowledge of the underlying $P(r)$ relationship(s) is sufficiently detailed.

B.3.1 *The surface type, being land or ocean, modifies the shape of* $P(r)$

As a first step, we compute $\chi_{rec}(t)$ based on one $P(r)$ relationship derived from all pairs (P, r) which assumes that the same $P(r)$ relationship holds across the full tropics and does not vary with time. This full tropical fit is shown in Figure 23a by the green line. Due to the high nonlinearity of $P(r)$, we use a logarithmic scale for the vertical axis. Further, for better visibility of the relevant ranges of r, we do not display values below $r = 0.3$ as they only contribute insignificantly small amounts of precipitation.

Figure 24a shows the corresponding reconstruction of $\chi(t)$ from the full tropical fit in blue as well as the benchmark in black. The reconstruction from the full tropical fit grossly overestimates $\chi_{bm}(t)$, especially in boreal summer. This overestimation is both due to an overestimation of $\overline{P_\ell}(t)$ by up to 24.58 % and an underestimation of $\overline{P_o}(t)$ by up to 1.23 %. That the reconstruction bias is dominated by a misrepresentation of land precipitation is a first indication for a systematic difference between the two surface types. The full tropical fit not only overestimates the overall magnitude of $\chi_{bm}(t)$, it also misrepresents the seasonal variations.

Both reconstruction biases resulting from the full tropical fit can also be seen in Figure 24b which shows a scatter plot of the monthly mean values of $\chi_{rec}(t)$ from all individual years against the respective benchmark values. The identity line is plotted as a gray dashed line for visual guidance. Most scatter points lie below the identity line, owing to the overestimation of $\chi_{bm}(t)$, and the spread of the scatter cloud is rather large due to the mismatch between the seasonal cycles of $\chi_{rec}(t)$ and $\chi_{bm}(t)$. This mismatch is quantified by the Pearson correlation coefficient c for which we obtain the relatively low value of $c = 0.68$.

In a second step, we test whether accounting for a potential modification of $P(r)$ by the underlying surface type improves the reconstruction. To this end, we compute separate fits $P_\ell(r)$ and $P_o(r)$ to data from land grid cells (P_ℓ, r_ℓ) and ocean grid cells (P_o, r_o), respectively. The two fits are displayed in Figure 23a, where the orange line represents $P_\ell(r)$ and the blue line represents $P_o(r)$. Not surprisingly, the ocean fit is similar to the full tropical fit due to the larger areal extent of the ocean compared to land. There exist notable differences between $P_\ell(r)$ and $P_o(r)$ which can be broadly described in terms of three regimes along r: For $r \lessgtr 0.6$, the mean precipitation is higher over ocean than over land, for $0.6 \lessgtr r \lessgtr 0.78$, the land fit exhibits a 'bump' such that the mean precipitation is higher over land than over ocean, and for values of $r \gtrsim 0.78$, the mean precipitation is again higher over ocean. These regimes of qualitatively different behavior over land and ocean hint at a complex interaction between surface type and $P(r)$ that may not necessarily lead to an enhancement of precipitation over land and which we disentangle further in Section B.4.

Figure 24c and 24d display how $\chi_{rec}(t)$ is improved by using the surface type-specific functions $P_\ell(r)$ and $P_o(r)$ for reconstructing precipitation over land and ocean, respectively. Accounting for the surface type corrects the general overestimation such that this time, $\chi_{rec}(t)$ and $\chi_{bm}(t)$ have the same 10-year mean value of 0.96 and scatter points in Figure 24d lie more symmetrically around the identity line. However, seasonal reconstruction biases persist with an overestimation from May to August, and an underestimation otherwise. Due to these seasonal biases, the correlation is only slightly improved with a correlation coefficient of $c = 0.72$.
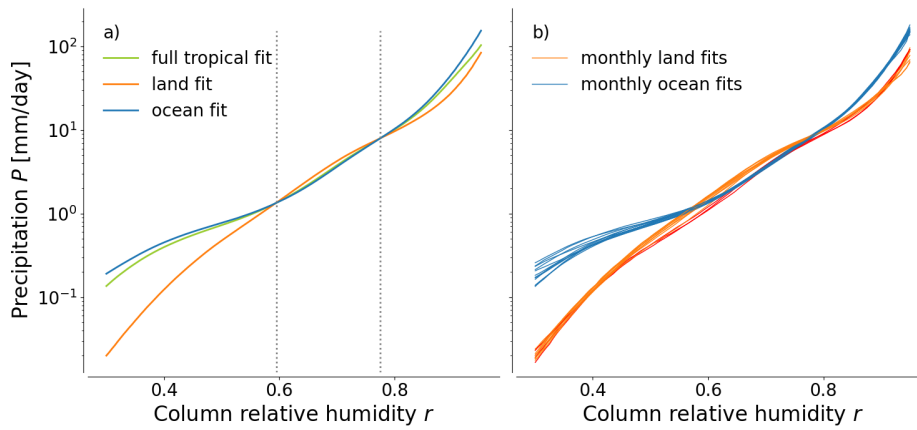
Figure 23: Empirical fit functions of the moisture-precipitation relationship in log-space obtained from different subsets of the underlying daily (P, r) data. The green line in panel a shows the full tropical fit based on all tropical grid points while the orange/red and blue lines in both panel a and b show the land and ocean fits, computed from tropical land and ocean grid points, respectively. Panel a displays fits based on the complete 10-year data set while panel b displays twelve fits derived for the individual months. Vertical dashed lines in panel a mark the approximate intersection points of the land and ocean relationships, and divide the humidity space into three different r-regimes. The land fits for June, July, and August in panel b are colored red to indicate that they do not exhibit the 'bump' relative to the ocean lines which characterizes the middle r-regime.

B.3.2 $P(r)$ *exhibits significant seasonal variations*

The seasonally varying biases in the reconstruction that remain after taking into account the land-sea contrast of the moisture-precipitation relationship suggest a distinct seasonal cycle of $P(r)$ over one or both of the two surface types. In a third step, we therefore derive twelve monthly relationships $P_{\ell,m}(r)$ and $P_{o,m}(r)$, for each surface type, respectively, and with m specifying the month. These monthly mean relationships, are shown in Figure 23b as orange/red lines for the land and blue lines for the ocean. The three red lines correspond to June, July, and August (JJA), and are highlighted due to their qualitatively distinct behavior relative to the corresponding ocean curve. Generally, the variability is stronger over land than over ocean, except for low r values. This variability leads to qualitative changes of the land-sea contrast of $P(r)$ over the course of the year in that the 'bump' in $P_\ell(r)$, constituting the middle r-regime where it rains more over land than over ocean, disappears during JJA. In JJA, there is consequently no range of r in which $P_\ell(r)$ lies above $P_o(r)$ which means that our initial hypothesis from our box model can already be refuted for these months.

As we account for the seasonal cycle of the moisture-precipitation relationship in the reconstruction of $\chi(t)$ by using the monthly fit functions $P_{o,m}(r)$ and $P_{\ell,m}(r)$, the seasonal biases disappear as shown in Figure 24e. The mean curves of $\chi_{rec}(t)$ and $\chi_{bm}(t)$ lie now nearly perfectly on top of each other and the correlation coefficient increases substantially to a value of $c = 0.91$. Note that the seasonal cycle over land is more relevant for a correct reconstruction of $\chi_{bm}(t)$ than the one over ocean but neglecting the seasonality of $P_o(r)$ nevertheless introduces reconstruction biases of up to 3.7 %. Even though the interquartile range in Figure 24e is still overestimated in most months, we deem this reconstruction from monthly land/ocean fits to be accurate enough to neglect higher-order spatial and temporal variations of $P(r)$.

One may ask whether accounting for monthly variations of $P(r)$ alone, i.e. monthly full tropical fit functions, would lead to a sufficiently accurate reconstruction, rendering the distinction between land and ocean obsolete. We computed the reconstruction from a month-dependent full tropical fit and found a very similar picture to the one presented in Figure 24a. This similarity is explained by the dominance of ocean grid points in setting the full tropical fit. Since the oceanic moisture-precipitation relationship shows only a weak seasonality, this feature is imposed on the full tropical relationship.

In conclusion, we find that the surface type is a meaningful criterion for the spatial variability of the moisture-precipitation relationship but that, on top of this, month-to-month variability needs to be taken into account in order to be able to adequately reconstruct characteristic features of the time evolution of the tropical precipitation ratio. Building on these insights, we can now investigate whether, at least in months other than JJA, the land-ocean differences in the moisture-precipitation relationship are responsible for precipitation enhancement over tropical land, and what role the underlying humidity distribution plays.

B.4 PRECIPITATION ENHANCEMENT OVER TROPICAL LAND

Following the theoretical results found by HS22, we diagnose precipitation enhancement over tropical land whenever $\chi > 0.86$. Figure 22 shows that the mean value of χ_{bm} lies above this threshold in all months, consistent with observations (see Fig. 5a in HS22), even though individual years sometimes fall below it.

B.4.1 *Is the land-sea contrast of $P(r)$ responsible for precipitation enhancement over land?*

One possible explanation for the precipitation enhancement over tropical land, inspired by a previous box model study based on water balance equations (SH23), is that the presence of land modifies the moisture-precipitation relationship such that P is larger over land than over ocean for a given value of r.

We test this explanation by conducting a sensitivity experiment: We assume that the land does not modify the moisture-precipitation relationship and reconstruct both land and ocean precipitation using the oceanic relationship $P_{o,m}(r)$. If the modification of $P(r)$ by the land surface is the key mechanism responsible for precipitation enhancement over tropical land, then we expect to see an underestimation of $\chi_{bm}(t)$ by $\chi_{rec}(t)$ due to an underestimation of mean land precipitation $\overline{P_\ell}$, and χ_{rec} values should typically lie below 0.86.

Given that $P_{o,m}(r)$ is very close to the tropical fit, we can already guess that this will not be the case. And indeed, Figure 25a reveals an overestimation in all months. Hence, all land-ocean differences in the moisture-precipitation relationships combined act to disfavor land precipitation and are generally not the reason why we observe precipitation enhancement over tropical land. Note, that this result is independent of the choice of applying $P_{o,m}(r)$ over both land and ocean, rather than $P_{\ell,m}(r)$.

What is not yet fully clear is whether the 'bump', as the only r-range in which precipitation rates over land are higher than over ocean, is needed for χ to lie above the threshold of 0.86. To investigate the role of the 'bump', we perform a similar experiment as before but this time, we only set $P_{\ell,m}(r) = P_{o,m}(r)$ within the range of r that constitutes the 'bump'. The corresponding reconstruction is shown in Figure 25b. As expected, χ_{rec} is reduced compared to χ_{bm} in all months in which a 'bump' was present. However, except for November,

where precipitation enhancement over land was very weak to begin with, the blue reconstruction curve still lies above the threshold of $\chi = 0.86$, implying that the 'bump' is not necessary for precipitation enhancement over land either.

B.4.2 *Precipitation enhancement over land due to different humidity distributions*

As the distinct moisture-precipitation relationships over land and ocean are not the reason for precipitation enhancement over land, the enhancement has to be due to distinct humidity distributions. This prompts the question of how the humidity distributions over land and ocean differ in the first place. In addition, we want to know which ranges of r are particularly relevant for explaining precipitation enhancement over land. The relevance of different ranges of r cannot be discerned from the humidity distributions alone but only from the combined effect of the distinct humidity distributions, which set how numerous grid cells with a given value of r are, and the effect of the distinct moisture-precipitation relationships, which set how much precipitation is expected from that given value of r.

Figure 26 shows the moisture-precipitation relationships (upper row) and probability density functions of column relative humidity $f(r)$ (second row) for three exemplary months. For each month, the underlying data is combined from all ten years. Land and ocean quantities are shown as orange and blue lines, respectively. In all months, the humidity distribution over land exhibits a much stronger bimodality than over ocean with a first peak around $r = 0.2$ and a second, stronger peak around $r = 0.75$. Over ocean, some bimodality can be discerned as well but peak magnitudes are more similar and the first peak occurs at a higher r value around 0.45 while the second peak appears close to the second land peak at around $r = 0.75$.

How these land-ocean differences in the humidity distribution matter for explaining the enhancement of precipitation over land depends on their combination with differences in the moisture-precipitation relationship. We selected March, July, and November as examples because these months represent three qualitatively distinct combinations of features of $P(r)$ and $f(r)$: March and July have in common that the land humidity distribution has a pronounced tail towards high r values but the two months differ in that March exhibits the 'bump' in the moisture-precipitation relationship over land, while July does not. November exhibits the 'bump' as well but is different from March in that its humidity distribution has a more pronounced high-r tail over ocean rather than over land. In the following, we analyze how these features interact to enhance precipitation over land and attribute the enhancement to specific ranges of r.

To this end, we recast the formulation of the 10-year monthly mean precipitation ratio $\chi_{\text{mean},m}$ in the framework of the moisture-precipitation relationship and humidity distribution,

$$\chi_{\text{mean},m} = \frac{\int_0^1 P_{\ell,m}(r) f_{\ell,m}(r)\,dr}{\int_0^1 P_{o,m}(r) f_{o,m}(r)\,dr}, \tag{30}$$

where $f_{\ell,m}(r)$ and $f_{o,m}(r)$ are the monthly land and ocean humidity distributions, respectively. To evaluate the integrals in Equation (30), we express the humidity distributions in terms of area fractions of grid cells with a given value of r,

$$f_{\ell,m}(r) = \frac{A_{\ell,m}(r)}{\int_0^1 A_{\ell,m}(r)\,dr} = \frac{A_{\ell,m}(r)}{\alpha A_{tr,m}}, \tag{31}$$

$$f_{o,m}(r) = \frac{A_{o,m}(r)}{\int_0^1 A_{o,m}(r)\,dr} = \frac{A_{o,m}(r)}{(1-\alpha)\,A_{tr,m}}, \tag{32}$$

where $A_{\ell/o,m}(r)$ denotes the 10-year total area of grid cells with the given value of r over either land or ocean, $\alpha \approx 0.26$ denotes the tropical land fraction, and $A_{tr,m}$ is the total area of the tropics between $\pm 30°$N multiplied by the number of days in month m from all 10 years. Even though mathematically not identical, $\chi_{mean,m}$ is practically equivalent to the mean seasonal cycle of $\chi(t)$ computed in Section B.3 (solid lines in Figure 24e). Replacing the humidity distributions in Equation (30) by the right hand side expressions of Equations (31) and (32), we can now formulate the condition for precipitation enhancement over tropical land as

$$\chi_{mean,m} = \frac{\frac{1}{\alpha} \int_0^1 P_{\ell,m}(r) A_{\ell,m}(r)\,dr}{\frac{1}{1-\alpha} \int_0^1 P_{o,m}(r) A_{o,m}(r)\,dr} > 0.86. \tag{33}$$

Since we want to assess which ranges of r contribute to precipitation enhancement over land, we make use of the fact that the integrals in Equation (33) are equivalent to the cumulative 10-year total rainfall over land and ocean, $P_{\ell,cum}(r_s, r_e)$ and $P_{o,cum}(r_s, r_e)$, respectively, where the accumulation is performed along r, starting from $r_s = 0$ and ending at $r_e = 1$. With $r_s = 0$ fixed and r_e as the variable end point of the accumulation, we rewrite Equation (33) as

$$\frac{P_{\ell,cum}(r_e)}{\alpha} - 0.86 \frac{P_{o,cum}(r_e)}{1-\alpha} > 0, \tag{34}$$

and identify ranges of r that contribute to precipitation enhancement over land as those in which the term on the left hand side (LHS) of Equation (34) increases.

We evaluate the LHS of Equation (34) and its derivative with respect to r from $r_e = 0$ to $r_e = 1$, using the same discretization as for the computation of the mean moisture-precipitation relationships with bin lengths $\Delta r = 0.01$. The results are shown in the third and bottom row of Figure 26 by the solid black lines. Gray shading in the third row marks the r-ranges that contribute to precipitation enhancement over land. The red dashed line in the bottom row indicates the location of maximum increase of the LHS of Equation (34) and, thus, the r value that contributes most to precipitation enhancement over tropical land. We see in all months that precipitation enhancement can be attributed to relatively large humidity values, above $r = 0.6$. The pattern of r-ranges identified as contributors can be classified into two types, depending on the considered month: First, a single broad range of values above some threshold value of r. This type is representative for the months from March to July and is the result of the combined effect of the 'bump' (if present) and the pronounced tail of the land humidity distribution. The threshold value of r for precipitation enhancement is located between 0.60 and 0.65 in months that exhibit a 'bump' and shifted to slightly higher values between 0.65 and 0.70 in months that do not. The second type is representative for the months from August to February and is characterized by an interruption of the broad r-range seen in type one by a range in which precipitation

is favored over ocean rather than land. Still, as a whole, precipitation remains favored over land as the LHS of Equation (34) does not become negative. The width of this interruption varies between months and is largest in November where the ocean has the pronounced high-r tail in its humidity distribution. Such a pronounced tail over ocean is, however, not a necessary condition for causing this interruption.

B.5 SENSITIVITY OF THE RESULTS TO THE CHOSEN FIT MODEL

The results presented so far were obtained using empirical fits of the moisture-precipitation relationships over narrow ranges of r, meaning that the shape of the relationships was captured very accurately. Previous studies on $P(r)$, however, have used simple exponential fit models to describe the nature of the relationship (Bretherton et al., 2004; Rushley et al., 2018). Looking at the fairly linear curves of $P(r)$ in log-space as displayed in Figure 23, such an exponential ansatz seems appropriate. In this section, we test whether an exponential ansatz is accurate enough to reconstruct $\chi_{bm}(t)$.

There are two ways to obtain a least squares fit function of the form $P_{fit}(r) = a \exp(b\,r)$ (analogous to Bretherton et al., 2004): Either by fitting $P_{fit}(r)$ directly to the data, or by transforming $P_{fit}(r)$ into the linear function $P_{fit,\,lin}(r) = b\,r + \ln(a)$ and then fitting $P_{fit,lin}(r)$ to the data in log-space. The former method minimizes the absolute error of the fit, while the latter method minimizes the relative error. We use both methods to compute reconstructions of $\chi_{bm}(t)$, accounting for distinct relationships over land and ocean and for the different months, analogous to what was done for Figure 24e with the empirical fit. The results are shown in Figure 27a and b. We find that the exponential ansatz is not able to capture basic characteristics of $\chi_{bm}(t)$ regardless of the chosen method (compare to Fig. 24e as well).

In Figure 27a, where the fit was obtained with $P_{fit,\,lin}(r)$, both shape and magnitude of the seasonal cycle seem to be captured to some extent but $\chi_{bm}(t)$ is overestimated or underestimated in all months. Looking at the monthly mean values of the precipitation ratio's constituents, $\overline{P_\ell}$ and $\overline{P_o}$, in Figure 27c, it becomes clear that the similarity between reconstruction and benchmark is spurious since both land and ocean precipitation rates are greatly overestimated throughout the year. This is because the optimization of the relative error leads to large absolute errors, especially for high values of r where precipitation rates are high. When the reconstruction is based on $P_{fit}(r)$, as shown in Figure 27b and d, neither shape nor magnitude of $\chi_{bm}(t)$ are captured by the reconstruction. In this case, land and ocean mean precipitation are both greatly underestimated. This is because the fit function optimizes for accuracy in the steep, high-r range of $P(r)$ at the expense of accuracy at intermediate r values. At intermediate r values, the fit function remains close to zero while the (P, r) bin-mean data already picks up. Thus, we conclude that the deviations of the $P(r)$ mean curves in Figure 23 from a simple analytical form such as an exponential function are significant if the goal is to reconstruct the land-ocean precipitation differences.

That the exponential ansatz is unable to capture the correct value and behavior of a basic mean characteristic of tropical precipitation such as χ raises questions about the usefulness of the concept of a simple, analytical moisture-precipitation relationship, for instance, in the context of conceptual models. In particular, when spatial differences in precipitation characteristics are of interest, a simple form of $P(r)$ will yield spurious results. This said, it needs to be noted that our analysis here is solely based on ERA5 reanalysis data which cannot be considered to be the ground truth. Final conclusions, thus, require a validation

of our findings using largely independent datasets such as observations or convection-resolving model output.

B.6 SUMMARY

This study investigated whether the moisture-precipitation relationship $P(r)$ is able to explain land-ocean differences in tropical precipitation, quantified by the tropical precipitation ratio χ, and whether the modification of $P(r)$ and/or the modification of the underlying humidity distribution by the land surface enhances land precipitation, as revealed by values of χ larger than 0.86.

To this end, we first derived the moisture-precipitation relationship from 10 years of daily ERA5 reanalysis data (1981–1990), and tested to which detail we need to know the spatial and temporal dependence of $P(r)$ in order to adequately reconstruct the mean seasonal cycle and year-to-year variability of $\chi(t)$. Two modes of the variability of $P(r)$ proofed to be essential:

1. $P(r)$ is distinct over land and ocean.

2. $P(r)$ exhibits a seasonal cycle.

Using the obtained relationships, $P_{\ell,m}(r)$ and $P_{o,m}(r)$, dependent on surface type (land/ocean) and month, we then showed that, despite the existence of a small range of r values in which $P_{\ell,m}(r)$ lies above $P_{o,m}(r)$ in the months from September to May, the net effect of distinct $P(r)$ relationships over land and ocean in all months is to counteract precipitation enhancement over land. Instead, the precipitation enhancement can be attributed to the influence of land on the humidity distribution.

Over land, the humidity distribution exhibits a more pronounced tail towards high r values. The abundance of these high r values, associated with high rain rates, overcompensates the fact that differences between $P_{\ell,m}(r)$ and $P_{o,m}(r)$ act to reduce precipitation over land compared to over ocean. An exception to this rule is November, where precipitation enhancement requires the additional 'support' of the range where $P_{\ell,m}(r) > P_{o,m}(r)$.

While a correct reconstruction of $\chi(t)$ from the moisture-precipitation relationship proofed to be insensitive to the temporal resolution of the underlying data, being averaged either daily or monthly, it does rest on a sufficiently accurate fit $P(r)$. An exponential fit model, as suggested e.g. by Bretherton et al., 2004, was unable to reproduce basic characteristics of $\chi(t)$ and to explain tropical land-ocean precipitation differences. This insight calls for caution when employing the moisture-precipitation relationship in simple models, especially when spatial variations of precipitation characteristics are of interest. We conclude that the moisture-precipitation relationship, if constructed with sufficient attention to detail, is a useful tool to probe interactions between tropical precipitation and the surface and that precipitation enhancement over tropical land is a consequence of how the land modulates column relative humidity, both through direct moistening and heating of the atmospheric column, and through synoptic- or large-scale moisture transport.
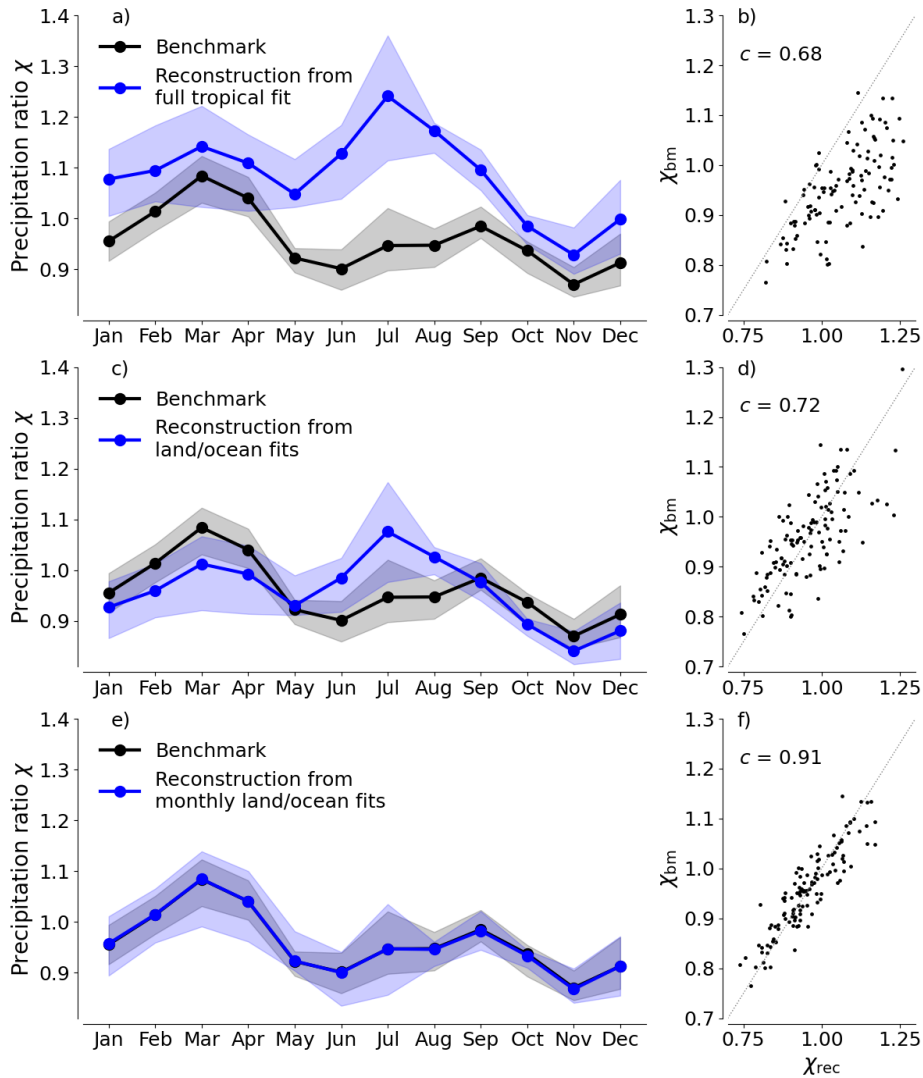
Figure 24: Comparison of benchmark $\chi_{bm}(t)$ with different reconstructions $\chi_{rec}(t)$ based on moisture-precipitation relationships that were fitted to different subsets of the data. Left panels: 10-year mean seasonal cycle (solid lines) and interquartile ranges of monthly mean values from individual years (shading). Right panels: Monthly mean values of individual years (1981–1990) from the benchmark and reconstruction plotted against each other. The gray dashed line shows the identity line, $\chi_{bm} = \chi_{rec}$, and c denotes the Pearson correlation coefficient.
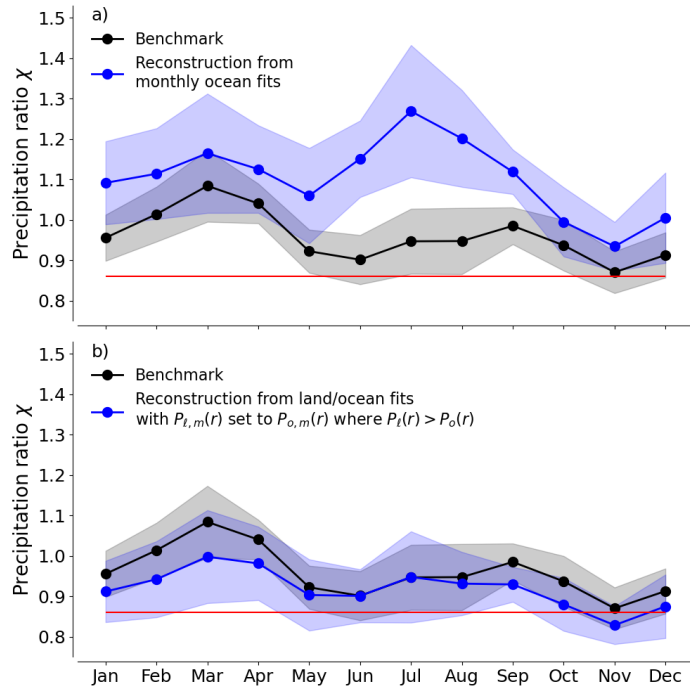
Figure 25: Comparison of the benchmark precipitation ratio with reconstructions from sensitivity experiments. Panel a: Reconstructed precipitation over both land and ocean was computed from the oceanic relationship $P_{o,m}(r)$. Panel b: Reconstructed ocean precipitation was computed from $P_{o,m}(r)$ and reconstructed land precipitation was computed from a modified land relationship which was set to $P_{o,m}(r)$ in the range where $P_{\ell,m}(r) > P_{o,m}(r)$, effectively removing the 'bump'. The threshold for precipitation enhancement over land is shown in red.
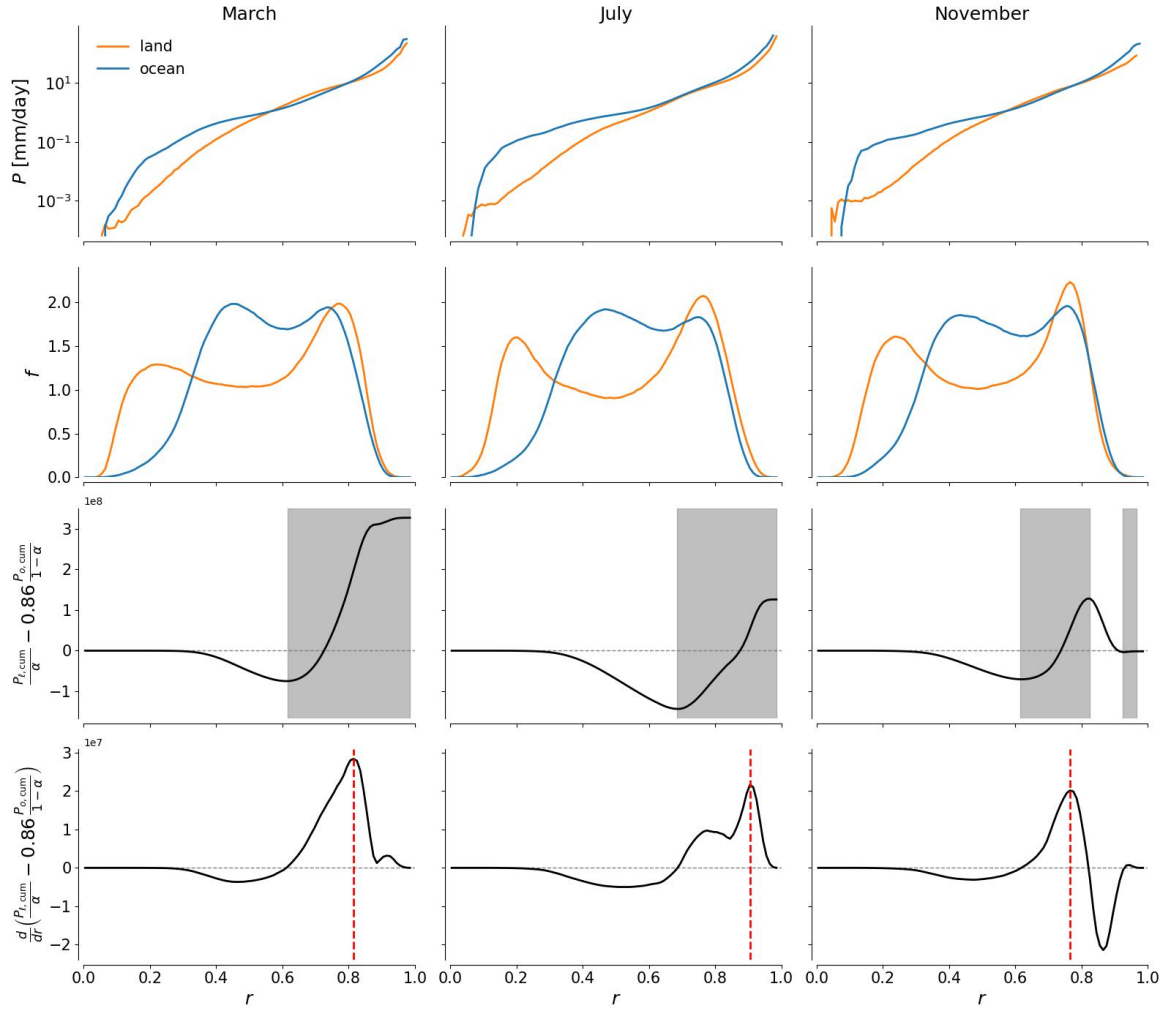
Figure 26: Land and ocean moisture-precipitation relationships (top row) and probability density functions of column relative humidity (second row) for three exemplary months. The third row shows the curves of the LHS of Equation (34) in black. Ranges of r that contribute to precipitation enhancement over land are those in which the black curves exhibit a positive slope and are marked with gray shading. The bottom row shows the rate of change of the LHS of Equation (34) along r with the red dashed line indicating the location of maximum increase.
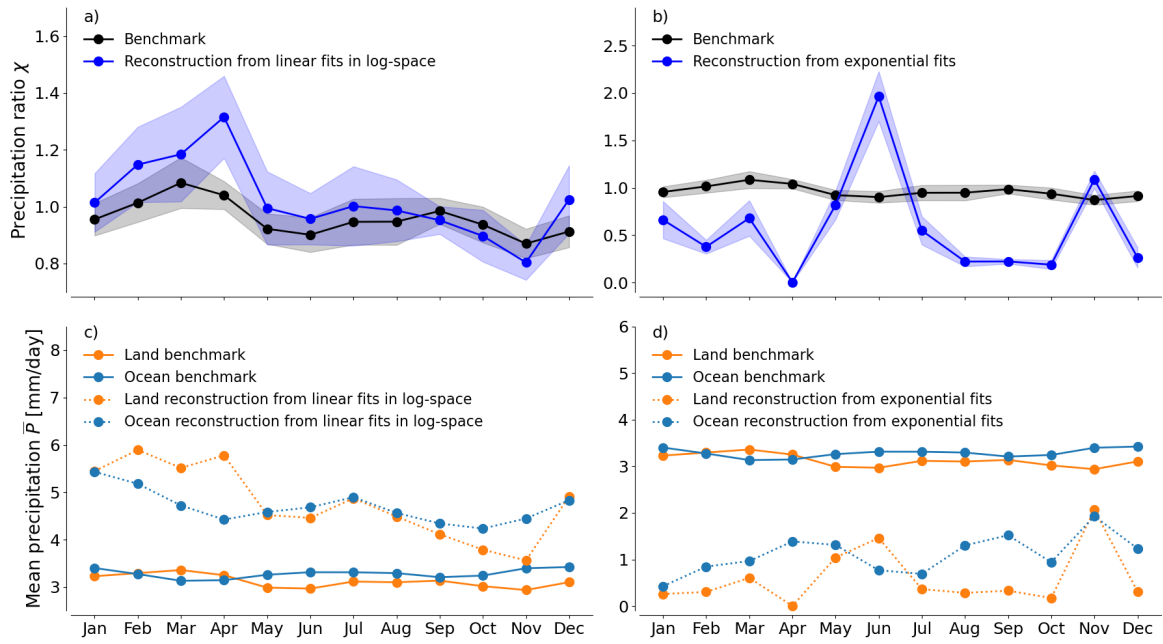
Figure 27: Comparison of benchmark values of the precipitation ratio (panel a and c) and monthly mean precipitation over land and ocean (panel b and d) with respective reconstructions based on different analytical fit models. Reconstructions in panel a and b are computed using the linear fit model $P_{fit,lin}(r)$ applied to data in log-space and reconstructions in panel c and d are based on the exponential fit model $P_{fit}(r)$ applied to data directly.

DATA AND TOOLS

The ICON simulations that form the basis of Chapter 5 were conducted within the third cycle of the NextGems project, which is funded by the EU Horizon 2020 program (project number 101003470).

Furthermore, the work for this dissertation heavily relied on open source software, some of which I would like to acknowledge explicitly:

- The conceptual box model was written in `Julia` (Bezanson et al., 2017), and made use of various julia-packages, including `DynamicalSystems.jl` (Datseris, 2018), `DifferentialEquations.jl` (Rackauckas and Nie, 2017), and `Makie.jl` (Danisch and Krumbiegel, 2021) for creating figures.

- For the second study, I mostly used `Python`, and especially the packages `numpy` (Harris et al., 2020), `xarray` (Hoyer and Hamman, 2017), `pandas` (team, 2020), and `matplotlib` (Hunter, 2007).

- I typeset this thesis using the `classicthesis` template developed by André Miede and Ivo Pletikosić (https://bitbucket.org/amiede/classicthesis/).

BIBLIOGRAPHY

Ahmed, Fiaz and J. David Neelin (2018). "Reverse Engineering the Tropical Precipitation–Buoyancy Relationship." In: *Journal of the Atmospheric Sciences* 75.5, pp. 1587–1608. ISSN: 0022-4928, 1520-0469. DOI: 10.1175/JAS-D-17-0333.1.

Ahmed, Fiaz and Courtney Schumacher (2017). "Geographical differences in the tropical precipitation-moisture relationship and rain intensity onset." In: *Geophysical Research Letters* 44.2, pp. 1114–1122. ISSN: 1944-8007. DOI: 10.1002/2016GL071980.

Allen, Myles R. and William J. Ingram (2002). "Constraints on future changes in climate and the hydrologic cycle." In: *Nature* 419.6903, pp. 224–232. ISSN: 1476-4687. DOI: 10.1038/nature01092.

Ananthakrishnan, R. (1977). "Some aspects of the monsoon circulation and monsoon rainfall." In: *pure and applied geophysics* 115.5, pp. 1209–1249. ISSN: 1420-9136. DOI: 10.1007/BF00874407.

Arraut, Josefina Moraes et al. (2012). "Aerial Rivers and Lakes: Looking at Large-Scale Moisture Transport and Its Relation to Amazonia and to Subtropical Rainfall in South America." In: *Journal of Climate* 25.2, pp. 543 –556. DOI: 10.1175/2011JCLI4189.1.

Augstein, Ernst, Heiner Schmidt, and Feodor Ostapoff (1974). "The vertical structure of the atmospheric planetary boundary layer in undisturbed trade winds over the Atlantic Ocean." In: *Boundary-Layer Meteorology* 6.1, pp. 129–150. ISSN: 1573-1472. DOI: 10.1007/BF00232480.

Austin, James M. (1948). "A note on cumulus growth in a nonsaturated environment." In: *Journal of the Atmospheric Sciences* 5.3, pp. 103–107. ISSN: 1520-0469. DOI: 10.1175/1520-0469(1948)005<0103:ANOCGI>2.0.CO;2.

Back, Larissa E. and Christopher S. Bretherton (2005). "The Relationship between Wind Speed and Precipitation in the Pacific ITCZ." In: *Journal of Climate* 18.20, pp. 4317–4328. ISSN: 0894-8755, 1520-0442. DOI: 10.1175/JCLI3519.1.

Becker, Tobias, Peter Bechtold, and Irina Sandu (2021). "Characteristics of convective precipitation over tropical Africa in storm-resolving global simulations." In: *Quarterly Journal of the Royal Meteorological Society* 147.741, pp. 4388–4407. ISSN: 1477-870X. DOI: 10.1002/qj.4185.

Bergemann, Martin and Christian Jakob (2016). "How important is tropospheric humidity for coastal rainfall in the tropics?" In: *Geophysical Research Letters* 43.11, pp. 5860–5868. ISSN: 1944-8007. DOI: 10.1002/2016GL069255.

Bezanson, Jeff et al. (2017). "Julia: A Fresh Approach to Numerical Computing." In: *SIAM Review* 59.1, pp. 65–98. DOI: 10.1137/141000671.

Bretherton, Christopher S., Matthew E. Peters, and Larissa E. Back (2004). "Relationships between Water Vapor Path and Precipitation over the Tropical Oceans." In: *Journal of Climate* 17.7, pp. 1517–1528. ISSN: 0894-8755, 1520-0442. DOI: 10.1175/1520-0442(2004)017<1517:RBWVPA>2.0.CO;2.

Brubaker, Kaye, Dara Entekhabi, and Peter Eagleson (1991). "Atmospheric water vapor transport: Estimation of continental precipitation recycling and parameterization of a simple climate model." In.

Brubaker, Kaye L., Dara Entekhabi, and P. S. Eagleson (1993). "Estimation of Continental Precipitation Recycling." In: *Journal of Climate* 6, pp. 1077–1089. ISSN: 0894-8755. DOI: 10.1175/1520-0442(1993)006<1077:EOCPR>2.0.CO;2.

Budyko, M. I. (1958). *Heat balance of the Earth's surface*. U.S. Dept. of Commerce, Weather Bureau.

Budyko, M. I. and O. A. Drozdov (1953). "Characteristics of the moisture circulation in the atmosphere." In: 4, pp. 5–14.

Chaboureau, J.-P. et al. (2004). "The role of stability and moisture in the diurnal cycle of convection over land." In: *Quarterly Journal of the Royal Meteorological Society* 130.604, pp. 3105–3117. ISSN: 1477-870X. DOI: 10.1256/qj.03.132.

Chahine, Moustafa T. (1992). "The hydrological cycle and its influence on climate." In: *Nature* 359.6394, pp. 373–380. ISSN: 1476-4687. DOI: 10.1038/359373a0.

Charney, Jule G. (1963). "A Note on Large-Scale Motions in the Tropics." In: *Journal of the Atmospheric Sciences* 20.6, pp. 607–609. ISSN: 0022-4928, 1520-0469. DOI: 10.1175/1520-0469(1963)020<0607:ANOLSM>2.0.CO;2.

Chou, C., J. D. Neelin, and H. Su (2001). "Ocean-atmosphere-land feedbacks in an idealized monsoon." In: *Quarterly Journal of the Royal Meteorological Society* 127.576, pp. 1869–1891. DOI: https://doi.org/10.1002/qj.49712757602.

Cronin, Timothy W., Kerry A. Emanuel, and Peter Molnar (2015). "Island precipitation enhancement and the diurnal cycle in radiative-convective equilibrium." In: *Quarterly Journal of the Royal Meteorological Society* 141.689, pp. 1017–1034. ISSN: 1477-870X. DOI: 10.1002/qj.2443.

Danisch, Simon and Julius Krumbiegel (2021). "Makie.jl: Flexible high-performance data visualization for Julia." In: *Journal of Open Source Software* 6.65, p. 3349. DOI: 10.21105/joss.03349.

Datseris, George (2018). "DynamicalSystems.jl: A Julia software library for chaos and nonlinear dynamics." In: *Journal of Open Source Software* 3, p. 598. DOI: 10.21105/joss.00598.

Datseris, George and Ulrich Parlitz (2022). *Nonlinear Dynamics*. 2192-4791. Springer International Publishing.

Dayem, Katherine E., David C. Noone, and Peter Molnar (2007). "Tropical western Pacific warm pool and maritime continent precipitation rates and their contrasting relationships with the Walker Circulation." In: *Journal of Geophysical Research: Atmospheres* 112 (D6). DOI: https://doi.org/10.1029/2006JD007870.

Derbyshire, S. H. et al. (2004). "Sensitivity of moist convection to environmental humidity." In: *Quarterly Journal of the Royal Meteorological Society* 130.604, pp. 3055–3079. ISSN: 1477-870X. DOI: 10.1256/qj.03.130.

Dessler, A. E. and K. Minschwaner (2007). "An analysis of the regulation of tropical tropospheric water vapor." In: *Journal of Geophysical Research: Atmospheres* 112 (D10). ISSN: 2156-2202. DOI: 10.1029/2006JD007683.

Dey, Dipanjan, Aitor Aldama Campino, and Kristofer Döös (2024). "Atmospheric water transport connectivity within and between ocean basins and land." In: *Hydrology and Earth System Sciences* 27.2, pp. 481–493. ISSN: 1027-5606. DOI: 10.5194/hess-27-481-2023.

Edelman, Alexandra et al. (June 2014). *State of the Tropics - 2014 Report*. ISBN: 978-0-9924023-4-1.

Eltahir, E. a. B. and R. L. Bras (1994). "Precipitation recycling in the Amazon basin." In: *Quarterly Journal of the Royal Meteorological Society* 120, pp. 861–880. ISSN: 1477-870X. DOI: 10.1002/qj.49712051806.

Ent, Rudi J. van der et al. (2010). "Origin and fate of atmospheric moisture over continents." In: *Water Resources Research* 46.9. ISSN: 1944-7973. DOI: 10.1029/2010WR009127.

Entekhabi, Dara, Ignacio Rodriguez-Iturbe, and Rafael L. Bras (1992). "Variability in Large-Scale Water Balance with Land Surface-Atmosphere Interaction." In: *Journal of Climate* 5.8, pp. 798–813. ISSN: 0894-8755. DOI: 10.1175/1520-0442(1992)005<0798:VILSWB>2.0.CO;2. URL: https://journals.ametsoc.org/jcli/article/5/8/798/35919/Variability-in-Large-Scale-Water-Balance-with-Land.

Fasullo, J. (2012). "A mechanism for land–ocean contrasts in global monsoon trends in a warming climate." In: *Climate Dynamics* 39.5, pp. 1137–1147. ISSN: 1432-0894. DOI: 10.1007/s00382-011-1270-3.

Fiedler, Stephanie et al. (2020). "Simulated Tropical Precipitation Assessed across Three Major Phases of the Coupled Model Intercomparison Project (CMIP)." In: *Monthly Weather Review* 148.9, pp. 3653–3680. ISSN: 1520-0493, 0027-0644. DOI: 10.1175/MWR-D-19-0404.1.

Gadgil, Sulochana, P. V. Joseph, and N. V. Joshi (1984). "Ocean–atmosphere coupling over monsoon regions." In: *Nature* 312.5990, pp. 141–143. ISSN: 1476-4687. DOI: 10.1038/312141a0.

Galewsky, Joseph, Adam Sobel, and Isaac Held (2005). "Diagnosis of Subtropical Humidity Dynamics Using Tracers of Last Saturation." In: *Journal of the Atmospheric Sciences* 62.9, pp. 3353–3367. ISSN: 0022-4928, 1520-0469. DOI: 10.1175/JAS3533.1.

Geen, Ruth et al. (2020). "Monsoons, ITCZs, and the Concept of the Global Monsoon." In: *Reviews of Geophysics* 58.4, e2020RG000700. DOI: https://doi.org/10.1029/2020RG000700.

Graham, N. E. and T. P. Barnett (1987). "Sea Surface Temperature, Surface Wind Divergence, and Convection over Tropical Oceans." In: *Science* 238.4827, pp. 657–659. DOI: 10.1126/science.238.4827.657.

Hagemann, Stefan and Tobias Stacke (2015). "Impact of the soil hydrology scheme on simulated soil moisture memory." In: *Climate Dyn.* 44, pp. 1731–1750. DOI: 10.1007/s00382-014-2221-6.

Halley, Edmond (1686). "An historical account of the trade winds, and monsoons, observable in the seas between and near the Tropicks, with an attempt to assign the physical cause of the said winds." In: *Philosophical Transactions of the Royal Society of London* 16.183, pp. 153–168. DOI: 10.1098/rstl.1686.0026.

Harris, Charles R. et al. (2020). "Array programming with NumPy." In: *Nature* 585.7825, pp. 357–362. DOI: 10.1038/s41586-020-2649-2.

Held, Isaac M and Arthur Y Hou (1980). "Nonlinear axially symmetric circulations in a nearly inviscid atmosphere." In: *Journal of the Atmospheric Sciences* 37.3, pp. 515–533.

Hersbach, H. et al. (2018a). *ERA5 hourly data on pressure levels from 1979 to present*. Copernicus Climate Change Service (C3S) Climate Data Store (CDS). accessed at DKRZ on <25-09-2023>. DOI: 10.24381/cds.bd0915c6.

— (2018b). *ERA5 hourly data on single levels from 1979 to present*. Copernicus Climate Change Service (C3S) Climate Data Store (CDS). accessed at DKRZ on <25-09-2023>. DOI: 10.24381/cds.adbb2d47.

Hohenegger, Cathy and Bjorn Stevens (2018). "The role of the permanent wilting point in controlling the spatial distribution of precipitation." In: *Proceedings of the National Academy of Sciences* 115.22, pp. 5692–5697. ISSN: 0027-8424, 1091-6490. DOI: 10.1073/pnas.1718842115.

— (2022). "Tropical Continents Rainier Than Expected From Geometrical Constraints." In: *AGU Advances* 3.4, e2021AV000636. ISSN: 2576-604X. DOI: 10.1029/2021AV000636.

Hohenegger, Cathy et al. (2023). "ICON-Sapphire: simulating the components of the Earth system and their interactions at kilometer and subkilometer scales." In: *Geoscientific Model Development* 16.2, pp. 779–811. ISSN: 1991-959X. DOI: 10.5194/gmd-16-779-2023.

Holloway, Christopher E. and J. David Neelin (2009). "Moisture Vertical Structure, Column Water Vapor, and Tropical Deep Convection." In: *Journal of the Atmospheric Sciences* 66.6, pp. 1665–1683. ISSN: 0022-4928, 1520-0469. DOI: 10.1175/2008JAS2806.1.

Horton, Robert e. (1943). "Hydrologic interrelations between lands and oceans." In: *Eos, Transactions American Geophysical Union* 24.2, pp. 753–764. ISSN: 2324-9250. DOI: 10.1029/TR024i002p00753.

Hoyer, S. and J. Hamman (2017). "xarray: N-D labeled arrays and datasets in Python." In: *Journal of Open Research Software* 5.1. DOI: 10.5334/jors.148.

Hu, Shineng et al. (2023). "Spatial and Seasonal Variations of Sea Surface Temperature Threshold for Tropical Convection." In: *Journal of Climate* 36.15, pp. 4899–4912. ISSN: 0894-8755, 1520-0442. DOI: 10.1175/JCLI-D-22-0545.1.

Hunter, J. D. (2007). "Matplotlib: A 2D graphics environment." In: *Computing in Science & Engineering* 9.3, pp. 90–95. DOI: 10.1109/MCSE.2007.55.

Insel, Nadja, Christopher J. Poulsen, and Todd A. Ehlers (2010). "Influence of the Andes Mountains on South American moisture transport, convection, and precipitation." In: *Climate Dynamics* 35.7, pp. 1477–1492. ISSN: 1432-0894. DOI: 10.1007/s00382-009-0637-1.

Koldunov, Nikolay et al. (2023). *nextGEMS: output of the model development cycle 3 simulations for ICON and IFS*. DOI: 10.26050/WDCC/nextGEMS_cyc3.

Krishna Kumar, K. et al. (2004). "Climate impacts on Indian agriculture." In: *International Journal of Climatology* 24.11, pp. 1375–1393. DOI: https://doi.org/10.1002/joc.1081.

Kumar, B. Praveen et al. (2017). "Latent Heat Flux Sensitivity to Sea Surface Temperature: Regional Perspectives." In: *Journal of Climate* 30.1, pp. 129–143. ISSN: 0894-8755, 1520-0442. DOI: 10.1175/JCLI-D-16-0285.1.

Lintner, Benjamin R. et al. (2013). "An Idealized Prototype for Large-Scale Land– Atmosphere Coupling." In: *Journal of Climate* 26.7, pp. 2379–2389. ISSN: 0894-8755, 1520-0442. DOI: 10.1175/JCLI-D-11-00561.1.

Liu, Zhengyu and Mike Alexander (2007). "Atmospheric bridge, oceanic tunnel, and global climatic teleconnections." In: *Reviews of Geophysics* 45.2. ISSN: 1944-9208. DOI: 10.1029/2005RG000172.

Manabe, S. et al. (1991). "Transient Responses of a Coupled Ocean–Atmosphere Model to Gradual Changes of Atmospheric CO2. Part I. Annual Mean Response." In: *Journal of Climate* 4.8, pp. 785–818. ISSN: 0894-8755, 1520-0442. DOI: 10.1175/1520-0442(1991)004<0785:TROACO>2.0.CO;2.

Mapes, Brian E. et al. (2018). "The Meandering Margin of the Meteorological Moist Tropics." In: *Geophysical Research Letters* 45.2, pp. 1177–1184. ISSN: 1944-8007. DOI: 10.1002/2017GL076440.

Masunaga, Hirohiko (2012). "Short-Term versus Climatological Relationship between Precipitation and Tropospheric Humidity." In: *Journal of Climate* 25.22, pp. 7983–7990. ISSN: 0894-8755, 1520-0442. DOI: 10.1175/JCLI-D-12-00037.1.

Masunaga, Hirohiko and Tristan S. L'Ecuyer (2014). "A Mechanism of Tropical Convection Inferred from Observed Variability in the Moist Static Energy Budget." In: *Journal of the Atmospheric Sciences* 71.10, pp. 3747–3766. ISSN: 0022-4928, 1520-0469. DOI: 10.1175/JAS-D-14-0015.1.

Masunaga, Hirohiko and Brian E. Mapes (2020). "A Mechanism for the Maintenance of Sharp Tropical Margins." In: *Journal of the Atmospheric Sciences* 77.4, pp. 1181–1197. ISSN: 0022-4928, 1520-0469. DOI: 10.1175/JAS-D-19-0154.1.

McBride, John L. and William M. Frank (1999). "Relationships between Stability and Monsoon Convection." In: *Journal of the Atmospheric Sciences* 56.1, pp. 24–36. ISSN: 0022-4928, 1520-0469. DOI: 10.1175/1520-0469(1999)056<0024:RBSAMC>2.0.CO;2.

Muller, Caroline J. et al. (2009). "A model for the relationship between tropical precipitation and column water vapor." In: *Geophysical Research Letters* 36.16. ISSN: 1944-8007. DOI: 10.1029/2009GL039667.

Murphy, D. M. and T. Koop (2005). "Review of the vapour pressures of ice and supercooled water for atmospheric applications." In: *Quarterly Journal of the Royal Meteorological Society* 131.608, pp. 1539–1565. ISSN: 1477-870X. DOI: 10.1256/qj.04.94.

Nepstad, Daniel C. et al. (1994). "The role of deep roots in the hydrological and carbon cycles of Amazonian forests and pastures." In: *Nature* 372.6507, pp. 666–669. ISSN: 1476-4687. DOI: 10.1038/372666a0.

Ogino, Shin-Ya et al. (2016). "How Much is the Precipitation Amount over the Tropical Coastal Region?" In: *Journal of Climate* 29.3, pp. 1231–1236. ISSN: 0894-8755, 1520-0442. DOI: 10.1175/JCLI-D-15-0484.1.

— (2017). "Tropical Coastal Dehydrator in Global Atmospheric Water Circulation." In: *Geophysical Research Letters* 44.22, pp. 11,636–11,643. ISSN: 1944-8007. DOI: https://doi.org/10.1002/2017GL075760.

Peixóto, José P. and Abraham H. Oort (1983). "The Atmospheric Branch Of The Hydrological Cycle And Climate." In: *Variations in the Global Water Budget*. Dordrecht: Springer Netherlands, pp. 5–65. DOI: 10.1007/978-94-009-6954-4_2.

Peters, Ole and J. David Neelin (2006). "Critical phenomena in atmospheric precipitation." In: *Nature Physics* 2.6, pp. 393–396. ISSN: 1745-2481. DOI: 10.1038/nphys314.

Phillips, Oliver L. et al. (2009). "Drought Sensitivity of the Amazon Rainforest." In: *Science* 323.5919, pp. 1344–1347. DOI: 10.1126/science.1164033.

Pierrehumbert, R. T. (1995). "Thermostats, Radiator Fins, and the Local Runaway Greenhouse." In: *Journal of the Atmospheric Sciences* 52.10, pp. 1784–1806. ISSN: 0022-4928, 1520-0469. DOI: 10.1175/1520-0469(1995)052<1784:TRFATL>2.0.CO;2.

Qian, Jian-Hua (2008). "Why Precipitation Is Mostly Concentrated over Islands in the Maritime Continent." In: *Journal of the Atmospheric Sciences* 65.4, pp. 1428–1441. ISSN: 0022-4928. DOI: 10.1175/2007JAS2422.1.

Rackauckas, Christopher and Qing Nie (2017). "DifferentialEquations.jl–a performant and feature-rich ecosystem for solving differential equations in Julia." In: *Journal of Open Research Software* 5.1.

Raymond, David J. and David J. Torres (1998). "Fundamental Moist Modes of the Equatorial Troposphere." In: *Journal of the Atmospheric Sciences* 55.10, pp. 1771–1790. ISSN: 0022-4928, 1520-0469. DOI: 10.1175/1520-0469(1998)055<1771:FMMOTE>2.0.CO;2.

Rocha, Humberto R. da et al. (2004). "Seasonality of Water and Heat Fluxes Over a Tropical Forest in Eastern Amazonia." In: *Ecological Applications* 14 (sp4), pp. 22–32. ISSN: 1939-5582. DOI: 10.1890/02-6001.

Rodriguez-Iturbe, Ignacio, Dara Entekhabi, and Rafael L. Bras (1991). "Nonlinear Dynamics of Soil Moisture at Climate Scales: 1. Stochastic Analysis." In: *Water Resources Research* 27, pp. 1899–1906. DOI: 10.1029/91WR01035.

Rushley, S. S. et al. (2018). "Reexamining the Nonlinear Moisture-Precipitation Relationship Over the Tropical Oceans." In: *Geophysical Research Letters* 45.2, pp. 1133–1140. ISSN: 1944-8007. DOI: 10.1002/2017GL076296.

Schiro, Kathleen A. et al. (2016). "Deep Convection and Column Water Vapor over Tropical Land versus Tropical Ocean: A Comparison between the Amazon and the Tropical Western Pacific." In: *Journal of the Atmospheric Sciences* 73.10, pp. 4043–4063. ISSN: 0022-4928, 1520-0469. DOI: 10.1175/JAS-D-16-0119.1.

Schiro, Kathleen A. et al. (2020). "Environmental Controls on Tropical Mesoscale Convective System Precipitation Intensity." In: *Journal of the Atmospheric Sciences* 77.12, pp. 4233–4249. ISSN: 0022-4928, 1520-0469. DOI: 10.1175/JAS-D-20-0111.1.

Schmidt, Luca and Cathy Hohenegger (2023). "Constraints on the Ratio between Tropical Land and Ocean Precipitation Derived from a Conceptual Water Balance Model." In: *Journal of Hydrometeorology* 24.6, pp. 1103–1117. ISSN: 1525-7541, 1525-755X. DOI: 10.1175/JHM-D-22-0162.1.

Seneviratne, Sonia I. et al. (2010). "Investigating soil moisture–climate interactions in a changing climate: A review." In: *Earth-Science Reviews* 99.3, pp. 125–161. ISSN: 0012-8252. DOI: 10.1016/j.earscirev.2010.02.004.

Shannon, C. E. (1948). "A mathematical theory of communication." In: *The Bell System Technical Journal* 27.3, pp. 379–423. ISSN: 0005-8580. DOI: 10.1002/j.1538-7305.1948.tb01338.x.

Sherwood, Steven and Qiang Fu (2014). "A Drier Future?" In: *Science* 343.6172, pp. 737–739. DOI: 10.1126/science.1247620.

Sivakumar, M. V. K., H. P. Das, and O. Brunini (2005). "Impacts of Present and Future Climate Variability and Change on Agriculture and Forestry in the Arid and Semi-Arid Tropics." In: *Climatic Change* 70.1, pp. 31–72. ISSN: 1573-1480. DOI: 10.1007/s10584-005-5937-9.

Sobel, A. H., C. D. Burleyson, and S. E. Yuter (2011). "Rain on small tropical islands." In: *Journal of Geophysical Research: Atmospheres* 116 (D8). ISSN: 2156-2202. DOI: 10.1029/2010JD014695.

Sobel, Adam H. and Gilles Bellon (2009). "The Effect of Imposed Drying on Parameterized Deep Convection." In: *Journal of the Atmospheric Sciences* 66.7, pp. 2085–2096. ISSN: 0022-4928, 1520-0469. DOI: 10.1175/2008JAS2926.1.

Stan, Cristiana et al. (2017). "Review of Tropical-Extratropical Teleconnections on Intraseasonal Time Scales." In: *Reviews of Geophysics* 55.4, pp. 902–937. ISSN: 1944-9208. DOI: 10.1002/2016RG000538.

Stevens, Bjorn and Sandrine Bony (2013). "What Are Climate Models Missing?" In: *Science* 340.6136, pp. 1053–1054. DOI: 10.1126/science.1237554.

Stone, Peter H. and Robert M. Chervin (1984). "The Influence of Ocean Surface Temperature Gradient and Continentality on the Walker Circulation. Part II: Prescribed Global Changes." In: *Monthly Weather Review* 112.8, pp. 1524 –1534. DOI: 10.1175/1520-0493(1984)112<1524:TIOOST>2.0.CO;2.

Sutton, Rowan T., Buwen Dong, and Jonathan M. Gregory (2007). "Land/sea warming ratio in response to climate change: IPCC AR4 model results and comparison with observations." In: *Geophysical Research Letters* 34.2. ISSN: 1944-8007. DOI: 10.1029/2006GL028164.

Taylor, Christopher M. et al. (2011). "Frequency of Sahelian storm initiation enhanced over mesoscale soil-moisture patterns." In: *Nature Geoscience* 4.7, pp. 430–433. ISSN: 1752-0908. DOI: 10.1038/ngeo1173.

Taylor, Christopher M. et al. (2012). "Afternoon rain more likely over drier soils." In: *Nature* 489.7416, pp. 423–426. ISSN: 1476-4687. DOI: 10.1038/nature11377.

Taylor, Christopher M. et al. (2013). "Modeling soil moisture-precipitation feedback in the Sahel: Importance of spatial scale versus convective parameterization." In: *Geophysical Research Letters* 40.23, pp. 6213–6218. DOI: https://doi.org/10.1002/2013GL058511.

team, The pandas development (2020). *pandas-dev/pandas: Pandas*. Version latest. DOI: 10.5281/zenodo.3509134.

Tian, Baijun and Xinyu Dong (2020). "The Double-ITCZ Bias in CMIP3, CMIP5, and CMIP6 Models Based on Annual Mean Precipitation." In: *Geophysical Research Letters* 47.8, e2020GL087232. ISSN: 1944-8007. DOI: 10.1029/2020GL087232.

Tomassini, L., A. Voigt, and B. Stevens (2015). "On the connection between tropical circulation, convective mixing, and climate sensitivity." In: *Quarterly Journal of the Royal Meteorological Society* 141.689, pp. 1404–1416. ISSN: 1477-870X. DOI: 10.1002/qj.2450.

Tompkins, Adrian M. (2001). "Organization of Tropical Convection in Low Vertical Wind Shears: The Role of Water Vapor." In: *Journal of the Atmospheric Sciences* 58.6, pp. 529–545. ISSN: 0022-4928, 1520-0469. DOI: 10.1175/1520-0469(2001)058<0529:OOTCIL>2.0.CO;2.

Trenberth, Kevin E. (1998). "Atmospheric Moisture Residence Times and Cycling: Implications for Rainfall Rates and Climate Change." In: *Climatic Change* 39.4, pp. 667–694. ISSN: 1573-1480. DOI: 10.1023/A:1005319109110.

Trenberth, Kevin E. and Christian J. Guillemot (1995). "Evaluation of the Global Atmospheric Moisture Budget as Seen from Analyses." In: *Journal of Climate* 8.9, pp. 2255–2272. ISSN: 0894-8755, 1520-0442. DOI: 10.1175/1520-0442(1995)008<2255:EOTGAM>2.0.CO;2.

Trenberth, Kevin E., David P. Stepaniak, and Julie M. Caron (2000). "The Global Monsoon as Seen through the Divergent Atmospheric Circulation." In: *Journal of Climate* 13.22, pp. 3969 –3993. DOI: 10.1175/1520-0442(2000)013<3969:TGMAST>2.0.CO;2.

Ulrich, Max and Gilles Bellon (2019). "Superenhancement of Precipitation at the Center of Tropical Islands." In: *Geophysical Research Letters* 46.24, pp. 14872–14880. ISSN: 1944-8007. DOI: 10.1029/2019GL084947.

Veiga, J. A. Paixão, V. Brahmananda Rao, and Sérgio H. Franchito (2005). "Heat and moisture budgets of the Walker circulation and associated rainfall anomalies during El Niño events." In: *International Journal of Climatology* 25.2, pp. 193–213. DOI: https://doi.org/10.1002/joc.1115.

Wang, Shuguang and Adam H. Sobel (2017). "Factors Controlling Rain on Small Tropical Islands: Diurnal Cycle, Large-Scale Wind Speed, and Topography." In: *Journal of the Atmospheric Sciences* 74.11, pp. 3515–3532. ISSN: 0022-4928. DOI: 10.1175/JAS-D-16-0344.1.

Wohl, Ellen et al. (2012). "The hydrology of the humid tropics." In: *Nature Climate Change* 2.9, pp. 655–662. ISSN: 1758-6798. DOI: 10.1038/nclimate1556.

Zhang, Chidong (1993). "Large-Scale Variability of Atmospheric Deep Convection in Relation to Sea Surface Temperature in the Tropics." In: *Journal of Climate* 6.10, pp. 1898–1913. ISSN: 0894-8755, 1520-0442. DOI: 10.1175/1520-0442(1993)006<1898:LSVOAD>2.0.CO;2.

Zhang, Guang Jun and Michael J. McPhaden (1995). "The Relationship between Sea Surface Temperature and Latent Heat Flux in the Equatorial Pacific." In: *Journal of Climate* 8.3, pp. 589–605. ISSN: 0894-8755, 1520-0442. DOI: 10.1175/1520-0442(1995)008<0589:TRBSST>2.0.CO;2.

Zhang, Xiaoxiao, Hailong Liu, and Minghua Zhang (2015). "Double ITCZ in Coupled Ocean-Atmosphere Models: From CMIP3 to CMIP5." In: *Geophysical Research Letters* 42.20, pp. 8651–8659. ISSN: 1944-8007. DOI: 10.1002/2015GL065973.

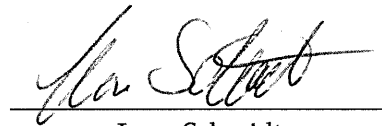# EIDESSTATTLICHE VERSICHERUNG | DECLARATION ON OATH

Hiermit erkläre ich an Eides statt, dass ich die vorliegende Dissertationsschrift selbst verfasst und keine anderen als die angegebenen Quellen und Hilfsmittel benutzt habe.

I hereby declare upon oath that I have written the present dissertation independently and have not used further resources and aids than those stated
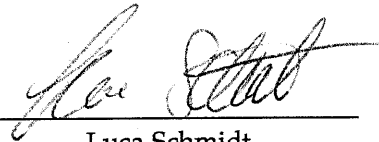
Hamburg, March 28, 2024

Luca Schmidt

EIDESSTATTLICHE VERSICHERUNG II | DECLARATION ON OATH II

Ich versichere, dass dieses gebundene Exemplar der Dissertation und das in elektronischer Form eingereichte Dissertationsexemplar (über den Docata-Upload) und das bei der Fakultät zur Archivierung eingereichte gedruckte gebundene Exemplar der Dissertationsschrift identisch sind.

I, the undersigned, declare that this bound copy of the dissertation and the dissertation submitted in electronic form (via the Docata upload) and the printed bound copy of the dissertation submitted to the faculty (responsible Academic Office or the Doctoral Office Physics) for archiving are identical.

Hamburg, March 28, 2024

Luca Schmidt

Hinweis / Reference

Die gesamten Veröffentlichungen in der Publikationsreihe des MPI-M
„Berichte zur Erdsystemforschung / Reports on Earth System Science",
ISSN 1614-1199

sind über die Internetseiten des Max-Planck-Instituts für Meteorologie erhältlich:
https://mpimet.mpg.de/forschung/publikationen

All the publications in the series of the MPI -M
„Berichte zur Erdsystemforschung / Reports on Earth System Science",
ISSN 1614-1199

are available on the website of the Max Planck Institute for Meteorology:
https://mpimet.mpg.de/en/research/publications